2006-03

Power losses and thermal modeling of a voltage source inverter

Oberdorf, Michael Craig.

Monterey California. Naval Postgraduate School

NAVAL POSTGRADUATE SCHOOL

MONTEREY, CALIFORNIA

THESIS

POWER LOSSES AND THERMAL MODELING OF A VOLTAGE SOURCE INVERTER

by

Michael Craig Oberdorf

March 2006

Thesis Advisor:	Alexander Julian
Second Reader:	Robert Ashton

Approved for public release; distribution is unlimited

THIS PAGE INTENTIONALLY LEFT BLANK

REPORT DOCUMENTATION PAGE			Form Approved OMB No. 0704-0188
Public reporting burden for this collection of information is estimated to average 1 hour per response, including the time for reviewing instruction, searching existing data sources, gathering and maintaining the data needed, and completing and reviewing the collection of information. Send comments regarding this burden estimate or any other aspect of this collection of information, including suggestions for reducing this burden, to Washington headquarters Services, Directorate for Information Operations and Reports, 1215 Jefferson Davis Highway, Suite 1204, Arlington, VA 22202-4302, and to the Office of Management and Budget, Paperwork Reduction Project (0704-0188) Washington DC 20503.			
1. AGENCY USE ONLY ***(Leave blank)***	**2. REPORT DATE** March 2006	**3. REPORT TYPE AND DATES COVERED** Master's Thesis	
4. TITLE AND SUBTITLE: Power Losses and Thermal Modeling of A Voltage Source Inverter			**5. FUNDING NUMBERS**
6. AUTHOR(S) Michael C. Oberdorf			
7. PERFORMING ORGANIZATION NAME(S) AND ADDRESS(ES) Naval Postgraduate School Monterey, CA 93943-5000			**8. PERFORMING ORGANIZATION REPORT NUMBER**
9. SPONSORING /MONITORING AGENCY NAME(S) AND ADDRESS(ES) N/A			**10. SPONSORING/MONITORING AGENCY REPORT NUMBER**
11. SUPPLEMENTARY NOTES The views expressed in this thesis are those of the author and do not reflect the official policy or position of the Department of Defense or the U.S. Government.			
12a. DISTRIBUTION / AVAILABILITY STATEMENT Approved for public release; distribution is unlimited			**12b. DISTRIBUTION CODE**

13. ABSTRACT (maximum 200 words)

This thesis presents thermal and power loss models of a three phase IGBT voltage source inverter used in the design of the 625KW fuel cell and reformer demonstration which is a top priority for the Office of Naval Research. The ability to generate thermal simulations of systems and to accurately predict a system's response becomes essential in order to reduce the cost of design and production, increase reliability, quantify the accuracy of the estimated thermal impedance of an IGBT module, predict the maximum switching frequency without violating thermal limits, predict the time to shutdown on a loss of coolant casualty, and quantify the characteristics of the heat-sink needed to dissipate the heat under worst case conditions. In order to accomplish this, power loss and thermal models were created and simulated to represent a three phase IGBT voltage source inverter in the lab. The simulated power loss and thermal model data were compared against the experimental data of a three phase voltage source inverter set up in the Naval Postgraduate School power systems laboratory.

14. SUBJECT TERMS Power Losses Model, Thermal Modeling, IGBT, Voltage Source Inverter DC-AC			**15. NUMBER OF PAGES** 125
			16. PRICE CODE
17. SECURITY CLASSIFICATION OF REPORT Unclassified	**18. SECURITY CLASSIFICATION OF THIS PAGE** Unclassified	**19. SECURITY CLASSIFICATION OF ABSTRACT** Unclassified	**20. LIMITATION OF ABSTRACT** UL

NSN 7540-01-280-5500 Standard Form 298 (Rev. 2-89)
Prescribed by ANSI Std. 239-18

THIS PAGE INTENTIONALLY LEFT BLANK

Approved for public release; distribution is unlimited

POWER LOSSES AND THERMAL MODELING OF A VOLTAGE SOURCE INVERTER

Michael C. Oberdorf
Lieutenant, United States Navy
B.S., Penn State University, 1999

Submitted in partial fulfillment of the
requirements for the degree of

MASTER OF SCIENCE IN ELECTRICAL ENGINEERING

from the

NAVAL POSTGRADUATE SCHOOL
March 2006

Author: Michael Craig Oberdorf

Approved by: Alexander Julian
Thesis Advisor

Robert Ashton
Second Reader

Jeffery B. Knorr
Chairman, Department of Electrical and Computer Engineering

THIS PAGE INTENTIONALLY LEFT BLANK

ABSTRACT

This thesis presents thermal and power loss models of a three phase IGBT voltage source inverter used in the design of the 625KW fuel cell and reformer demonstration which is a top priority for the Office of Naval Research. The ability to generate thermal simulations of systems and to accurately predict a system's response becomes essential in order to reduce the cost of design and production, increase reliability, quantify the accuracy of the estimated thermal impedance of an IGBT module, predict the maximum switching frequency without violating thermal limits, predict the time to shutdown on a loss of coolant casualty, and quantify the characteristics of the heat-sink needed to dissipate the heat under worst case conditions. In order to accomplish this, power loss and thermal models were created and simulated to represent a three phase IGBT voltage source inverter in the lab. The simulated power loss and thermal model data were compared against the experimental data of a three phase voltage source inverter set up in the Naval Postgraduate School power systems laboratory.

THIS PAGE INTENTIONALLY LEFT BLANK

TABLE OF CONTENTS

LIST OF FIGURES

LIST OF TABLES

THIS PAGE INTENTIONALLY LEFT BLANK

ACKNOWLEDGMENTS

First, I would like to thank my advisor, Professor Alex Julian for his guidance in this thesis research. He always had suggestions and new ideas when I ran into problems with the modeling of the system, and his help in understanding the hardware was invaluable. I would like to thank my Co-Advisor Professor Ashton for all the help he gave me on my introduction and background information. I would like to thank Tom Fikse from, Naval Surface Warfare Center for the funding and equipment which allowed me to complete my thesis. Several of my fellow students also deserve to be recognized. Carl Trask and Greg Moselle were always willing to help out with brainstorming, troubleshooting, and coding. I would like to thank my parents for the love and support they have given me. Finally, I would like to thank my wife for her support through all the years we have been married, I am the man I am today because of her.

THIS PAGE INTENTIONALLY LEFT BLANK

LIST OF ABBREVIATIONS, ACRONYMS, AND SYMBOLS

VSI	Voltage Source Inverter
ONR	Office of Naval Research
FPGA	Field Programmable Gate Array
NPS	Naval Postgraduate School
LOCC	Loss of Coolant Casualty
IPS	Integrated Power System
COTS	Commercial Off The Shelf Technology
PEBB	Power Electronics Building Block
AC	Alternating Current
DC	Direct Current
EMALS	Electromagnetic Aircraft Launching System
IGBT	Insulated Gate Bipolar Transistor
OOD	Officer Of the Deck
FEL	Free Electron Laser
NWSC	Naval Warfare Service Center
TMS	Thermal Management System
EM	Electro Magnetic

THIS PAGE INTENTIONALLY LEFT BLANK

EXECUTIVE SUMMARY

The goal of this thesis was to accurately simulate power loss and thermal behavior of a Voltage Source Inverter (VSI) using vendor data and a validated electrical model of a VSI. The model overview is shown below in **Figure 1**. Successful creation and implementation of these models can reduce the cost of design and production, increase reliability, quantify the accuracy of the estimated thermal impedance of an IGBT module, predict the maximum switching frequency without violating thermal limits, predict the time to shutdown on a Loss of Coolant Casualty (LOCC), and quantify the characteristics of the heat-sink needed to dissipate the heat under worst case conditions. This thesis particularly was focused on a VSI used in the development of a 625KW fuel cell and reformer demonstration for Office of Naval Research (ONR).

A thermal model was defined, created in Simulink, and calibrated to the Semikron VSI Module and its heatsink. The input required for the thermal model was the average power output of the semiconductor devices on the VSI module. A power losses model of the Semikron VSI module was created in Simulink to obtain the average power outputs of the semiconductor devices for the thermal model. The power losses model input variables were set to obtainable lab conditions (defined in the simulations chapter) so that experimental data could be collected. The power losses model was then simulated and data was collected. The thermal model was then simulated with the average power outputs of the semiconductor devices from the power losses model simulation. The lab equipment and experimental lab conditions were then set up to match the simulated conditions. Two experimental data runs were performed; one with coolant and one without coolant. The experimental data run without coolant was completed in order to compute the time to shutdown for a LOCC. The experimental data run with coolant was compared to the simulated data and it was determined that a strong correlation was present between the experimental data and the simulated data.

The percent error between the simulated and experimental power losses of the three phase VSI inverter was 11%. The percent error between the simulated and experimental IGBT Junction temperature of a half-bridge VSI inverter was 27%. The

extrapolated time to shutdown for a LOCC was 68 seconds. The power losses and thermal simulation were run multiple times to determine the maximum PWM switching frequency for the 625 KW fuel cell reformer project of ONR. The maximum PWM switching frequency for the 625kW fuel cell reformer project was determined to be 7 kHz which allowed a 20% margin to the lowest over temperature protection set point of 110°C. This thesis shows that by taking the vendor data one can accurately define, create, and simulate power loss and thermal models of a half bridge VSI which accurately predict the systems response.

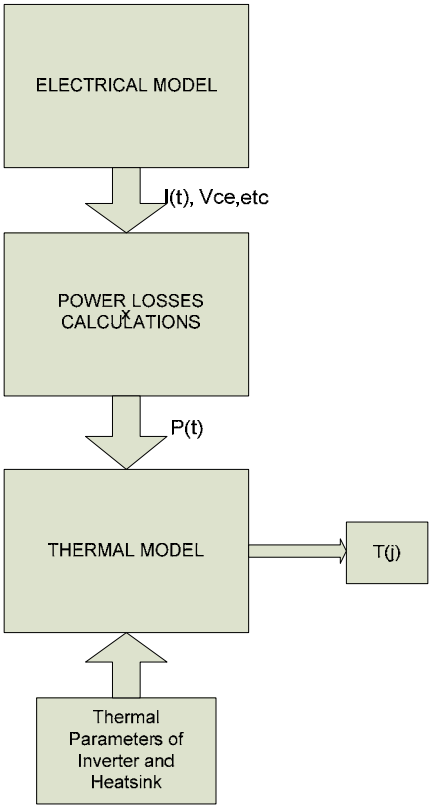

Figure 1. Overview of Thesis Model

I. INTRODUCTION

A. OVERVIEW

As the U. S. Navy moves toward a smaller more sophisticated fleet whose ships require less military personnel to operate them and becomes more dependent on electronics, the need to quantify the heat dissipated by electronic loads becomes paramount. As the number of electronic devices and inefficient weapon systems increase the ability to accurately quantify and predict the heat loads will allow ships to move from concentrated heat loads (i.e. propulsion system) to distributed heat loads (i.e. multiple electronic converters).

Today, one of the acronyms of interest is COTS (Commercial Off The Shelf) technology. The secretary of the Navy stated in January 2000 that electric drive would be used to propel all future Navy warships.

"Changes in propulsion systems fundamentally change the character and the power of our forces. This has been shown by the movement from sails to steam or from propeller to jet engines… More importantly, electric drive, like other propulsion changes, will open immense opportunities for redesigning ship architecture, reducing manpower, improving ship life, reducing vulnerability and allocating a great deal more power to war-fighting applications" [From 1].

The Navy's DD(X) ship program will be constructed with an Integrated Power System (IPS) to utilize all available shipboard power more efficiently and to unlock propulsion power for high-powered advanced electric launch, weapons, and sensor systems [3].

The Navy has had many transitions in its lineage that have changed the way we fight wars and build ships. The battleship was considered a measure of a country's naval strength during World War I and World War II. But in World War II, the aircraft carrier proved to be superior to the battleship during the Battle of Midway and the age of the carrier began. The submarine also proved to be a stealthy and effective weapon during World War II. The submarine from its beginning days of the Turtle to the newest Virginia Class nuclear submarine, has truly redefined the battle space. Although there

have been many inventions and changes within the Navy the standard power distribution architecture has remained the same for the last hundred years although electrical power demand has increased (**Figure 2**), [2].

INCREASING SHIPBOARD POWER DEMAND

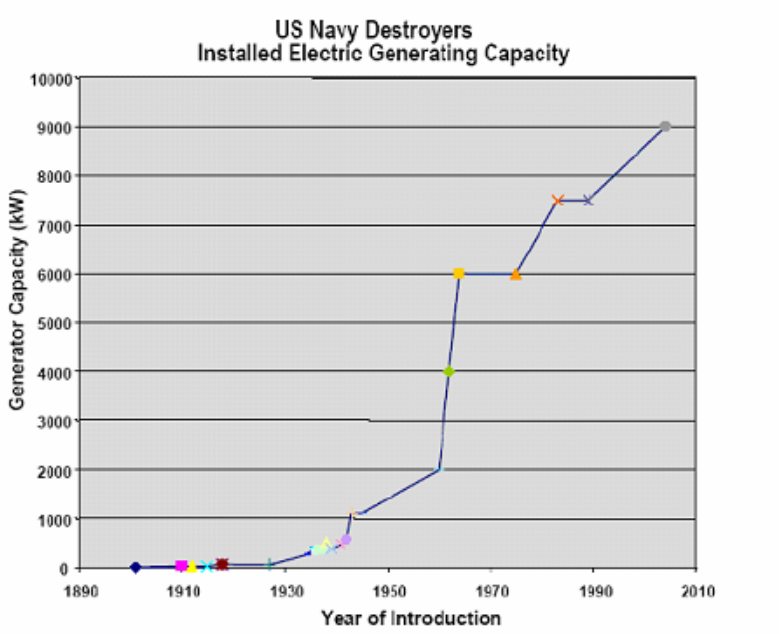

Figure 2. Historic Shipboard Electrical Generator Capacities [From 3]

So, why is the amount of power demand increasing and what does that have to do with power loss and thermal modeling of a Voltage Source Inverter (VSI)? The amount of increased power demand stems from the introduction of new technology such as the Electro-Magnetic Aircraft Launching System (EMALS), Electro-Magnetic (EM) rail-gun, Free Electron Laser (FEL), and high power radar. One technical report from the Naval Surface Warfare Center (NSWC) dated July 2003 concluded that the new generation ship will not be able to incorporate all these above listed thermal loads without a more modernized cooling system [4]. Further, compounding the thermal load is the introduction of distributed heat sources in the form of electronic converters. The objective of the thermal survey was to identify, quantify and document heat loads generated by naval systems in order to project cooling requirements for the future [4].

The following quotation is the summary of this study:

"The implementation of the design features of new electric distributed loads to achieve these objectives for the next generation of warships results in the generation of additional waste heat. Thermal issues are key in electronic product development at all levels of the electronic product hierarchy, from components such as the chip to the transfer of heat throughout ship systems and out to sea. Shrinking component sizes are resulting in increasing the volumetric heat generation rates and surface heat fluxes in many devices. The rate of heat flux is expected to eventually top 1000W/cm^2 due to material advances, smaller electronics components and faster switching speeds. The addition of advanced power electronics, advanced radar, dynamic armor, and weapons systems such as the EM railgun and the Free Electron Laser in future Naval Combatants, will result in heat loads eventually requiring a significant increase in cooling capacity" [From 4].

As the Navy moves towards IPS and away from conventional propulsion it introduces more heat generation from power electronic loads that will need to be quantified in order to accurately design cooling systems for future ships. The power requirements for the new high power weapons such as the EM railgun and the FEL are so demanding on the cooling system a Thermal Management System (TMS) for the entire ship might need to be designed [4]. The TMS would contain thermal models of all dissipatory equipment and its heat load given its current readiness condition. For instance, once an Officer Of the Deck (OOD) gives the command to fire the EM railgun, the TMS may override the command until there is sufficient cooling capacity. The ability to provide a robust cooling system capable of handling all heat loads becomes a difficult problem when one tries to minimize the size, weight and cost of the ship. The thermal loads of COTS equipment may also necessitate the inclusion of a TMS; COTS equipment generally dumps heat directly into the occupied area. This distributed thermal loading may quickly overwhelm Heating Ventilation and Air Conditioning (HVAC) systems. Further, new modern reduced sized electronics may require special attention, because the power density and thus heat generation have been increased. The ships cooling capacity

might need to be modified in order to handle these newly introduced loads. IPS versus conventional propulsion is shown in **Figure 3** [5].

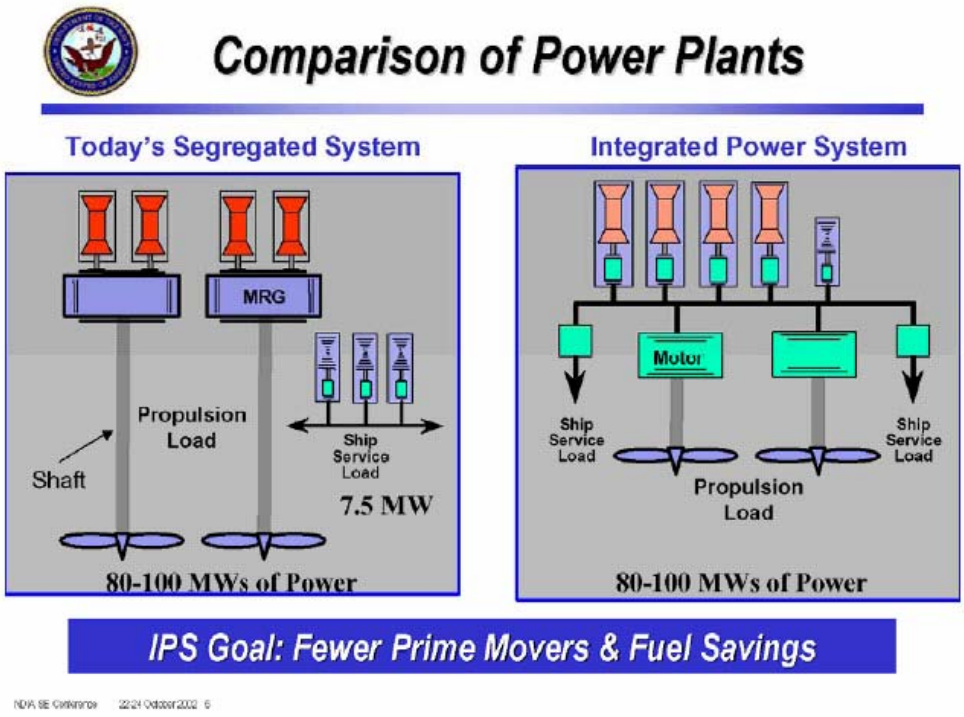

Figure 3. Comparison of IPS vs. Conventional Power Plants[From 5]

So why is the navy going to IPS? IPS has less prime mover machinery which equates to less infrared and acoustic signatures. IPS requires a smaller machinery room and propulsion plant which will reduce the fuel consumption over the life of the ship by an anticipated 15-20%. The reduction in weight will equate to reduced ships displacement and a faster ship. IPS is a modular design which will reduce construction, repair, and modernization costs. IPS technology has longer Mean Time Between Failures (MBTF) of propulsion components. The above characteristics equates to reduced manpower for operations up to 50% and reduced life cycle costs up to 50%. IPS propulsion motors have shorter electrical drive shafts when compared to the legacy systems, allowing an increase in the ships compartmentalization and survivability. Most importantly, the mechanical power only available for propulsion is unleashed for other

high power loads that could not possibly be energized by the ships service bus. The overall design of the IPS system doesn't require the extensive hydraulic and pneumatic systems, but instead utilizes electro-mechanical systems which reduce both overall cost and weight. It provides a more robust electrical power system capable of handling the next generation weapons such as the EM railgun and the FEL [5].

The ships zonal power distribution architecture utilizes both converters and inverters. The inverters and converters of the future could be made of Power Electronic Building Blocks (PEBB) technology. The PEBB will be able to convert ac to dc, buck and/or boost dc to dc, convert ac from one frequency to another, and invert dc back to ac. Since PEBB are pre-tested "plug and play" models, any system assembled with PEBB is pre-engineered and pre-tested to a certain extent. architecture. PEBB philosophy dictates that large converters will be constructed by series and/or parallel combinations of common blocks; Voltage can be increased by series connected PEBB while current can be increased by parallel connected PEBB (**Figure 4**) [4, 5].

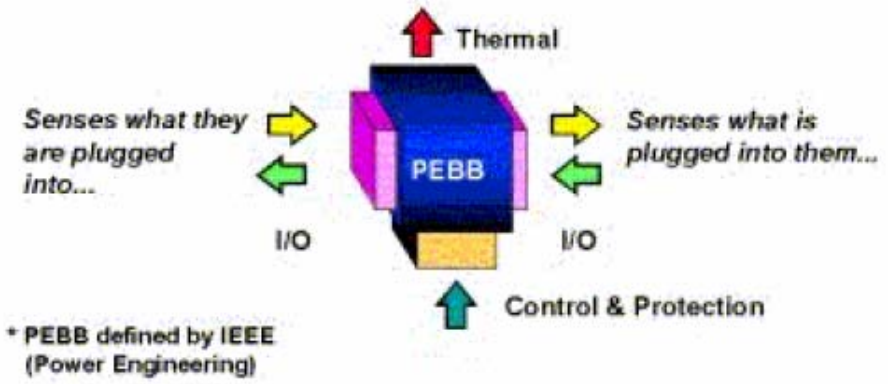

Figure 4. Power Electronics Building Blocks [From 5]

The concept PEBB contains a microprocessor/FPGA controller that allows the module to be programmed for a variety of different functions as listed in the previous paragraph. Ultimately, the PEBB constructed will be able to self-protect and limit stress to other common bus connected electronic equipment. The PEBB itself is made up of IGBT (or other electronic switching devices), diodes, laminate buses, isolated gate drivers, controller interface card, electrolytic capacitors, etc. The switching devices and diodes dissipate the majority of the heat as they conduct and switch from one state to

another. The thermal properties of the PEBB must be understood and tabulated in order to properly integrate a useable converter into a military environment. Thus, this thesis addresses the thermal characterization of a 625KW fuel cell converter constructed from COTS PEBB. The ability to account for the heat generated so that it may be dissipated is why the PEBB and IPS are relevant to this thesis.

Further, as industry constantly decreases the size of electronics the efficiency doesn't increase at the same rate which causes increased thermal stresses. The ability to characterize the thermal constraints of components based on the given controller architecture, layout, and environment becomes essential in order to reduce costs of design and production.

B. RESEARCH GOALS

During the development of a controller for a 625KW fuel cell inverter, it became necessary to determine the maximum switching frequency of the semiconductors in the PEBB without violating thermal limits. A high switching frequency is generally desired to reduce the size of the filtering components. However, thermal losses increase as frequency increases. This necessitated a study of the power losses and thermal characteristics of the VSI. The following are the thesis goals for the power loss and thermal modeling of a VSI :

- Model the power losses for a three phase VSI system using Simulink.
- Model the thermal behavior of a VSI system using Simulink.
- Compare the simulations to experimental measurements in order to validate models.
- Quantify the accuracy of the estimated thermal impedance of an IGBT module.
- Predict the maximum switching frequency without violating thermal limits.
- Predict the time to shutdown on a Loss of Coolant Casualty (LOCC).
- Quantify the characteristics of the heat-sink needed to dissipate the heat under worst case conditions.

The Comparison of the simulated data and the experimental data will be used to validate the computer modeling of the system.

C. APPROACH

The thermal model was defined and then created in Simulink given a valid electrical model. The thermal model was calibrated to the Semikron VSI module (i.e. PEBB) and its heatsink [6]. The input required in the thermal model was the average power output of the semiconductor devices on the VSI module. In order to simulate the average power output of the semiconductor devices, a power loss model of the Semikron VSI module was created in Simulink. The power loss model input variables were set to obtainable lab conditions. The model was then simulated and data was collected for verification with experimental results. The thermal model was then simulated with the average power outputs of the semiconductor devices from the power loss model simulation. The lab equipment and experimental lab conditions were then set up to match the simulated conditions. Two experimental data runs were performed: one with coolant and one without coolant. The experiment without coolant was completed in order to compute shutdown time for an LOCC. The experiment with coolant was compared to the simulated data to determine if a correlation was present. Models were validated based on the results.

D. THESIS ORGANIZATION

Chapter I is an overview of the research effort and the layout of the thesis.

Chapter II is a presents the thermal model of the IGBT half bridge dc-ac voltage source inverter.

Chapter III presents the power losses model which computes the amount of power losses inside the voltage source inverter along with the load in order to verify the thermal model.

Chapter IV presents the power losses and thermal model simulation results.

Chapter V Experimental Data Acquisition: experimental results from the lab built prototype in order to verify thermal model.

Chapter VI Validation of Models by comparisons between the simulated and experimental data and readdressing the research questions.

Chapter VII provides conclusions and future research opportunities.

The appendices provide Matlab computer code, data sheets, and application notes for the models constructed in this thesis.

II. THERMAL MODEL

A. INTRODUCTION

In order to accomplish the research goals of this thesis a thermal model of a voltage source inverter (VSI) was created. Specifically, it was created for a Semikron SKiiP 942GB120-317CTV VSI. The Semikron SKiiP package was chosen because it was the VSI that was used in the design of ONR's 625KW fuel cell and reformer demonstration. It was also used because it had a thermal resistor in close proximity to the IGBT junction. The thermal resistor allowed experimental temperature to be collected which could be compared to the simulated thermal model data of the IGBT junction temperature. Without this feature a contact pyrometer or other thermal device would have to be installed in order to measure the actual IGBT junction temperature.

The thermal model of the system was characterized by using the vendor application notes and data sheets. Once the thermal model was defined, a mathematical model representation of the system was created and solved. The mathematical model was then implemented in a Simulink Model. The Simulink Model was then calibrated to the data sheets for the Semikron SKiiP 942GB120-317CTV by creating a Matlab M-File for the initial variables of the thermal model. The input required for the thermal model was average power of the semiconductor devices on the Semikron module. Therefore, in order to determine the thermal response of the system a power losses model was created which is discussed in Chapter III.

The following are the benefits of creating a valid thermal model which predicts the temperature of the IGBT and diode junctions in a voltage source inverter:

- To reduce the cost of design and production.
- Increase reliability.
- Quantify the accuracy of the estimated thermal impedance of an IGBT module.
- Predict the maximum switching frequency without violating thermal limits.

- Predict the time to shutdown on a Loss of Coolant Casualty (LOCC).
- To quantify the characteristics of the heat-sink needed to dissipate the heat under worst case conditions.

B. THERMAL MODEL GENERATION

1. Thermal System Defined

The first step in thermal modeling of a VSI was to characterize the system. Although a more detailed system model is a ninth order system represented in **Figure 5**. The vendor has stated and showed that the thermal response of the IGBT and diode junction-case temperatures can be approximated by the solution of a fourth order system. The data necessary to represent the fourth order approximation of the system is provided in the vendor's data sheet located in **Appendix A**. Each fourth order system from a thermal stand point can be characterized as a fourth order R||C Load as seen in **Figure 6 [6].**

The model of the system is based on the vendor's representation of a fourth ordered system. As seen in **Figure 7**, the topology of the thermal model is made up of half of a half bridge inverter which includes one IGBT and one free wheeling diode. The vendors thermal model in the application notes makes some notable assumptions. First, the temperature drop from the case of the IGBT module to the heat sink is neglected. Second, the thermal coupling between the IGBT and the free wheeling diode is neglected. Instead of coupling, the application notes inform the user to use the hottest modeled semiconductor device junction temperature to be the junction temperature of both devices. This assumption is made due to the semiconductor devices close proximity to each other. The validity of these assumptions will be discussed in the conclusions chapter [6].

In order to determine the temperature of the IGBT junction temperature ($T_{j/T1}$) (**Figure 7**), a model of three systems must be created. One of the systems is a fourth order system, which is the model of thermal resistance and capacitance($R_{th}C$) from IGBT junction to case, which represents the temperature drop from the IGBT junction to case of

the SKiiP package. The next thermal boundary is the $R_{th}C$ from the case of the SKiiP package to attached heatsink. These thermal constants are due to the thermal paste applied and the amount of surface area for heat to dissipate. The vendor has determined that difference in temperature between the case of the IGBT module and the heat sink is negligible compared to the other thermal transfer functions and this system also neglected. The last system represents the $R_{th}C$ model is from the water-cooled heatsink to ambient temperature and is represented by a first ordered model.

In order to determine the temperature at the junction of the free wheeling diode another 4^{th} order system was created as seen in **Figure 7**. The system was that of a diode junction to inverter module case. Again, the thermal boundary from the case of the SKiiP package to attached heatsink is neglected. The last system represents the $R_{th}C$ model is from the water-cooled heatsink to ambient temperature and is represented by a first ordered model.

2. Mathematical Model and Solution

The next step that was taken was to derive the transfer function that characterized a fourth order RC system shown above. The value for thermal resistances and tau=R*C were taken from the Semikron data sheet for a SKiiP 942GB120-317CTV see **Appendix A**. The proof of a solution to one of the RC thermal model transfer functions is shown in **Equation 1**. The complete solution to a fourth order transfer function of a RC network shown in **Figure 6** is shown in **Equation 2 [6].**

3. Simulink Model

The thermal model of the system with its individual characteristics was then built using Simulink modeling software. Taking the vendors simplified model of the system a fourth order transfer function was created by using the **Figure 7** as a reference. The first transfer function created was the one that corresponded to the IGBT junction to module case system. In order to accomplish this, four transfer function equations were generated and their outputs were summed together as seen in **Figure 8**. Next, the sum of the output transfer functions were scaled by a constant since the thermal impedance was given in

milli-Kelvin/Watt in the vendor datasheet (see **Appendix A)**. The output of the sum of the transfer functions in **Figure 8** represents a change in temperature.

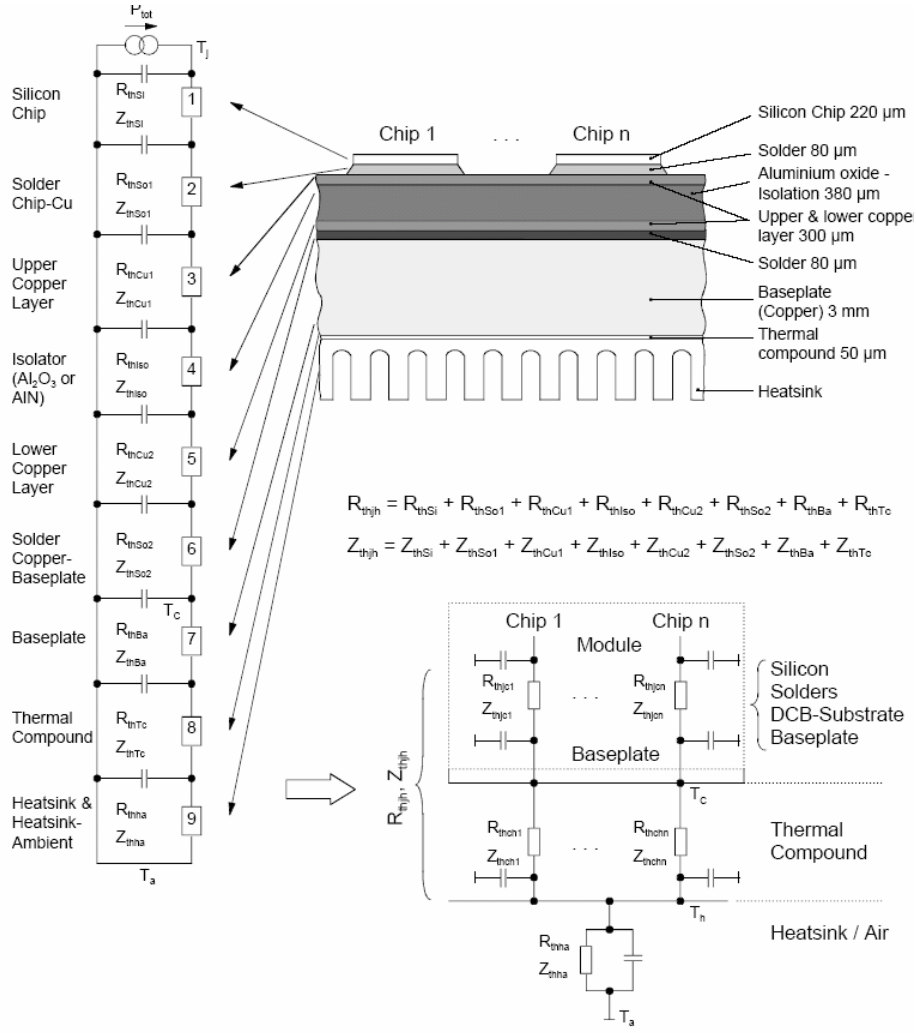

Figure 5. Semikron Thermal Model of System showing 9th Order System Reduced to three 4th Order Systems [From 6]

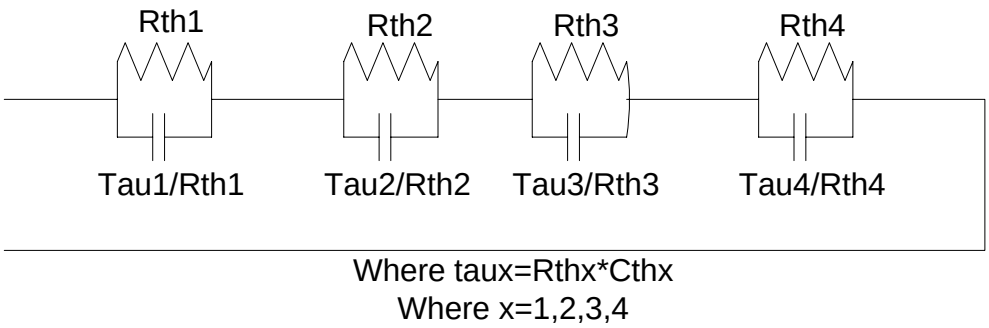

Figure 6. Thermal Model of a Fourth Order System [After 6]

$$\frac{r_1 \times \left[\frac{1}{sc_1}\right]}{r + \left[\frac{1}{sc_1}\right]} = \left[\frac{r_1 \times \left[\frac{1}{sc_1}\right]}{r_1 + \left[\frac{1}{sc_1}\right]}\right] \times \frac{sc_1}{sc_1} = \frac{r_1}{r_1 sc_1 + 1}, \text{where } \tau_1 = r_1 c_1 \Rightarrow \frac{r_1}{\tau_1 s + 1} \quad (1)$$

Equation 1. Solution to the Transfer Function of the Thermal Model for R||C Network [7]

$$\frac{R_1}{\tau_1 s + 1} + \frac{R_2}{\tau_2 s + 1} + \frac{R_3}{\tau_3 s + 1} + \frac{R_4}{\tau_4 s + 1} \text{ (Units: Temp/Power)} \quad (2)$$

Equation #2 Solution to the Transfer Function of the Thermal Model for 4th with units of Temp/Power [7]

.

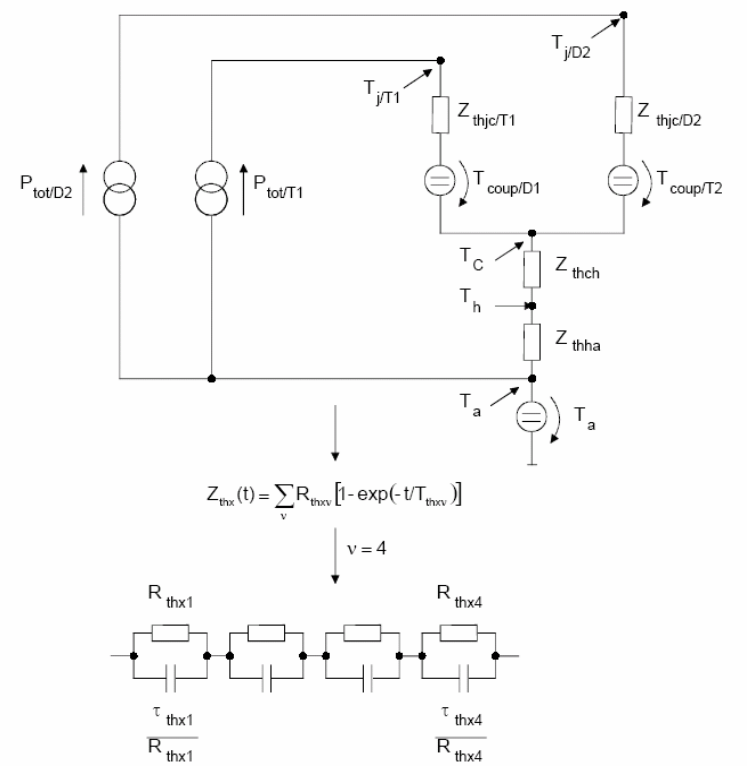

Figure 7. Semikrons Simplified Thermal Model for IGBT and Free Wheeling Diode [From 6]

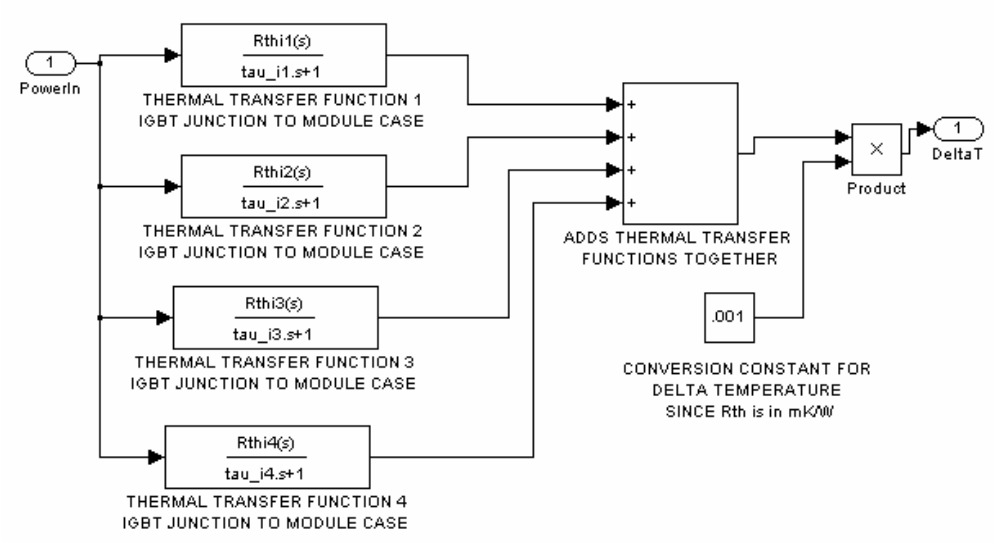

Figure 8. Simulink Model of 4th Order Transfer Function Representing the Thermal model of the IGBT junction to Module Case system

The next thermal boundary modeled in Simulink, as a 4th order transfer function, was from the diode junction to the case of inverter module. In order to accomplish this, four transfer function equations were generated and there outputs were summed to together as seen in **Figure 9**. Next, the sum of the output transfer functions were scaled by a constant since the thermal impedance was given in milli-Kelvin/Watt in the vendor datasheet (see **Appendix A)**. The output of the sum of the transfer functions in **Figure 9** represents a change in temperature.

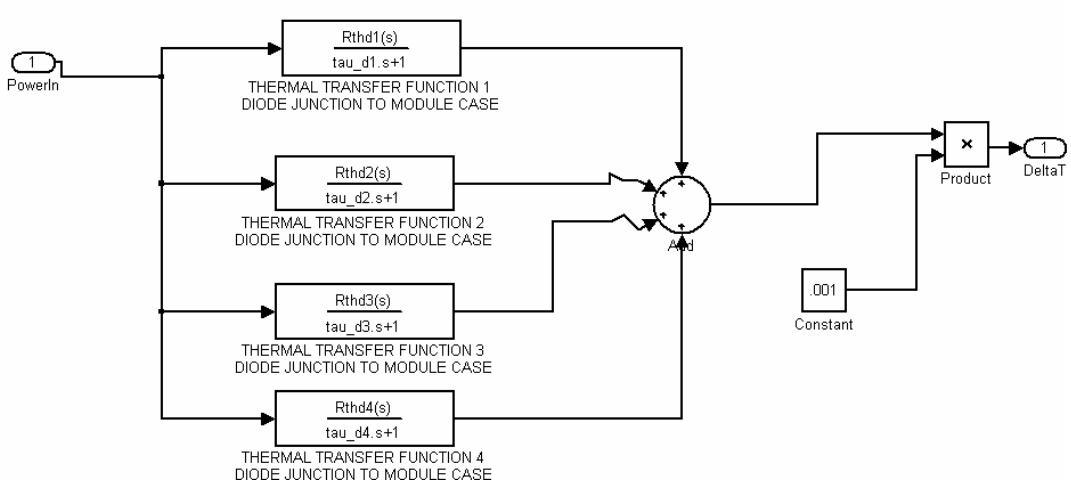

Figure 9. Simulink Model of 4th Order Transfer Function Representing the Thermal model of the Diode junction to Module Case system

The thermal model in **Figure 10** represents the $R_{th}C$ from the heatsink to ambient temperature. This transfer function was needed in order to simulate the temperature at the IGBT and diode junction. This model was a single order transfer function because it was the water cooled heatsink used versus the air cooled heatsink. Therefore a single transfer function equation was generated as seen in **Figure 10**. The output of the transfer functions wasn't scaled by a constant since the thermal impedance was given in Kelvin/Watt in the vendor datasheet (**Appendix A**). The output of the sum of the transfer functions in **Figure 10** represents a change in temperature.

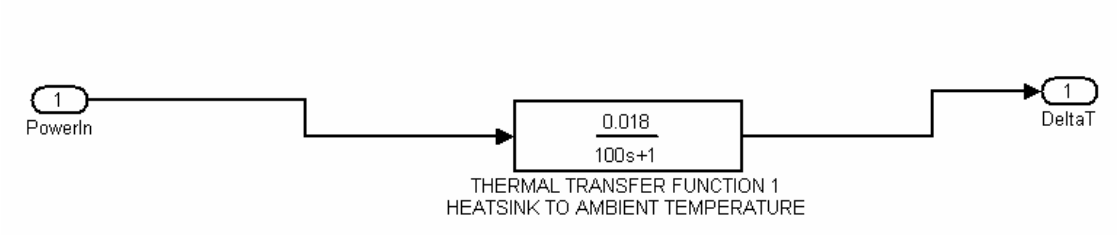

Figure 10. Simulink Model of 1st Order Transfer Function Representing the Thermal model of the Heatsink to Ambient Temperature

The final step was to connect up the subsystems in order to predict IGBT and diode junction temperatures. Using **Figure 7** as a reference, the temperature at the IGBT junction would be equal to **Equation 3**. The ambient temperature is a constant and $\Delta T_{\text{Ambient to Heatsink}}$ represents the temperature drop across the heatsink and the input to that system is the total power losses from the IGBT and the diode see **Figure 7**. The ΔT_{IGBT} module case to IGBT junction represents the temperature drop across the IGBT module case to the IGBT junction and its input is the total power losses from the IGBT see **Figure 7.** The subsystems were connected in accordance with **Figure 7** from the vendor in order to provide IGBT junction temperature and can be seen in **Figure 11**.

The temperature of the diode junction was calculated because depending on the switching frequency using PWM either semiconductor device might be thermal limiting one. The temperature of the diode junction was calculated using **Equation 4**. The ambient temperature is a constant and ΔT Ambient to Heatsink represents the temperature drop across the heatsink and the input to that system is the total power losses from the IGBT and the diode see **Figure 7**. The $\Delta T_{\text{Inverter module case to Diode junction}}$ represents the temperature drop across the inverter module case to the diode junction and its input is the total power losses from the diode see **Figure 7**. The subsystems were connected in accordance with **Figure 7** from the vendor in order to provide diode junction temperature and can be seen in **Figure 11**. The final step in building the thermal model was to create an initialization file in Matlab with all the vendor data. This is described in the simulation Chapter IV.

$$T_{IGBT\ JUNCTION} = T_{ambient} + \Delta T_{\text{Ambient to Heatsink}} + \Delta T_{\text{Inverter module case to IGBT junction}} \quad (3)$$

Equation 3. Solution to the IGBT junction temperature [6]

$$T_{\text{DIODE } JUNCTION} = T_{ambient} + \Delta T_{\text{Ambient to Heatsink}} + \Delta T_{\text{Inverter module case to Diode junction}} \quad (4)$$

Equation 4. Solution to the Diode junction temperature [6]

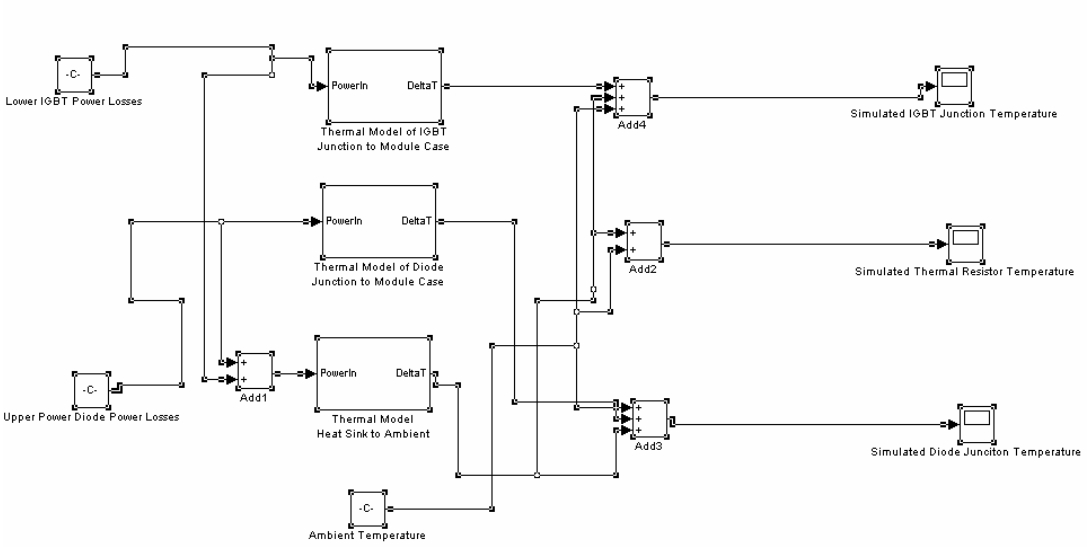

Figure 11. Total Thermal Model of Inverter Module which includes the IGBT and Diode junction temperatures

C. SUMMARY

The thermal model created in this chapter represents the thermal model that the vendor states approximates the thermal response of the system. The solution to the thermal model has many assumptions worth mentioning. First, it ignores the thermal losses between the inverter case and the heatsink. Normally, a thermal model would be generated to account for the thermal losses due to the thermal paste that is applied between the inverter case and the heatsink. The vendor in the application notes indicates

that the thermal losses due to the thermal paste boundary are insignificant compared to the other thermal losses. Second, the thermal coupling between the IGBT and the Diode due to there close proximity is ignored because the vendor states that the thermal coupling is minimal in the application notes. Instead of coupling, the application notes suggest to use the hottest modeled semiconductor device junction temperature to be the junction temperature of both devices. The relevancy and accuracy of these assumptions will be further discussed in the simulations and conclusions chapters. In order to compute the junction temperature using the thermal model developed in this chapter the power losses must be computed. The power losses model is described and developed in the next chapter.

III. POWER LOSSES MODEL

A. REASON FOR DEVELOPMENT

The power losses model was developed because the input required for the thermal model created in chapter II is the average power dissipated by the semiconductor devices in the VSI module. The simulation of thermal model is only made possible with power data from a power losses model. After a successful thermal simulation, experimental data will be collected in order to validate the thermal simulation data. After the validation of the thermal model further simulation of the power losses and thermal models will allow the research questions of Chapter I to be answered.

B. OVERVIEW

To accurately predict and validate a thermal model of a VSI you must be able to accurately predict the power losses of the system. In this thesis, a power losses model of the semiconductor devices in the SKiiP 942GB120-317CTV was created in Simulink using the vendor's application notes and data given a valid electrical Simulink model of a three phase VSI using PWM **(see Appendix's A)** [6]. The power losses model was experimentally compared to a controlled output of the VSI on a purely inductive load with a 100 V_{rms} output.

The power losses of the semiconductor devices were divided into the static power losses and the non-static power losses based on the vendors application notes [6]. The static power losses were the on-state losses (conduction losses) and the blocking losses. The non-static losses were divided into the switching losses (turn on/off) and driving losses. The driving losses and blocking losses were neglected since they accounted for a small portion of the overall power losses. An overview of the total power losses can be seen in **Figure 12 [6].**

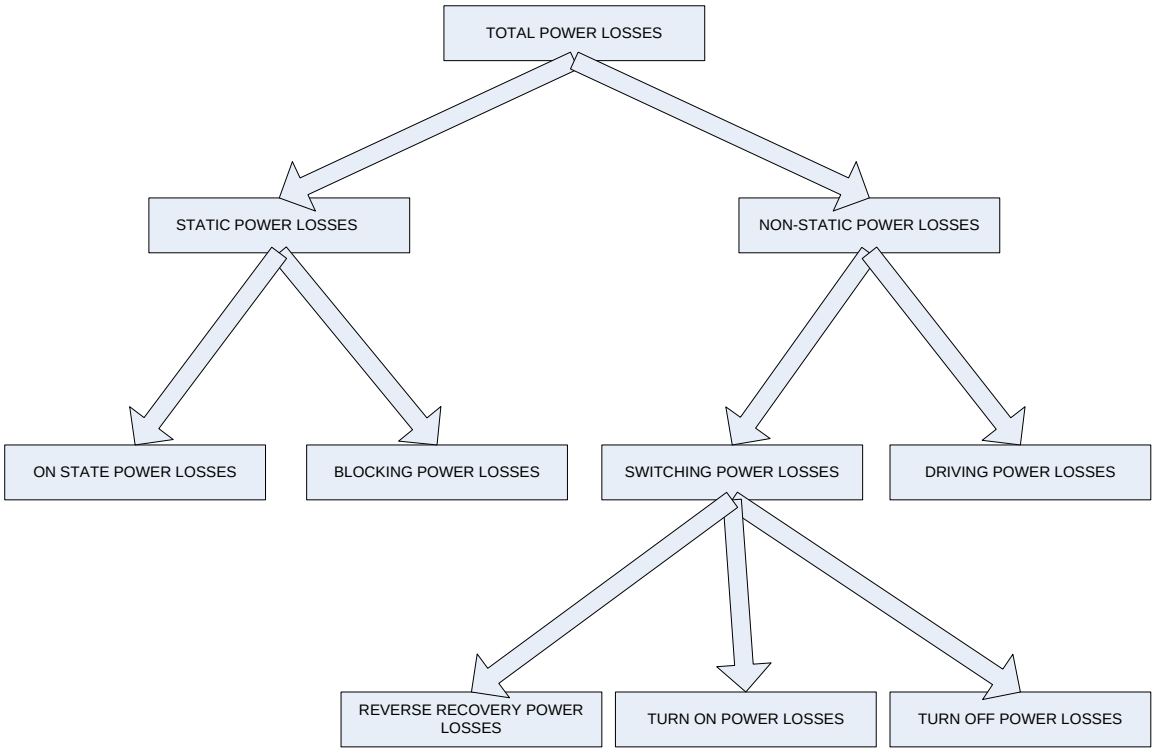

Figure 12. Overview and Breakdown of Total Power Losses[From 6]

C. DEVELOPMENT OF POWER LOSSES MODEL

1. Static Power Losses

The first step in development of a power losses model was the development of a validated electrical model. Since this thesis focuses on the power losses and thermal models it is noted that without a validated electrical model of the VSI the power losses model and thermal model couldn't have been implemented. The electrical model will only be referenced in order to clarify the power losses modeling. With that being said the static power losses are made up of the on-state power losses (conduction losses) and the blocking losses.

a. Conduction Losses

The conduction losses for the SKiiP 942GB120-317CTV VSI are from the four semiconductor devices found on the module. The topology of the SKiiP 942GB120-317CTV VSI is made up of two IGBT's (Insulated Gate Bipolar Transistors) and two power diodes shown in **Figure 13**.

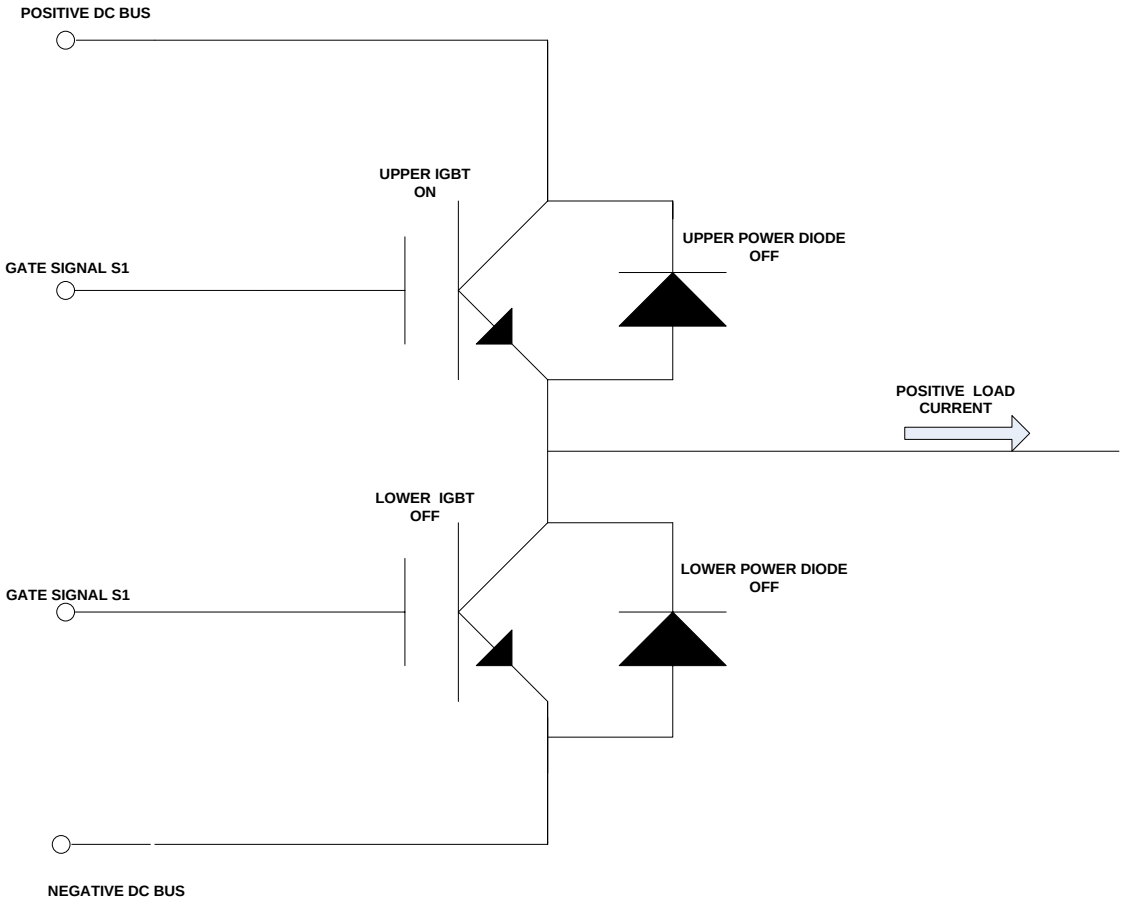

Figure 13. SKiiP 942GB120-317CTV Module Topology showing user defined positive current direction [From Ref 6]

In the electrical model, the gating signal S1 has a magnitude of either one or zero. The magnitude of one indicates that the upper IGBT is on (i.e. conducting). Therefore the user defined polarity of the current across the inductor would be positive. These were the two conditions used to determine the amount of time the upper IGBT was

on. This time was used to calculate the amount of conduction energy losses of the upper IGBT. The Simulink model describing this condition is shown in **Figure 14.**

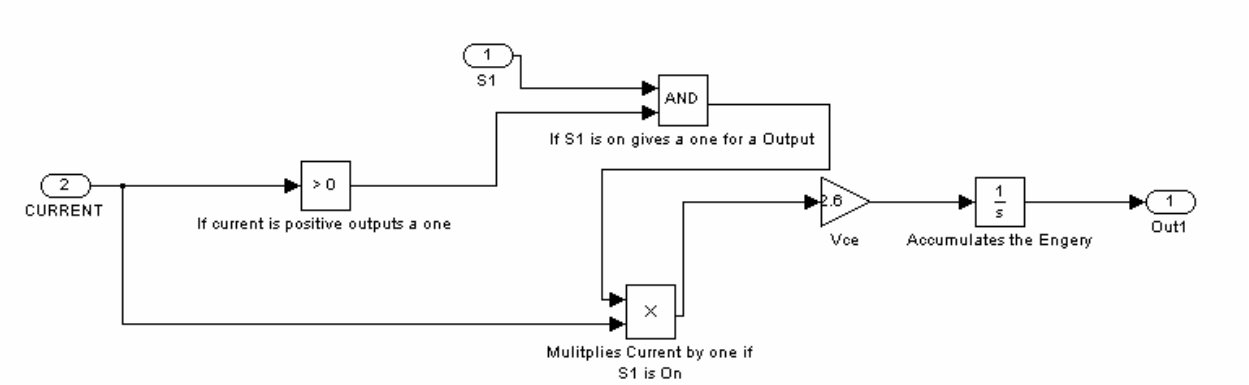

Figure 14. Simulink Model of Upper IGBT Conduction Losses

In order to calculate the amount of conduction power losses for the upper IGBT the magnitude of the current was then multiplied by the $V_{CE\ of}$ the IGBT and accumulated with an integrator. This number represents the amount of energy losses of the upper IGBT. In order to extract the power losses of the upper IGBT vice energy losses, the energy was divided by the period of the simulation to get an energy per unit time (Avg. Power). The mathematical equation is shown in **Equation 5**.

$$P_{\text{Upper IGBT}} = \frac{1}{T} \cdot \sum_{i=1}^{n} \left[\int_{t_0}^{t_1} v_{CE}(t) \cdot i(t)\, dt \right] \qquad (5)$$

Equation 5. Conduction Power Losses of the Upper IGBT [**8]**

In **Equation 5,** t_o represents the time when the upper IGBT turns on and t_1 represents the time when the upper IGBT turns off. The summation from I to n sums up each discrete conduction loss period for the entire simulation. Lastly, in order to extract

the amount of power losses from the upper IGBT vice energy losses the energy losses are divided by the simulation time to give a energy per unit time (Avg. Power).

The conduction losses of the lower power diode were calculated next. The conditions in the electrical model that indicate the lower power diode is conducting is when the gating signal S1 was off and the polarity of the current was positive. This condition can be seen in **Figure 15**.

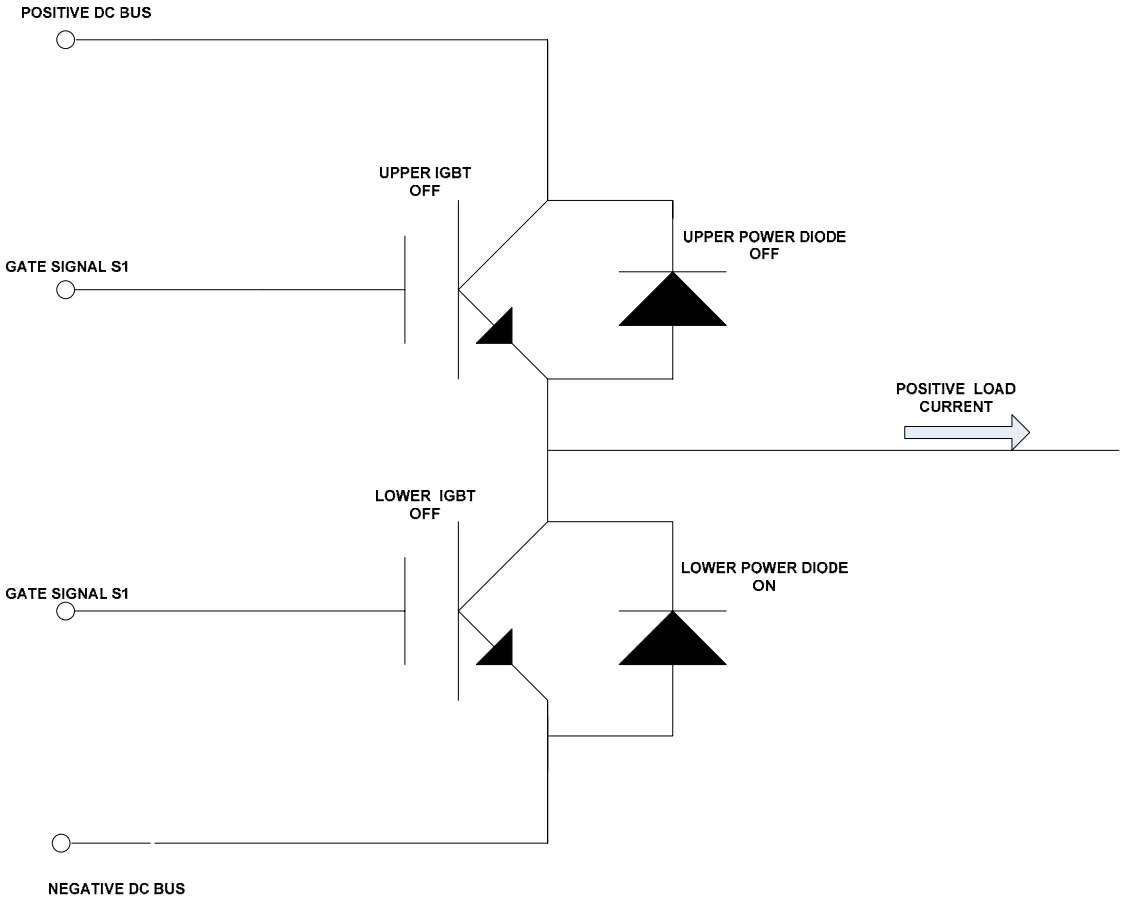

Figure 15. SKiiP Module Topology showing Lower Power Diode Conduction conditions [From 6]

The two conditions that were used to determine whether or not the lower power diode was conducting in the Simulink model were if the polarity of the current was positive and the upper IGBT was off. The Simulink model describing this condition is shown in **Figure 16**.

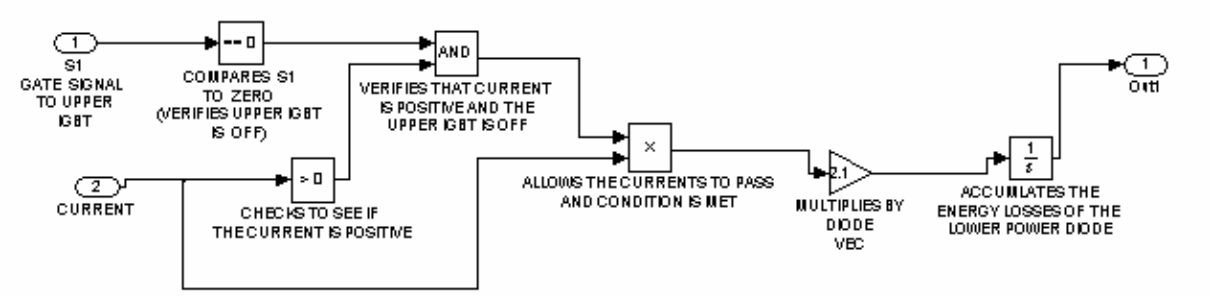

Figure 16. Simulink Model of Lower Power Diode Conduction Losses

In order to calculate the amount of conduction power losses for the lower power diode the magnitude of the current was then multiplied by the V_{EC} of the lower power diode and accumulated with an integrator. This number represents the amount of energy. In order to extract the power losses vice energy losses, the energy was divided by the period of the simulation to get an energy per unit time (Power). The mathematical equation is shown below in **Equation 6**.

$$P_{\text{Lower Power DIODE}} = \frac{1}{T} \cdot \sum_{i=1}^{n} \left[\int_{t_0}^{t_1} v_{EC}(t) \cdot i(t)\, dt \right] \tag{6}$$

Equation 6. Conduction Power Losses Calculation for Lower Power Diode [8]

In **Equation 6**, $\mathbf{t_o}$ represents the time when the lower power diode turns on and $\mathbf{t_1}$ represents the time when the lower power diode turns off. The summation from I to n sums up each discrete lower power diode conduction loss period for the entire simulation. Lastly, in order to extract the amount of conduction power losses from the lower power diode vice energy losses the energy losses are divided by the simulation time to give a energy per unit time (Avg. Power).

The conduction losses of the lower IGBT were calculated next. The conditions of the Semikron VSI electrical model built in Simulink that indicate a lower

IGBT is conducting is when the gating signal S1 was 0 indicating the bottom IGBT was on and the polarity of the current was negative. This condition can be seen in **Figure 17.**

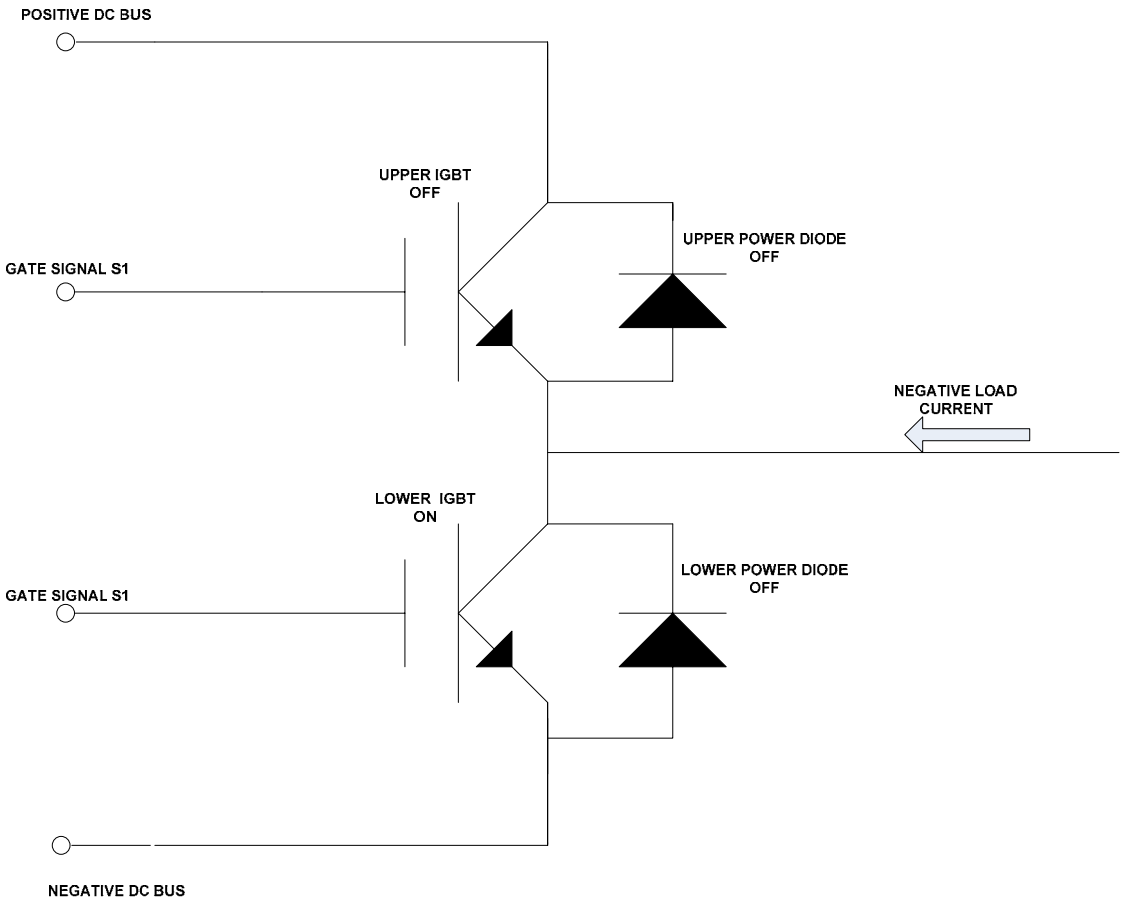

Figure 17. Electrical Model of SKiiP Module Topology showing user defined negative current direction [From 6].

In the electrical model the gating signal S1 has a magnitude of either 1 or 0. The magnitude of 0 indicates that the lower IGBT is on (i.e. conducting). Therefore the polarity of the current across the inductor would be negative. These were the two conditions used to determine the amount of time the lower IGBT was on. The Simulink model describing this condition is shown in **Figure 18.**

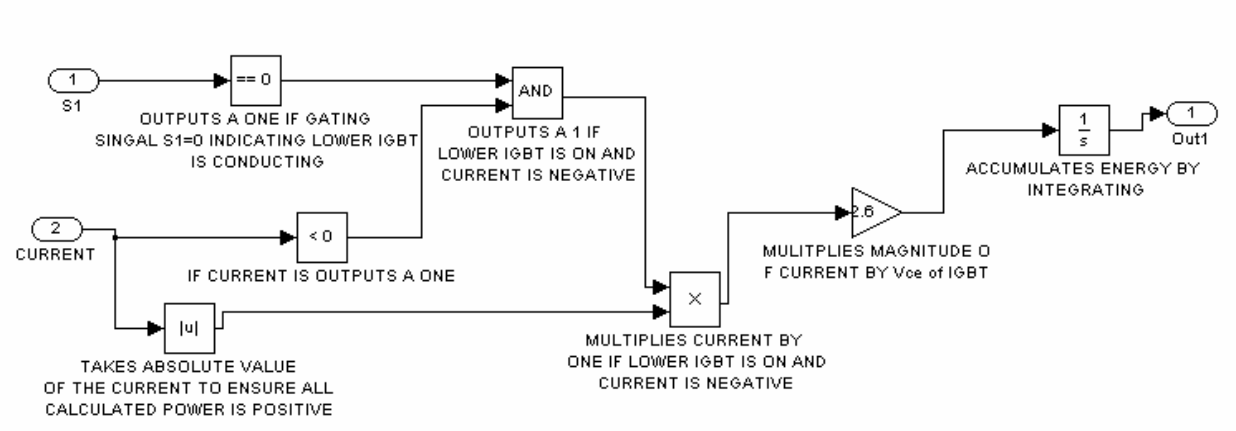

Figure 18. Simulink Model of Lower IGBT Conduction Losses

In order to calculate the amount of conduction power losses for the lower IGBT the magnitude of the current was then multiplied by the $V_{CE\ of}$ the IGBT and accumulated with an integrator. This number represents the amount of conduction energy losses of the lower IGBT. In order to extract the conduction power losses of the lower IGBT vice energy losses, the energy was divided by the period of the simulation to get an energy per unit time (Avg. Power). The mathematical equation is shown in **Equation 7**.

$$P_{\text{Lower IGBT}} = \frac{1}{T} \cdot \sum_{i=1}^{n} \left[\int_{t_0}^{t_1} v_{CE}(t) \cdot i(t)\, dt \right] \tag{7}$$

Equation 7. Conduction Power Losses for the Lower IGBT [8]

In **Equation 7**, t_o represents the time when the lower IGBT turns on and t_1 represents the time when the lower IGBT turns off. The summation from I to n sums up each discrete conduction energy loss period for the entire simulation. Lastly in order to extract the amount of power losses from the lower IGBT vice energy losses the energy losses are divided by one over the simulation time to give a energy per unit time (Avg. Power).

The conduction losses of the upper power diode were calculated next. The conditions of the Semikron VSI electrical model built in Simulink that indicate the upper power diode is conducting is when the gating signal S1 was off and the polarity of the current was negative. This condition can be seen in **Figure 19**.

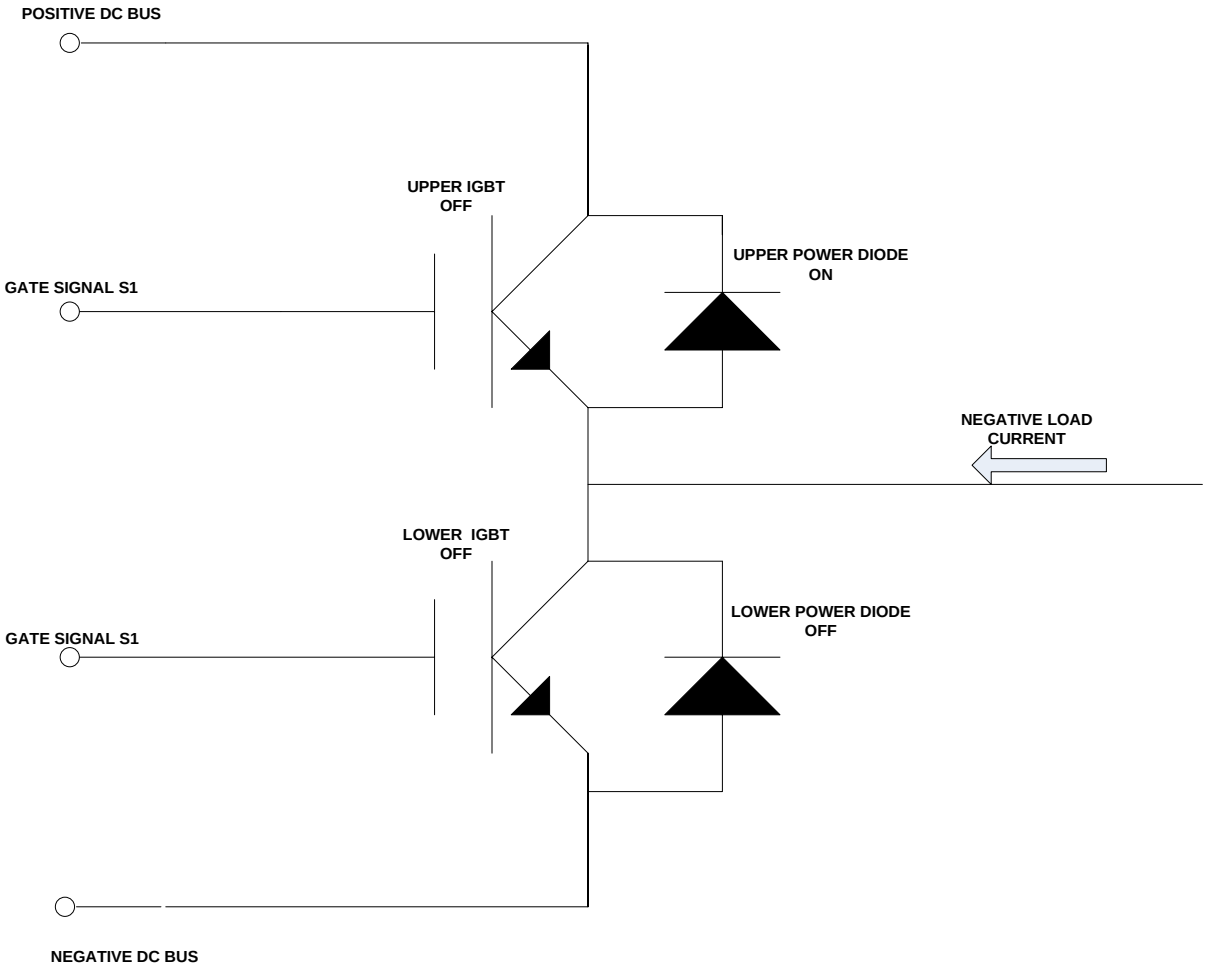

Figure 19. SKiiP Module Topology showing Upper Power Diode Conduction conditions [From 6]

The two conditions that were used to determine whether or not the upper power diode was conducting in the Simulink model were if the polarity of the current was negative and the lower IGBT was off. The Simulink model describing this condition is shown in **Figure 20**.

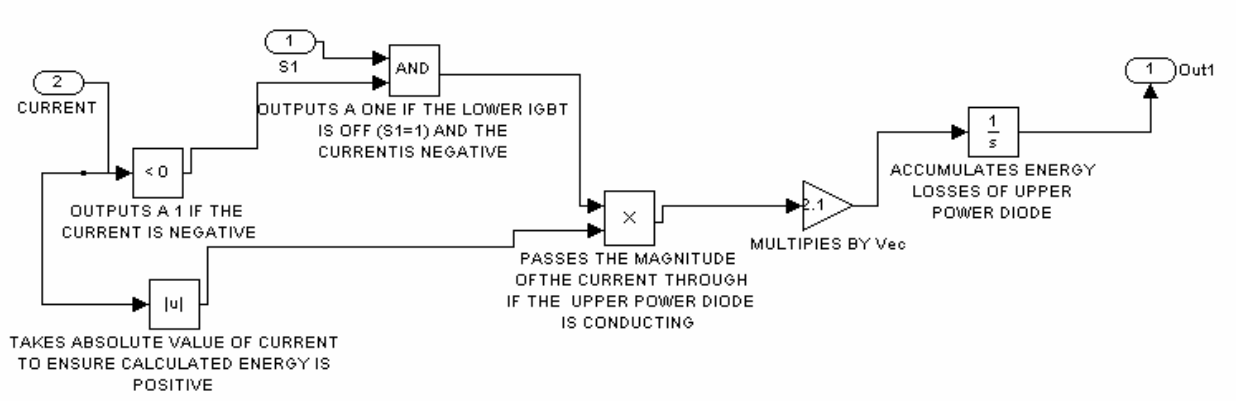

Figure 20. Simulink Model of Upper Power Diode Conduction Losses

In order to calculate the amount of conduction power losses for the upper power diode the magnitude of the current was then multiplied by the V_{EC} of the upper power diode and accumulated with an integrator. This number represents the upper power diode energy losses. In order to extract the power losses vice energy losses, the energy losses were divided by the period of the simulation to get an energy per unit time (Avg. Power). The mathematical equation is shown in **Equation 8**.

$$P_{\text{UPPER POWER DIODE}} = \frac{1}{T} \cdot \sum_{i=1}^{n} \left[\int_{t_0}^{t_1} v_{EC}(t) \cdot i(t)\, dt \right] \tag{8}$$

Equation 8: Conduction Power Losses Calculation for the Upper Power Diode [8]

In **Equation 8**, t_o represents the time when the upper power diode turns on and t_1 represents the time when the upper power diode turns off. The summation from I to n sums up each discrete upper power diode conduction energy loss period for the entire simulation. Lastly, in order to extract the amount of power losses from the upper power diode vice energy losses the energy losses are divided by the simulation time to give a energy per unit time (Avg. Power).

b. Blocking Losses

The blocking losses for this thesis will be neglected. The hypothesis is that the amount of forward blocking losses will be orders of magnitude smaller than the conduction losses, turn on/off losses, and reverse recovery losses. This hypothesis is based on the given vendor data sheets and application notes supplied from Semikron for the VSI modeled for this thesis.

2. Non-Static Power Losses

The non-static power losses are made up of the switching power losses and the driver power losses for the IGBT's. The switching power losses are made up of the turn on/ off losses of the upper and lower IGBT and the reverse recovery losses as the diode junctions transition from a reverse biased state to a forward biased state.

a. Turn on/off Losses for the Upper IGBT

The turn on/off losses for upper IGBT were calculated using the given data sheet from Semikron for the SKiiP 942GB120-317CTV (**Appendix A**). In order to calculate the amount of turn on/off cycles of the upper IGBT a rise detector was created in Simulink for the gating signal S1. Since the Semikron gave a value for the amount of energy per turn on/off cycle it was only necessary to count the entire event. Therefore the number of turn on events equaled the number of turn off events which was equal to the number of rise detects. The way to determine whether or not it was the upper IGBT turning on or off was to verify that the rise event happened while the current was positive. Therefore the two conditions required to count the number of turn on/off events for the upper IGBT was to count the number of rise events with the current being positive assuming that for every turn on event there was a turn off event. The value of the turn on/off losses was given by the vendor in the data sheet (see **Appendix A**) was related to a maximum current and voltage. In order to scale the turn on/off losses for the actual used voltage and current two gains were used.

The first gain block takes the absolute value of the current and multiplies it by the turn on/off losses and then divides it by the maximum value of current referenced in the vendor data sheet (See **Appendix A**). The second gain block takes the

current scaled turn on/off losses out of gain block one and multiplies it by the V_{dc} and then divides it by the maximum value of voltage referenced in the vendor data sheet (See **Appendix A**). The Simulink model coded for this event is shown in **Figure 21**. The Simulink model detects switching events of the upper IGBT and adds a current and voltage scaled turn on/off energy losses which is accumulated for the entire simulation period. The mathematical equation describing the calculation of the upper IGBT turn on/off Power losses is shown in **Equation 9**.

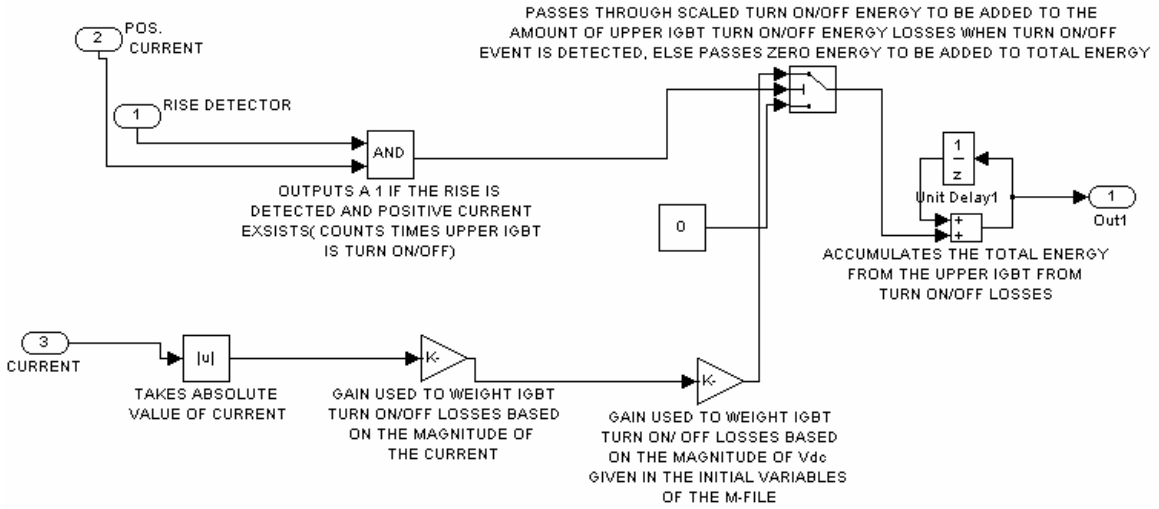

Figure 21. Simulink Model of Upper IGBT Turn On/Off Power Losses

$$\mathrm{P}_{\substack{\text{UPPER IGBT}\\ \text{TURN ON/OFF}\\ \text{POWER LOSSES}}} = \frac{1}{T}\cdot\sum_{i=1}^{n}\left[i * \frac{\left(225*10^{-3}\right)}{750} * \frac{\left(V_{dc}\right)}{600} \right] \tag{9}$$

Equation 9: Turn On/Off Power Losses Calculation for Upper IGBT Diode [8]

b. Turn on/off Losses for the Lower IGBT

The turn on/off losses for lower IGBT were calculated using the given data sheet from Semikron for the SKiiP 942GB120-317CTV (**Appendix A**). In order to calculate the amount of turn on/off cycles of the lower IGBT a rise detector was created in Simulink for the gating signal S1. Since the Semikron gave a value for the amount of

energy per turn on/off cycle it was only necessary to count the entire event. Therefore the number of turn on events equaled the number of turn off events which was equal to the number of rise detects. The way to determine whether or not it was the lower IGBT turning on or off was to verify that the rise event happened while the current was negative. Therefore the two conditions required to count the number of turn on/off events for the lower IGBT was to count the number of rise events with the current being negative assuming that for every turn on event there was a turn off event. The value of the turn on/off losses was given by the vendor in the data sheet (see **Appendix A**) was related to a maximum current and voltage. In order to scale the turn on/off losses for the actual used voltage and current two gains were used. The first gain block takes the absolute value of the current and multiplies it by the turn on/off losses and then divides it by the maximum value of current referenced in the vendor data sheet (See **Appendix A**). The second gain block takes the current scaled turn on/off losses out of gain block one and multiplies it by the V_{dc} and then divides it by the maximum value of voltage referenced in the vendor data sheet (See **Appendix A**).

The Simulink model coded for this event is shown in **Figure 22**. The Simulink model detects switching events of the lower IGBT and adds a current and voltage scaled turn on/off energy losses which is accumulated for the entire simulation period. The mathematical equation describing the calculation of the lower IGBT turn on/off Power losses is shown in **Equation 10**.

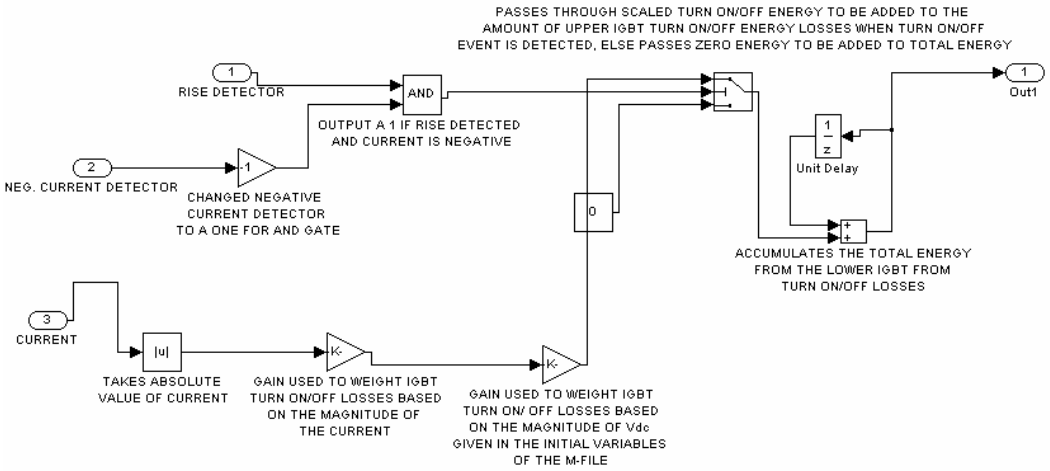

Figure 22. Simulink Model of Lower IGBT Turn On/Off Power Losses

$$P_{\substack{\text{LOWER IGBT}\\ \text{TURN ON/OFF}\\ \text{POWER LOSSES}}} = \frac{1}{T}\cdot\sum_{i=1}^{n}\left[i*\frac{\left(225*10^{-3}\right)}{750}*\frac{\left(V_{dc}\right)}{600}\right] \quad (10)$$

Equation 10. Turn On/Off Power Losses Calculation for Upper IGBT Diode [8]

c. Reverse Recovery Losses for the Lower Power Diode

The reverse recovery losses for the lower power diode were computed similar to that of the turn on/off losses for lower IGBT. The reverse recovery losses for the lower power diode were calculated using the given data sheet from Semikron for the SKiiP 942GB120-317CTV (**Appendix A**). Since the vendor gave a value for the amount of energy per reverse recovery cycle it was only necessary to count the entire event. In order to calculate the amount of reverse recovery losses of the lower power diode a rise detector was created in Simulink for the gating signal S1. Therefore the reverse recovery events equaled the number of reverse recovery events which was equal to the number of rise detects. The way to determine whether or not it was the lower power diode was having a reverse recovery event was to verify that the rise event happened while the current was positive. Therefore the two conditions required to count the reverse recovery events of the lower power diode was to count the number of rise events with the current being positive assuming that for every forward biased condition of the power diode there was a reverse biased condition. The value of the reverse recovery losses was given by the vendor in the data sheet (see **Appendix A**) was related to a maximum current and voltage. In order to scale the reverse recovery losses for the actual used voltage and current two gains blocks were used. The first gain block takes the absolute value of the current and multiplies it by the reverse recovery losses and then divides it by the maximum value of current referenced in the vendor data sheet (See **Appendix A**). The second gain block takes the current scaled reverse recovery losses out of gain block one and multiplies it by the V_{dc} and then divides it by the maximum value of voltage referenced in the vendor data sheet (See **Appendix A**).

The Simulink model coded for this event is shown in **Figure 23**. The Simulink model detects reverse recovery events of the lower power diode and accumulates a current and voltage scaled reverse recovery energy losses for the entire simulation period. The mathematical equation describing the calculation of the lower power diode reverse recovery Power losses is shown in **Equation 11**.

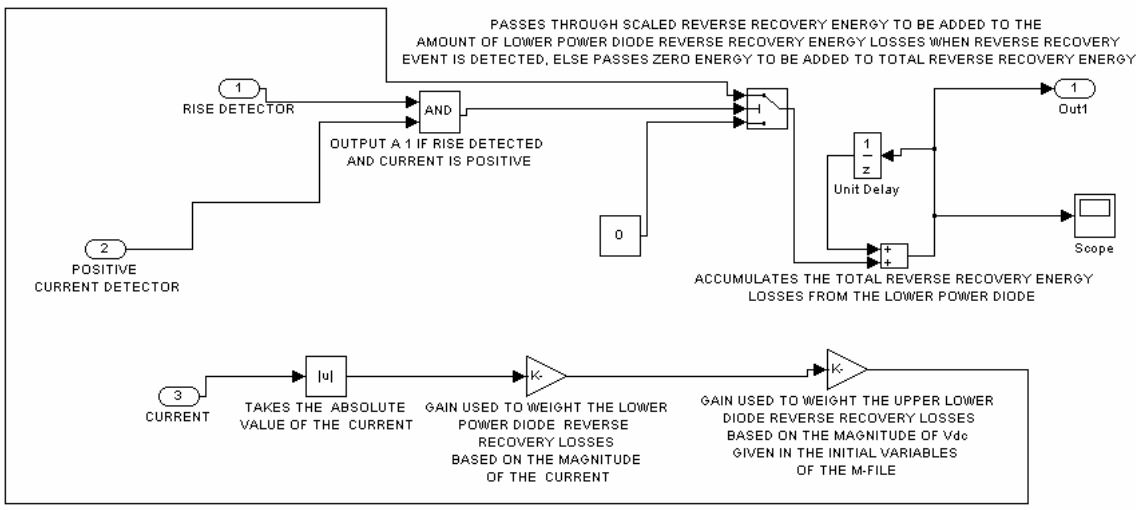

Figure 23. Simulink Model of Lower Power Diode Reverse Recovery Power Losses

$$P_{\substack{\text{LOWER POWER}\\ \text{DIODE REVERSE}\\ \text{RECOVERY POWER}\\ \text{LOSSES}}} = \frac{1}{T}\cdot\sum_{i=1}^{n}\left[i * \frac{\left(30*10^{-3}\right)}{750} * \frac{\left(V_{dc}\right)}{600} \right] \tag{11}$$

Equation 11. Reverse Recovery Power Losses Calculation for Lower Power Diode [8]

d. Reverse Recovery Losses for the Upper Power Diode

The reverse recovery losses for the upper power diode were computed similar to that of the turn on/off losses for upper IGBT. The reverse recovery losses for the upper power diode were calculated using the given data sheet from Semikron for the SKiiP 942GB120-317CTV (**Appendix A**). Since the vendor gave a value for the amount

of energy per reverse recovery cycle it was only necessary to count the entire event. In order to calculate the amount of reverse recovery losses of the upper power diode a rise detector was created in Simulink for the gating signal S1. Therefore the reverse recovery events equaled the number of reverse recovery events which was equal to the number of rise detects. The way to determine whether or not it was the upper power diode was having a reverse recovery event was to verify that the rise event happened while the current was negative. Therefore the two conditions required to count the reverse recovery events of the upper power diode was to count the number of rise events with the current being negative assuming that for every forward biased condition of the power diode there was a reverse biased condition. The value of the reverse recovery losses was given by the vendor in the data sheet (see **Appendix A**) was related to a maximum current and voltage. In order to scale the reverse recovery losses for the actual used voltage and current two gains blocks were used. The first gain block takes the absolute value of the current and multiplies it by the reverse recovery losses and then divides it by the maximum value of current referenced in the vendor data sheet (See **Appendix A**). The second gain block takes the current scaled reverse recovery losses out of gain block one and multiplies it by the V_{dc} and then divides it by the maximum value of voltage referenced in the vendor data sheet (See **Appendix A**).

The Simulink model coded for this event is shown in **Figure 24**. The Simulink model detects reverse recovery events of the upper power diode and accumulates a current and voltage scaled reverse recovery energy losses for the entire simulation period. The mathematical equation describing the calculation of the upper power diode reverse recovery Power losses is shown in **Equation 12**.

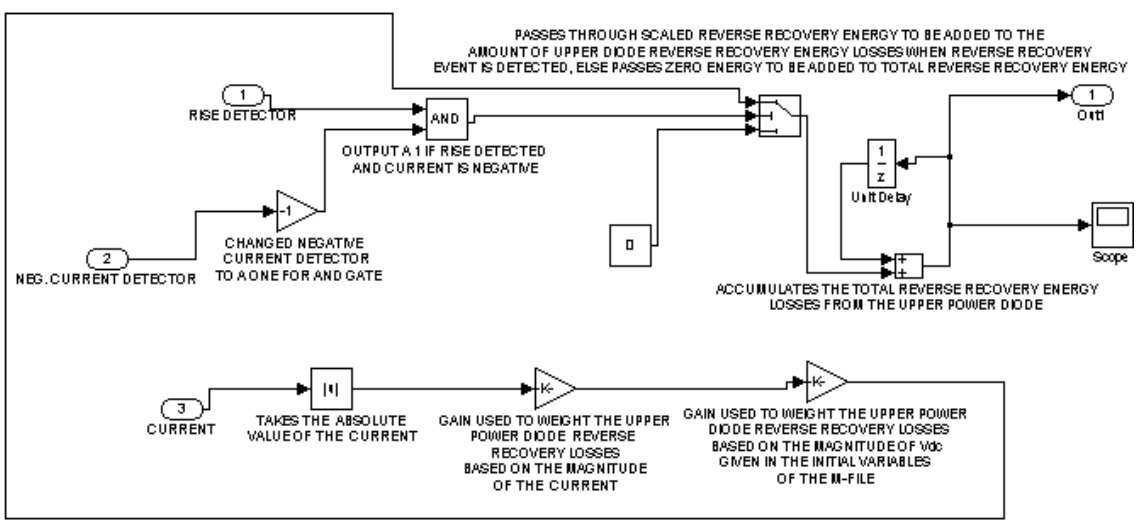

Figure 24. Simulink Model of Upper Power Diode Reverse Recovery Power Losses

$$P_{\substack{\text{UPPER POWER}\\ \text{DIODE REVERSE}\\ \text{RECOVERY POWER}\\ \text{LOSSES}}} = \frac{1}{T}\cdot\sum_{i=1}^{n}\left[i * \frac{\left(30*10^{-3}\right)}{750} * \frac{\left(V_{dc}\right)}{600} \right] \qquad (12)$$

Equation 12. Reverse Recovery Power Losses Calculation for Lower Power Diode [8]

e. Driving Power Losses

The driving losses for this thesis will be neglected. The hypothesis is that the amount of driver losses will be orders of magnitude smaller than the conduction losses, turn on/off losses, and reverse recovery losses. This hypothesis is based on the given data sheets and application notes supplied from Semikron for the 3 phase VSI modeled for this thesis.

D. CREATING A THREE PHASE VSI POWER LOSSES MODEL

The entire description so far only described the modeling of power losses of one Semikron SKiiP 942GB120-317CTV inverter pole separately. The model of all the power losses of one inverter pole is shown in **Figure 25**. The outputs of each individual type of power losses were summed together and all power losses of one IGBT and its corresponding diode were outputted to the workspace in Matlab for input to the thermal

model. The thermal model only requires the power losses one IGBT and its corresponding power diode. The rest of the power losses model was built to resemble the experimental equipment in the lab. The system in the lab consisted of three Semikron SKiiP 942GB120-317CTV connected as a three phase VSI DC-AC. The other two phases were modeled identically to the phase that has been described. The output of all energy from the three phases of voltage source inverter were then summed together and divided by the simulation time in order to produce the total power losses and is shown in the Simulink model(**Figure 26)**.

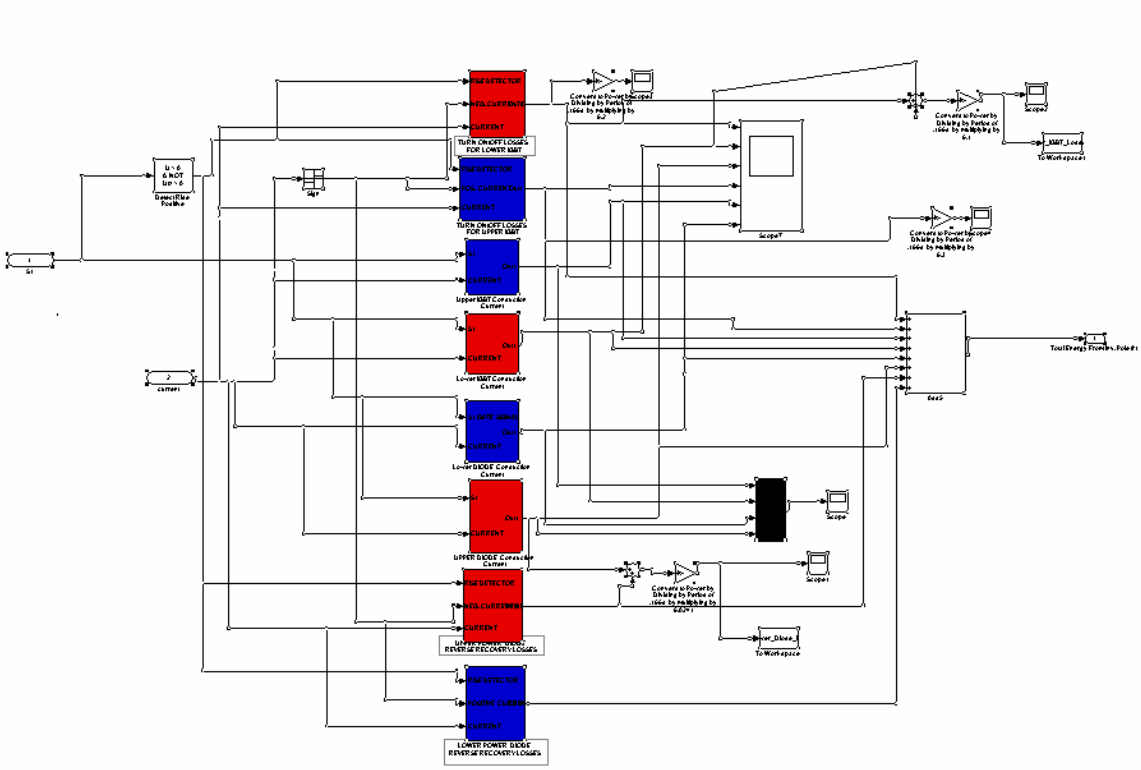

Figure 25. Simulink Model of Summation of Power Losses for one SKiiP 942GB120-317CTV VSI

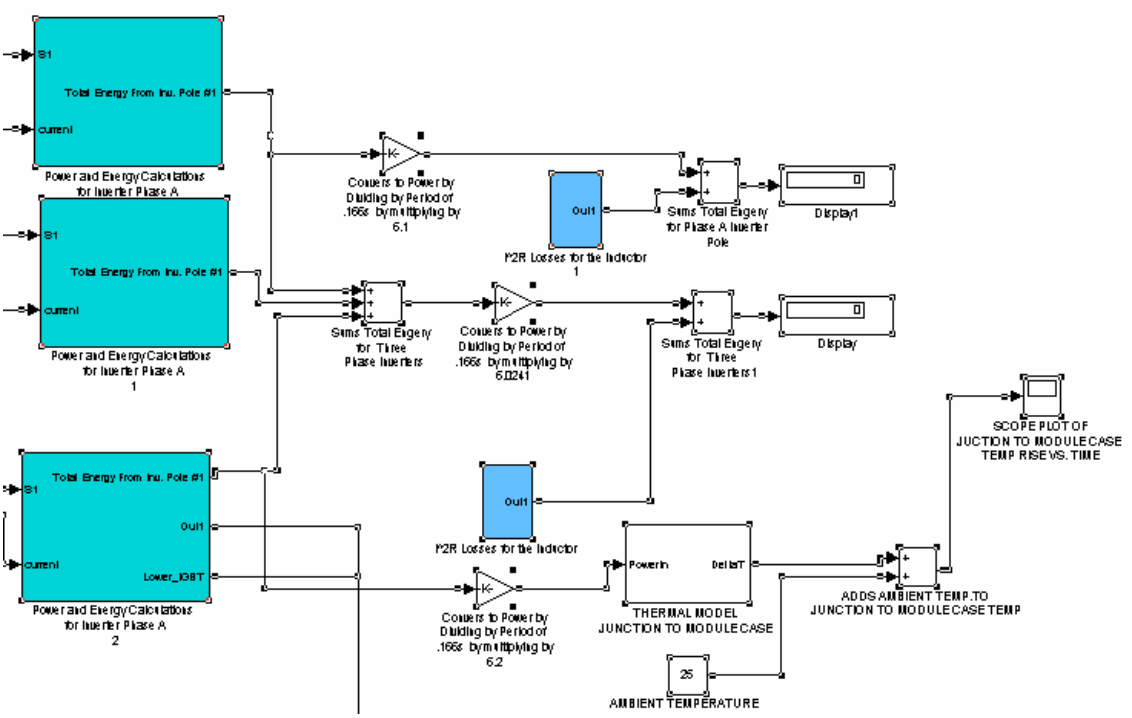

Figure 26. Simulink Model of Summation of Power Losses for Three SKiiP 942GB120-317CTV VSI

E. SUMMARY

The power losses model created in this chapter represents the model that the vendor states approximates the power losses response of the system. The solution to the power losses model has many assumptions worth mentioning. It ignores the blocking losses and the driver power losses. In the application notes the vendor indicates that these losses are insignificant compared to the conduction, turn on/off, and reverse recovery power losses. The relevancy and accuracy of these assumptions will be further discussed in the simulations and conclusions chapters. In order to simulate the junction temperature of the IGBT and power diode a simulation of the power losses must be performed. Then the data from the power losses model may be applied to the thermal model. The simulation of the power losses and thermal models are described in the next chapter.

THIS PAGE INTENTIONALLY LEFT BLANK

IV. INITIAL SIMULATIONS

A. INTRODUCTION

In this chapter, a power losses simulation was conducted on the model created in the previous chapter to produce power losses of a three phase DC-AC VSI based on three Semikron SKiiP 942GB120-317CTV modules. The simulation was calibrated to a pre-chosen experimental condition on which the actual lab equipment was set to and tested at. The power losses simulation data will then be collected and used as the input to the thermal model. In the next chapter a lab experiment will be setup and ran in order to collect experimental data to compare against the simulated data in order to validate the simulated models.

B. POWER LOSSES SIMULATION

In order to run the power losses model simulation in Simulink, some initial conditions for the electrical model needed to be defined. First, the input dc bus voltage (V_{dc}) voltage was chosen such that it could be easily reproduced in the lab. The value of 100 V_{dc} was chosen because it could be easily made with an input of 230 VAC into a VARIAC and then the output adjusted and rectified to 100V_{dc}. Next, the output current level need to be selected that was within the wiring capability of the wire stock and current measuring devices found in the power lab. The current level selected was 100 Amps since it both measured and the 4 AWG wire could handle 100Amps. The load was chosen to be a purely inductive load. The inductance was chosen to be the available 0.30mH 3 phase inductors available in the lab. Although the load was purely inductive it had some small value of AC resistance. The inductor losses were selected based on the measured resistance of the inductor to be used in the lab experiment and was .02 ohms per phase. The inductor power losses were computed using **Equations 13 & 14.** The initial variables were then inputted into a Simulink M-File. (**Appendix B)**

$$L_{\phi}\ I\hat{}2R\ \text{Losses} = (100A)\hat{}2 \cdot (.02\ \Omega) = 20\ W \qquad (13)$$

Equation 13. Power Losses Calculation Single Phase Inductor

$$L_{3\phi} I^{\wedge 2} R \text{ Losses} = 3 \cdot (20\text{W}) = 60 \text{ W} \qquad (14)$$

Equation 14. Power Losses Calculation for Three Phase Inductor

The next step was to run the simulation with the lab calibrated input values. The output of the simulation is seen in **Figure 27**. The results of the simulation were that for the Semikron three phase VSI using PWM at a switching frequency of 5 kHz with an input voltage of $100V_{dc}$ and a output current of 100A and output voltage of 100 VAC at 60Hz, the total power losses were **635.7 Watts** as seen in **Figure 27**. The Outputs of the IGBT and its corresponding diode extracted out of there respective subsystems as shown in **Figure 28&29**. In the next section, the power losses of one IGBT and its corresponding diode are placed in the thermal model created in Chapter II.

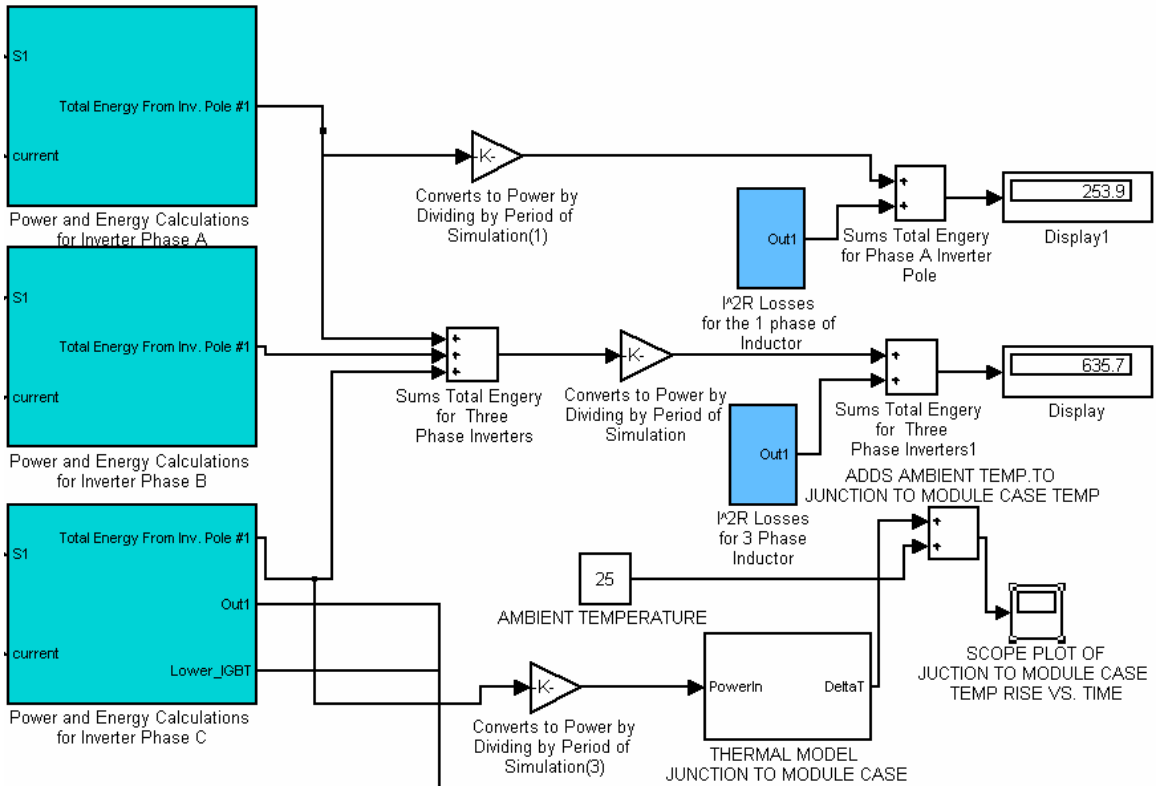

Figure 27. Simulink Simulation of Power Losses for Semikron Three Phase VSI

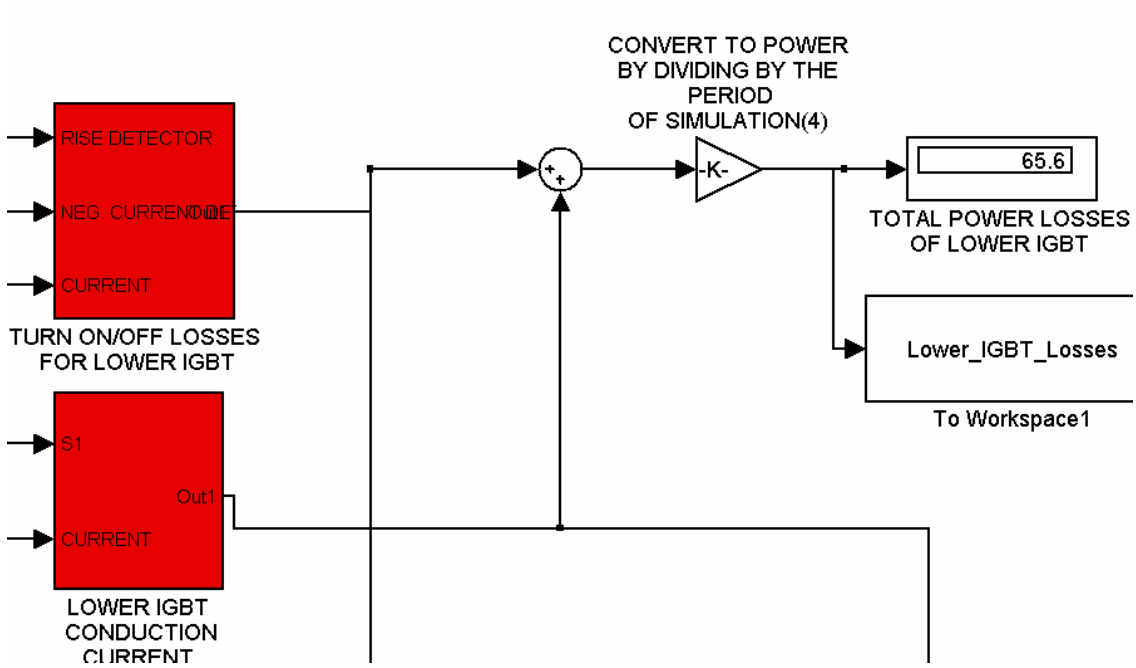

Figure 28. Simulink Simulation Showing 65.6 Watts of Power Losses for Lower IGBT

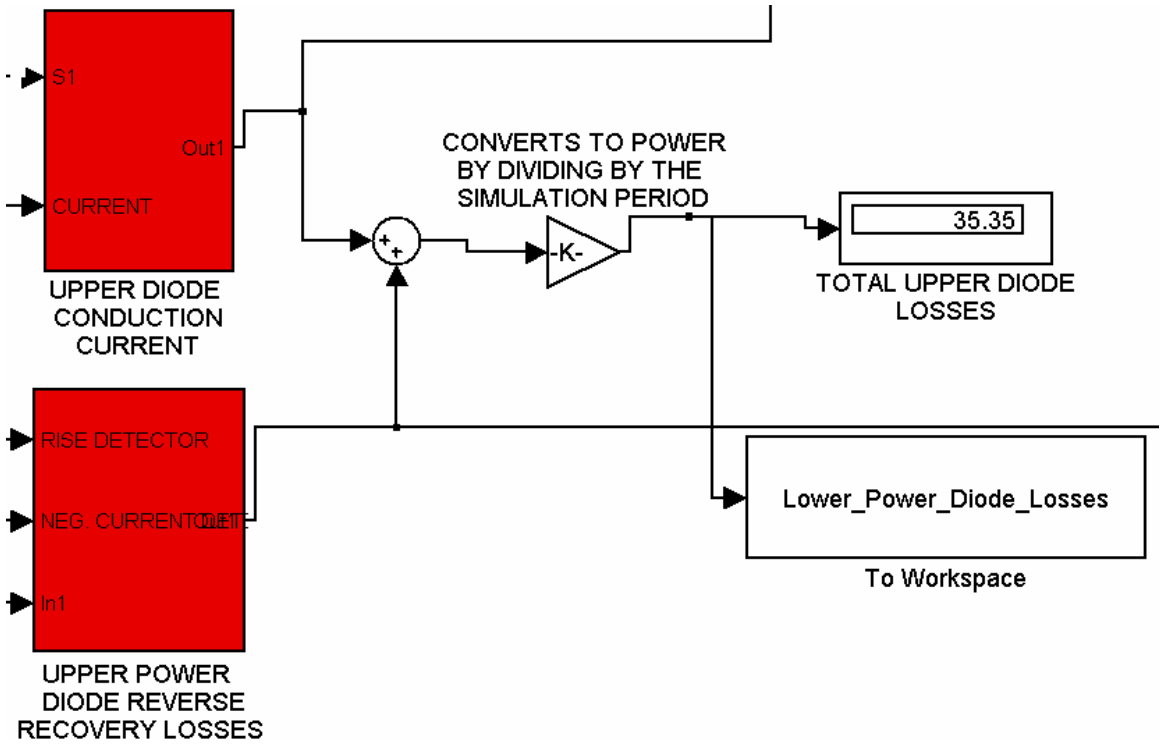

Figure 29. Simulink Simulation of 35.5 Watts of Power Losses for Upper Power Diode

C. THERMAL MODEL SIMULATION

In order to run the thermal model simulation in Simulink, some initial conditions for the thermal model from the Semikron data sheets (**Appendix A**) needed to be defined and are shown in **Table 1**. Also since the heatsink used was the water cooled heatsink (NWK 40) the thermal resistance of the heatsink was calculated by assuming a given flow rate of 5.3l/min and a R_{th} of 0.018 °C/W (**Figure 30**). This rate was chosen after determining that the available equipment in the lab could support this flow rate for the experimental data collection. After the thermal model was calibrated, the average power of the IGBT and diode collected in the previous section were placed into the thermal model by exporting them to Matlab workspace as variables to be used by the thermal model.

%Thermal Model Initial Variables
%IGBT junction to Case Variables
Rthi1=3
Rthi2=2
Rthi3=4
Rthi4=0
tau_i1=1
tau_i2=0.13
tau_i3=0.001
tau_i4=0
% Diode junction to Case Variables
Rthd1=9
Rthd2=64
Rthd3=10
Rthd4=0
tau_d1=1
tau_d2=0.13
tau_d4=0
%Heatsink to Ambient Variables
Rthhx1=0.018
tau_hx1=100
%Ambient Temperature
ambient_temp=25.5

Table 1. List of initial Variables for Thermal Model.

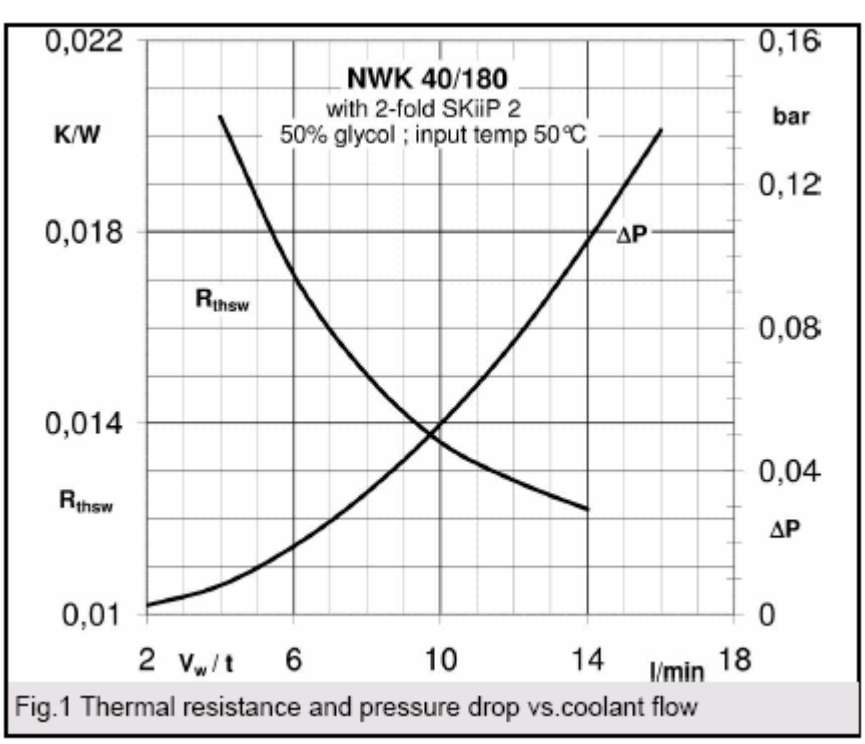

Figure 30. Thermal Resistance of NWK 40 Water Cooled Heatsink. [From 6]

The next step was to run the thermal simulation with those input values. The output of the simulation is seen in **Figure 31, 32 & 33**. The results of the simulation were that for the Semikron three phase VSI using PWM at a switching frequency of 5 kHz with an input voltage of 100Vdc and a output current of 100A and output voltage of 100 VAC at 60Hz. A summary of the results of the thermal simulation are shown in **Table 2**. In the next section, a brief summary of the initial power losses and thermal model simulations will be discussed.

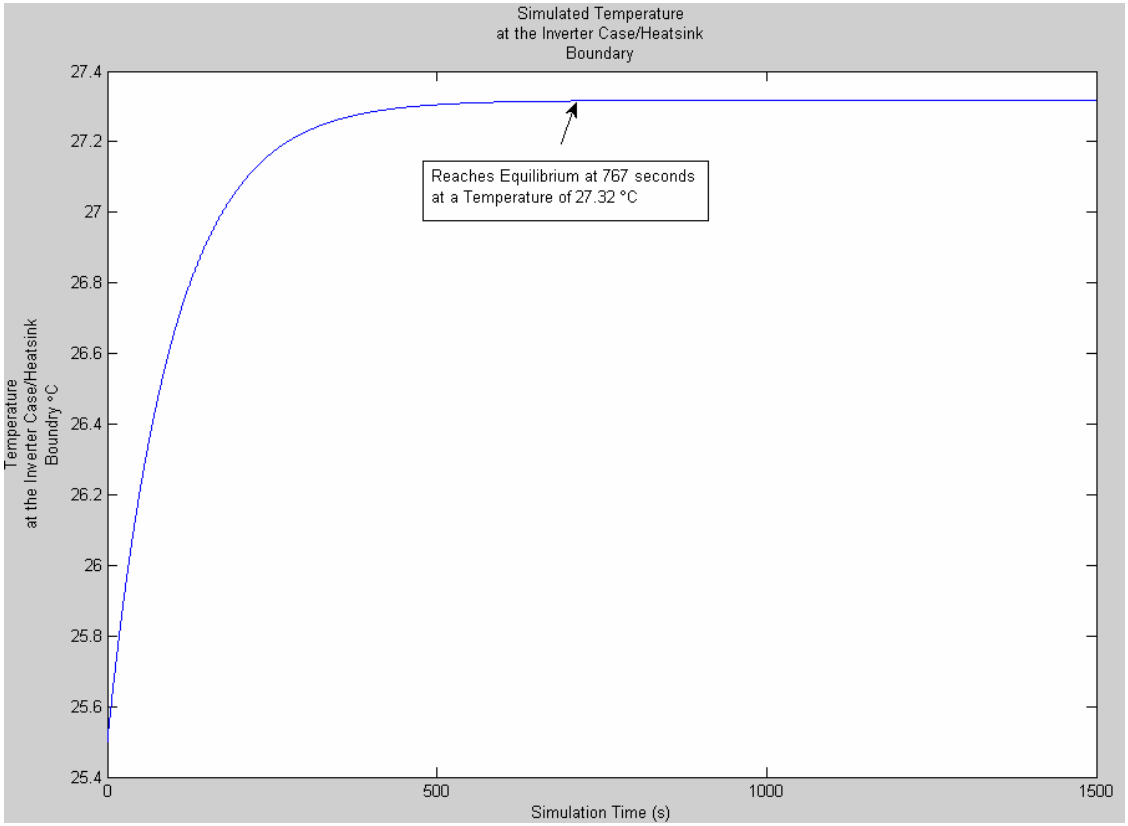

Figure 31. Simulink Simulated Temperature at Inverter Case/Heatsink Boundary from Thermal Model Using Power Losses Generated from Power Losses Simulation

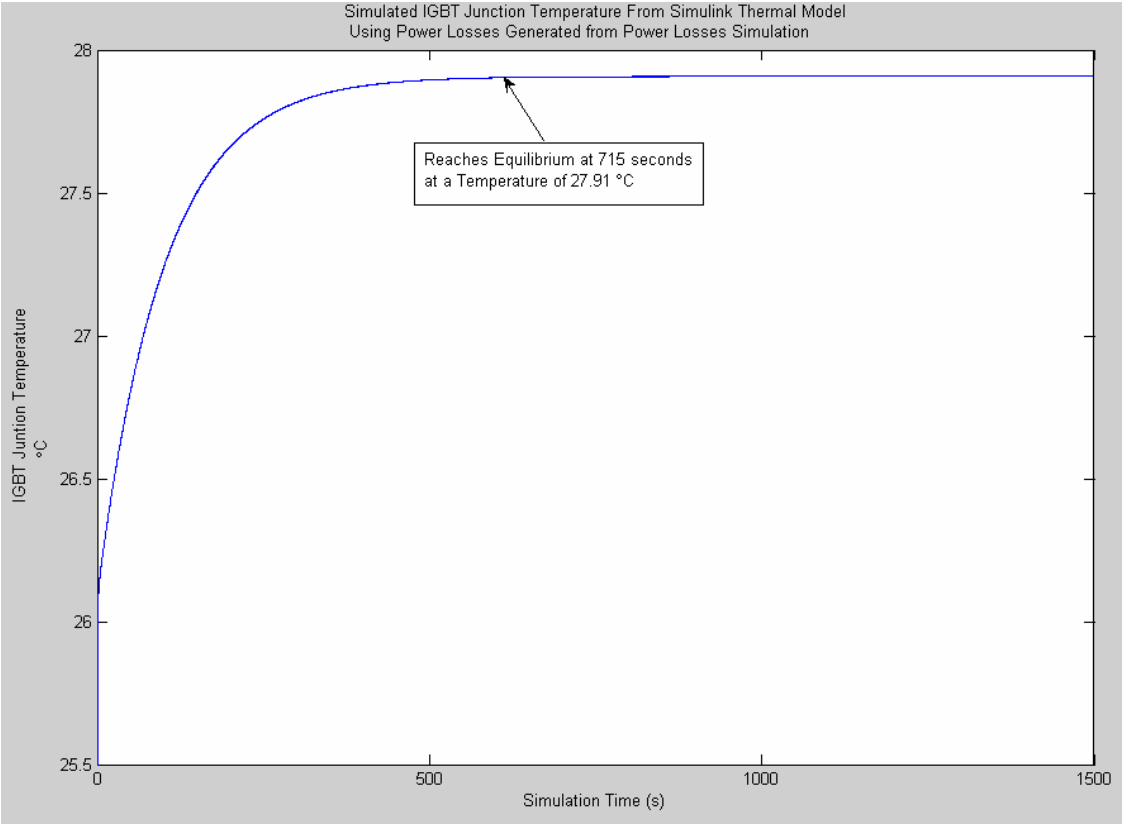

Figure 32. Simulink Simulated IGBT Junction Temperature from Thermal Model Using Power Losses Generated from Power Losses Simulation

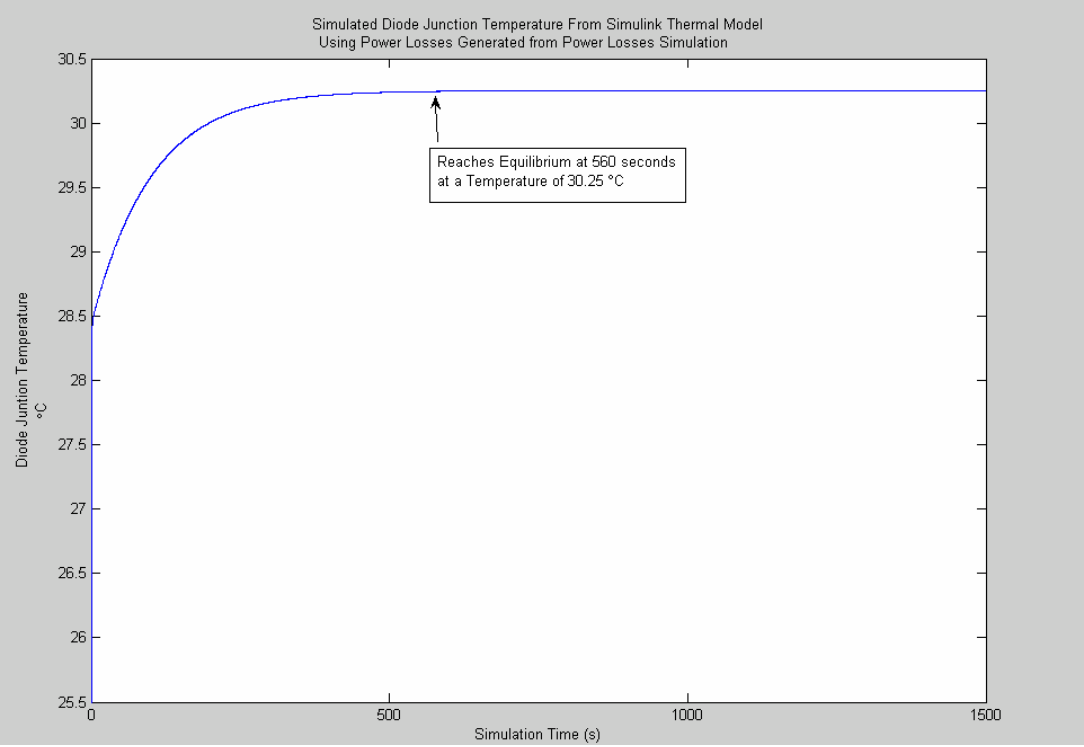

Figure 33. Simulink Simulated Diode Junction Temperature from Thermal Model Using Power Losses Generated from Power Losses Simulation

	Simulated IGBT Junction Temperature	Simulated Diode Junction Temperature	Simulated Temperature at Inverter Case/Heatsink Boundary
Final Simulation Temperature	27.91°C	30.25 °C	27.32 °C
Time till Equilibrium (seconds)	715	560	767

Table 2. Summary of Simulated Temperatures of a Semikron Skip Semikron three phase VSI using PWM at a switching frequency of 5 kHz with an input voltage of 100Vdc, output current of 100A, and an output voltage of 100 VAC at 60Hz with an ambient temperature of 25.5°C.

D. SUMMARY

The results of the initial simulation show an exponential build up function with a rising temperature that reaches equilibrium at around 700 seconds which was the expected response. The unexpected result obtained was that the diode junction temperature was higher than that of the IGBT junction even though the power losses of the diode were less than that of the IGBT. The reason for this is the values of thermal resistance in diode provided by the vendor (**Appendix A)** are greater than the thermal resistances values of the IGBT. Since there time constants are identical it makes sense that the one with the higher power isn't necessary the one with the higher temperature rise. Also the input voltage was low (100Vdc) compared to its maximum (350 Vdc) and this also contributed to the diode temperature being hottest. In the next chapter, lab equipment will be set up to match the simulation and experimental data will be collected in order to validate the simulated models.

THIS PAGE INTENTIONALLY LEFT BLANK

V. EXPERIMENTAL DATA ACQUISTION

A. INTRODUCTION

In order to validate the simulated data of the power losses and thermal models a DC-AC VSI inverter was setup as in the lab to match the simulated conditions. The controller for the DC-AC VSI used a PWM scheme at 5 kHz just like the electrical model did for the simulations. The VSI used was the Semikron SKiiP 942GB120-317CTV, because the hardware was available in the lab. The setup of the experimental system used for data collection is shown in a basic block diagram in **Figure 34.** The experimental data will be collected in order to determine the heat capacity of the system and also to validate the Simulink models. The heat capacity of the system will then be used in order to find out how long it would take for system to shutdown on over temperature protection on a loss of coolant casualty (LOCC).

B. CONSTRUCTION

The construction of the three phase DC-AC VSI system in **Figure 35** was accomplished in three steps. First, the input power to the DC-AC VSI needed to be created from available AC from the wall outlet. Next, the three phase inductive load needed to be connected to output of phase A, B and C of the DC-AC VSI. Finally, the measurement devices were added in order to monitor the DC input voltage and current and the output voltage and current and the thermal resistor voltage representing IGBT junction temperature. The wires that were chosen to connect the given components were chosen based on 100 Amps of current. The 4 AWG wire was used since its current capacity was in excess of 100 Amps.

1. Input Power

The input voltage required for the DC Bus of the VSI was created by taking three phase 208VAC 60Hz from the wall outlet and applying it to a STATCO ENERGY PRODUCTS CO. 12.1kVA VARIAC (**Figure 36**). The output of the VARIAC was applied to a CRYDOM M-50 six pack diode rectifier which rectifies the output to DC.

The output of the CRYDON M-50 six pack rectifier was connected directly to the DC input buses of the DC-AC VSI which was set to 100 V_{dc} to match simulated conditions by adjusting the VARIAC.

2. Three Phase Inductive Load

The output of the three phases of the voltage source inverter were connected to a Y connected MTE RL-10002 0.30mH inductor (**Figure 37**) using 4 AWG.

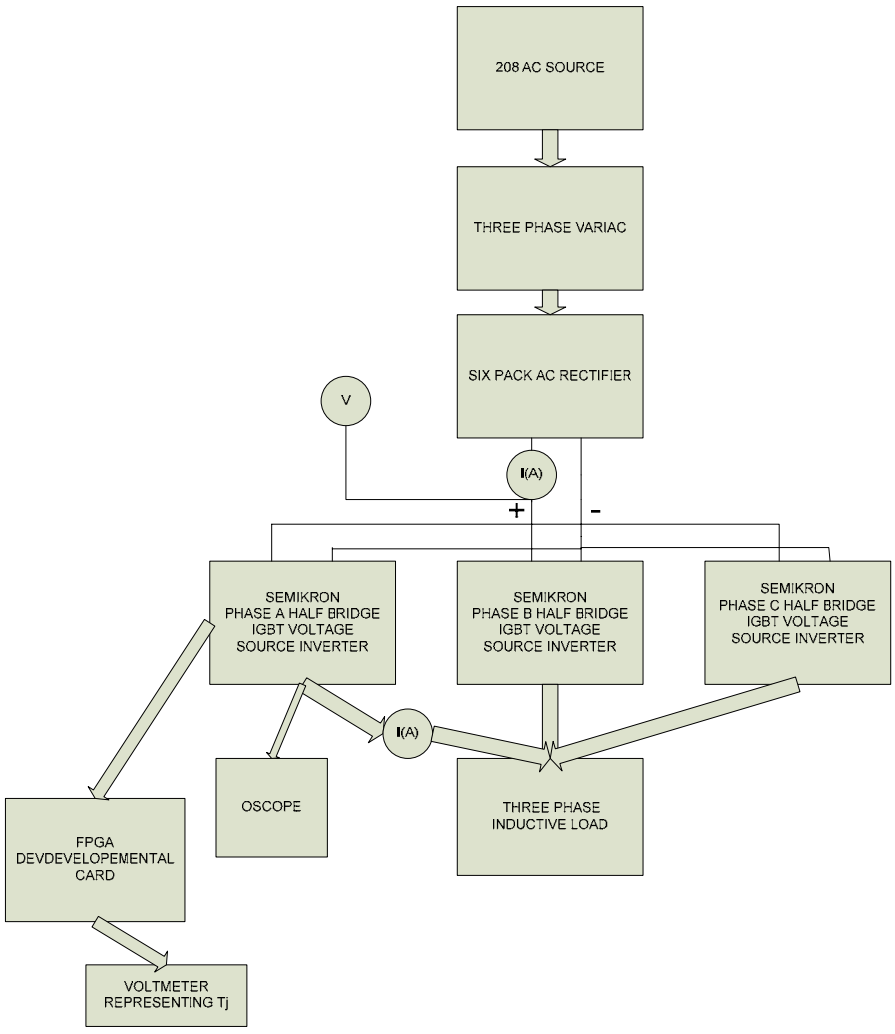

Figure 34. Basic Block Diagram of Lab Equipment Setup for Experimental Data Collection

3. Measurement Devices

The variables that needed to monitored and measured were the thermal resistor voltage, dc input current, dc input voltage, ac output voltage and ac output current. The output current of the CRYDOM six pack was measured with an AEMC SL206 AC/DC current probe that was connected to a EXTECH INSTRUMENTS MultiMaster 560 True RMS meter set to the V_{DC} mode. The output of the current probe was a voltage that represented the current level with a scaling factor of 10mv/A. The DC bus input voltage was measured with a EXTECH INSTRUMENTS MultiMaster 560 True RMS set to the V_{DC} mode. The DC voltage that represented the junction temperature was routed from the SKiiP module through the FPGA based controller card to a EXTECH INSTRUMENTS MultiMaster 560 True RMS set to the V_{DC} mode. The Load current was measure with two TEXTRONIC AS6303 current probes. Two probes were required since each one maximum capability was 50A. The Load Voltage was monitored and recorded on a TEXTRONIC TDS 3012B Oscilloscope via a TEXTRONIC P5200 High Voltage Differential Probe.

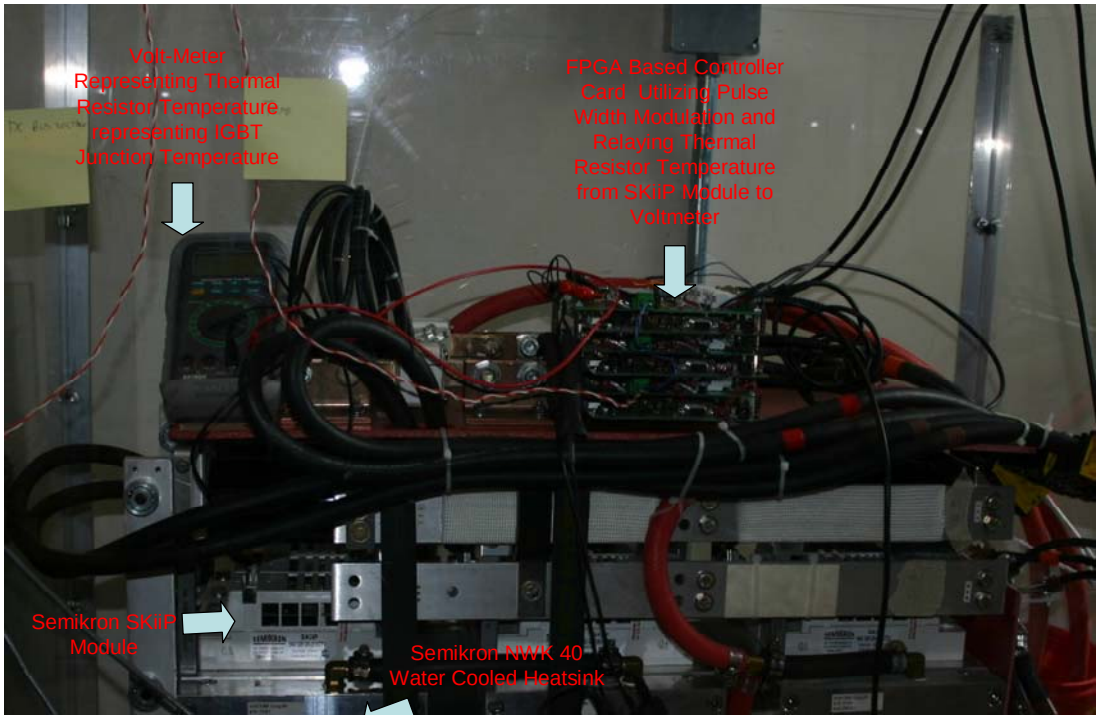

Figure 35. Semikron DC-AC VSI Module used for the 625KW Fuel Cell and Reformer Demonstration Set Up to Match Simulink Models

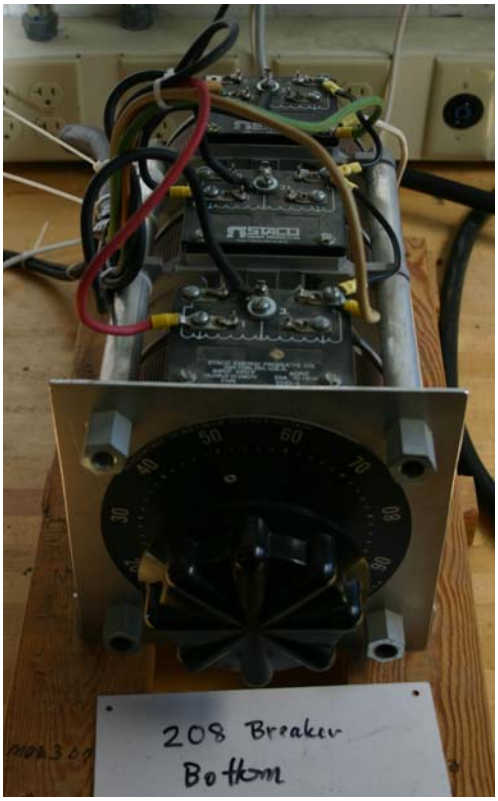

Figure 36. STATCO ENERGY PRODUCTS CO. 12.1kVA VARIAC

Figure 37. Y Connected MTE RL-10002 0.30mH Inductor

C. DATA COLLECTION

The experimental VSI system was connected as previously discussed and the controller card was programmed in order to get a current of $100A_{rms}$ and a voltage $100V_{rms}$. Next, all measuring equipment was calibrated and current probes were degaussed. Two data runs were completed. The first data run was run without any coolant flow to the heat exchanger. This data set will be used to determine the heat capacity of the system and later determine how long it would take for the system to shutdown on over temperature protection on a loss of coolant casualty. The second data run was run with cooling water applied to the heat sink in order to validate the simulated power losses and thermal models data.

1. First Data Run with No Coolant Flow Conducted on 08Jun05

The controller card was configured to provide a load current of 100 A_{rms} and a load voltage of 100 V_{rms}. The DC bus was set to 51 V_{DC} by adjusting the VARIAC and the measured DC bus current was 12.6Amps which was measured on an AEMC SL206 AC/DC current probe that was connected to a EXTECH INSTRUMENTS MultiMaster 560 True RMS meter set to the V_{DC} mode. The actual voltage that was measured was 126mV with a scaling factor of 10mV/A was 12.6Amps. The DC Bus voltage was measured with a EXTECH INSTRUMENTS MultiMaster 560 True RMS meter set to the V_{DC} mode measured 51VDC. The Output Current was measured with two TEXTRONIC AS6303 current probes that were inputted to the two channels of a TEXTRONIC TDS 3012B Oscilloscope and summed together using the summing function. Two current probes were used because the value of current was above 100Amps which was the rating of each individually current probe. The load voltage was measured to be 100VAC and is shown in **Figure 38** calculated in **Equation 15**. The current was measure to be 100 Amps shown in **Figure 39** and calculated in **Equation 16**. The ambient room temperature was recorded to be 24°C with a BRAUN SS CO. CAT. No. 610 Laboratory Grade Thermometer. The experimental time was measured with a SEIKO ARCTURA stopwatch. The thermal data was collected and recorded every thirty seconds for 125 minutes and is shown in **Table 3.**

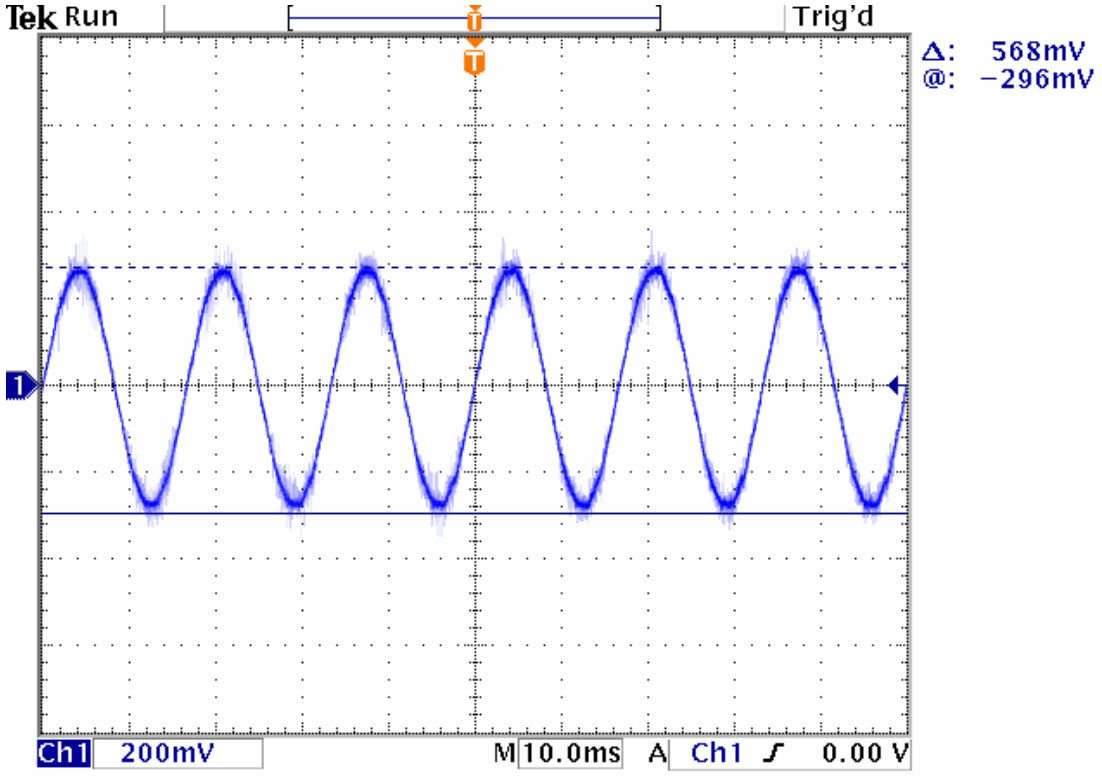

Figure 38. Load Voltage 568mVpp using a High Voltage Differential Probe on Scale 1/500: Therefore showing $100V_{rms}$ (Equation 15).

$$V_{LOAD\,(RMS)} = \left[\frac{\left(568*10^{-3}\right)}{2}*\frac{500}{\sqrt{2}}\right] = 102.19\ V_{rms} \approx 100\ V_{rms} \quad (15)$$

Equation 15. Calculation of Load Voltage for Data Run #1

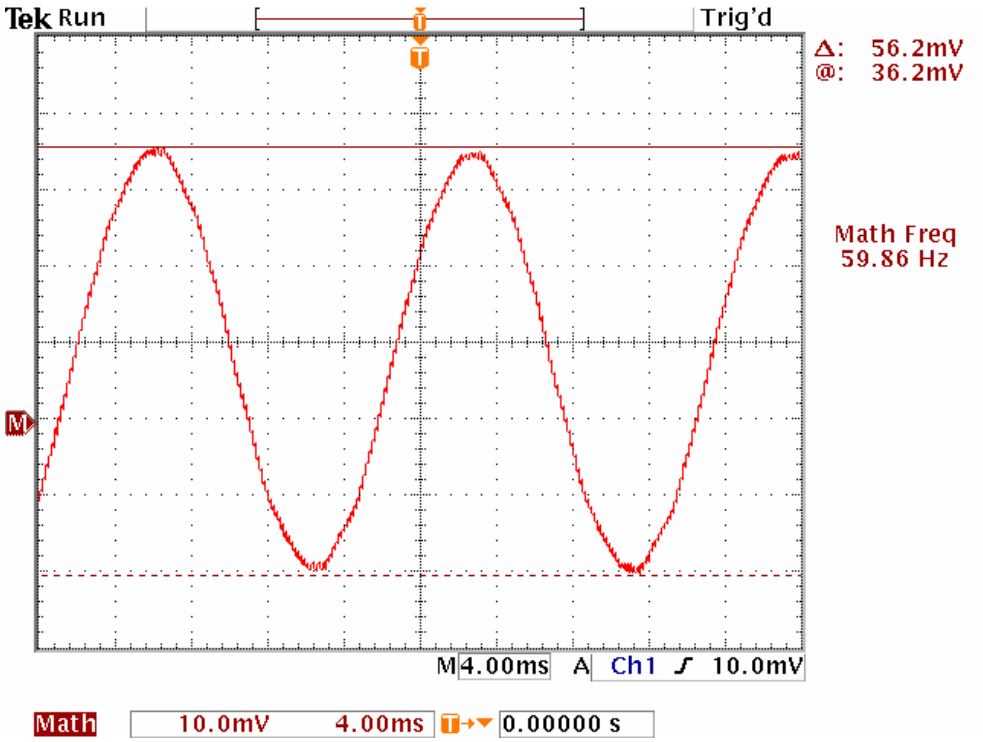

Figure 39. Load Current for Data Run #1 of 56.2mVpp using two current probes and the summing function with 50A/div at the 10mV scale (Equation 16).

$$I_{LOAD\,(RMS)} = \left[\frac{\left(56.2 * 10^{-3}\, mV_{pp}\right)}{div} * \frac{50 Amps}{div} * \frac{div}{10mV} * \frac{1A_p}{2A_{pp}} * \frac{1A_{rms}}{\sqrt{2}A_p} \right] = 99.36\ A_{rms} \approx 100\ A_{rms} \quad (16)$$

Equation 16. Calculation of Load Current Voltage for Data Run #1

Table 3: Data Run#1 Conducted on 08Jun05 Recorded Data for Voltage Source Inverter with no water supplied to heat sink							
Experimental Time (Seconds)	Ambient Temperature (°C)	Analog Voltage (Volts)	ΔT_j (°C)	DC Bus Voltage (Volts)	DC Current from Rectifier (Amps)	Load Voltage (Volts)	Load Current (Amps)
0	24	0.62	24	51	12.6	100	100
30	24	0.85	27.6	51	12.6	100	100
60	24	0.94	28.5	51	12.6	100	100
90	24	1.01	30.1	51	12.6	100	100
120	24	1.08	30.8	51	12.6	100	100
150	24	1.14	31.4	51	12.6	100	100
180	24	1.21	32.1	51	12.6	100	100
210	24	1.27	32.7	51	12.6	100	100
240	24	1.33	33.3	51	12.6	100	100
270	24	1.4	34	51	12.6	100	100
300	24	1.46	34.6	51	12.6	100	100
330	24	1.51	35.1	51	12.6	100	100
360	24	1.57	35.7	51	12.6	100	100
390	24	1.63	36.3	51	12.6	100	100
420	24	1.69	36.9	51	12.6	100	100
450	24	1.74	37.4	51	12.6	100	100
480	24	1.8	38	51	12.6	100	100
510	24	1.85	38.5	51	12.6	100	100
540	24	1.9	39	51	12.6	100	100

Table 3: Data Run#1 Conducted on 08Jun05 Recorded Data for Voltage Source Inverter with no water supplied to heat sink							
Experimental Time (Seconds)	Ambient Temperature (°C)	Analog Voltage (Volts)	ΔT_j (°C)	DC Bus Voltage (Volts)	DC Current from Rectifier (Amps)	Load Voltage (Volts)	Load Current (Amps)
570	24	1.95	39.5	51	12.6	100	100
600	24	2	40	51	12.6	100	100
630	24	2.06	40.6	51	12.6	100	100
660	24	2.11	41.1	51	12.6	100	100
690	24	2.16	41.6	51	12.6	100	100
720	24	2.21	42.1	51	12.6	100	100
750	24	2.26	42.6	51	12.6	100	100
780	24	2.3	43	51	12.6	100	100
810	24	2.35	43.5	51	12.6	100	100
840	24	2.4	44	51	12.6	100	100
870	24	2.44	44.4	51	12.6	100	100
900	24	2.49	44.9	51	12.6	100	100
930	24	2.53	45.3	51	12.6	100	100
960	24	2.58	45.8	51	12.6	100	100
990	24	2.62	46.2	51	12.6	100	100
1020	24	2.66	46.6	51	12.6	100	100
1050	24	2.71	47.1	51	12.6	100	100
1080	24	2.75	47.5	51	12.6	100	100
1110	24	2.79	47.9	51	12.6	100	100

Table 3: Data Run#1 Conducted on 08Jun05 Recorded Data for Voltage Source Inverter with no water supplied to heat sink							
Experimental Time (Seconds)	Ambient Temperature (°C)	Analog Voltage (Volts)	ΔT_j (°C)	DC Bus Voltage (Volts)	DC Current from Rectifier (Amps)	Load Voltage (Volts)	Load Current (Amps)
1140	24	2.83	48.3	51	12.6	100	100
1170	24	2.87	48.7	51	12.6	100	100
1200	24	2.91	49.1	51	12.6	100	100
1230	24	2.95	49.5	51	12.6	100	100
1260	24	2.99	49.9	51	12.6	100	100
1290	24	3.03	50.3	51	12.6	100	100
1320	24	3.07	50.7	51	12.6	100	100
1350	24	3.1	51	51	12.6	100	100
1380	24	3.14	51.4	51	12.6	100	100
1410	24	3.18	51.8	51	12.6	100	100
1440	24	3.21	52.1	51	12.6	100	100
1470	24	3.25	52.5	51	12.6	100	100
1500	24	3.29	52.9	51	12.6	100	100
1530	24	3.32	53.2	51	12.6	100	100
1560	24	3.36	53.6	51	12.6	100	100
1590	24	3.39	53.9	51	12.6	100	100
1620	24	3.42	54.2	51	12.6	100	100
1650	24	3.45	54.5	51	12.6	100	100
1680	24	3.49	54.9	51	12.6	100	100

Table 3: Data Run#1 Conducted on 08Jun05 Recorded Data for Voltage Source Inverter with no water supplied to heat sink							
Experimental Time (Seconds)	Ambient Temperature (°C)	Analog Voltage (Volts)	ΔT_j (°C)	DC Bus Voltage (Volts)	DC Current from Rectifier (Amps)	Load Voltage (Volts)	Load Current (Amps)
1710	24	3.52	55.2	51	12.6	100	100
1740	24	3.55	55.5	51	12.6	100	100
1770	24	3.58	55.8	51	12.6	100	100
1800	24	3.61	56.1	51	12.6	100	100
1830	24	3.64	56.4	51	12.6	100	100
1860	24	3.68	56.8	51	12.6	100	100
1890	24	3.7	57	51	12.6	100	100
1920	24	3.73	57.3	51	12.6	100	100
1950	24	3.77	57.7	51	12.6	100	100
1980	24	3.79	57.9	51	12.6	100	100
2010	24	3.82	58.2	51	12.6	100	100
2040	24	3.85	58.5	51	12.6	100	100
2070	24	3.88	58.8	51	12.6	100	100
2100	24	3.9	59	51	12.6	100	100
2130	24	3.93	59.3	51	12.6	100	100
2160	24	3.96	59.6	51	12.6	100	100
2190	24	3.99	59.9	51	12.6	100	100
2220	24	4.01	60.1	51	12.6	100	100
2250	24	4.04	60.4	51	12.6	100	100

Table 3: Data Run#1 Conducted on 08Jun05 Recorded Data for Voltage Source Inverter with no water supplied to heat sink							
Experimental Time (Seconds)	Ambient Temperature (°C)	Analog Voltage (Volts)	ΔT_j (°C)	DC Bus Voltage (Volts)	DC Current from Rectifier (Amps)	Load Voltage (Volts)	Load Current (Amps)
2280	24	4.06	60.6	51	12.6	100	100
2310	24	4.09	60.9	51	12.6	100	100
2340	24	4.11	61.1	51	12.6	100	100
2370	24	4.14	61.4	51	12.6	100	100
2400	24	4.16	61.6	51	12.6	100	100
2430	24	4.19	61.9	51	12.6	100	100
2460	24	4.21	62.1	51	12.6	100	100
2490	24	4.23	62.3	51	12.6	100	100
2520	24	4.26	62.6	51	12.6	100	100
2550	24	4.28	62.8	51	12.6	100	100
2580	24	4.3	63	51	12.6	100	100
2610	24	4.33	63.3	51	12.6	100	100
2640	24	4.35	63.5	51	12.6	100	100
2670	24	4.37	63.7	51	12.6	100	100
2700	24	4.39	63.9	51	12.6	100	100
2730	24	4.41	64.1	51	12.6	100	100
2760	24	4.43	64.3	51	12.6	100	100
2790	24	4.46	64.6	51	12.6	100	100
2820	24	4.48	64.8	51	12.6	100	100

Table 3: Data Run#1 Conducted on 08Jun05 Recorded Data for Voltage Source Inverter with no water supplied to heat sink							
Experimental Time (Seconds)	Ambient Temperature (°C)	Analog Voltage (Volts)	ΔT_j (°C)	DC Bus Voltage (Volts)	DC Current from Rectifier (Amps)	Load Voltage (Volts)	Load Current (Amps)
2850	24	4.5	65	51	12.6	100	100
2880	24	4.52	65.2	51	12.6	100	100
2910	24	4.54	65.4	51	12.6	100	100
2940	24	4.56	65.6	51	12.6	100	100
2970	24	4.58	65.8	51	12.6	100	100
3000	24	4.6	66	51	12.6	100	100
3030	24	4.62	66.2	51	12.6	100	100
3060	24	4.64	66.4	51	12.6	100	100
3090	24	4.65	66.5	51	12.6	100	100
3120	24	4.67	66.7	51	12.6	100	100
3150	24	4.69	66.9	51	12.6	100	100
3180	24	4.71	67.1	51	12.6	100	100
3210	24	4.73	67.3	51	12.6	100	100
3240	24	4.74	67.4	51	12.6	100	100
3270	24	4.76	67.6	51	12.6	100	100
3300	24	4.78	67.8	51	12.6	100	100
3330	24	4.8	68	51	12.6	100	100
3360	24	4.81	68.1	51	12.6	100	100
3390	24	4.83	68.3	51	12.6	100	100

Table 3: Data Run#1 Conducted on 08Jun05 Recorded Data for Voltage Source Inverter with no water supplied to heat sink							
Experimental Time (Seconds)	Ambient Temperature (°C)	Analog Voltage (Volts)	ΔT_j (°C)	DC Bus Voltage (Volts)	DC Current from Rectifier (Amps)	Load Voltage (Volts)	Load Current (Amps)
3420	24	4.84	68.4	51	12.6	100	100
3450	24	4.86	68.6	51	12.6	100	100
3480	24	4.88	68.8	51	12.6	100	100
3510	24	4.89	68.9	51	12.6	100	100
3540	24	4.91	69.1	51	12.6	100	100
3570	24	4.92	69.2	51	12.6	100	100
3600	24	4.94	69.4	51	12.6	100	100
3630	24	4.95	69.5	51	12.6	100	100
3660	24	4.97	69.7	51	12.6	100	100
3690	24	4.98	69.8	51	12.6	100	100
3720	24	5	70	51	12.6	100	100
3750	24	5.01	70.1	51	12.6	100	100
3780	24	5.03	70.3	51	12.6	100	100
3810	24	5.04	70.4	51	12.6	100	100
3840	24	5.05	70.5	51	12.6	100	100
3870	24	5.07	70.7	51	12.6	100	100
39000	24	5.08	70.8	51	12.6	100	100
3930	24	5.1	71	51	12.6	100	100
3960	24	5.11	71.1	51	12.6	100	100

Table 3: Data Run#1 Conducted on 08Jun05 Recorded Data for Voltage Source Inverter with no water supplied to heat sink							
Experimental Time (Seconds)	Ambient Temperature (°C)	Analog Voltage (Volts)	ΔT_j (°C)	DC Bus Voltage (Volts)	DC Current from Rectifier (Amps)	Load Voltage (Volts)	Load Current (Amps)
3990	24	5.12	71.2	51	12.6	100	100
4020	24	5.14	71.4	51	12.6	100	100
4050	24	5.15	71.5	51	12.6	100	100
4080	24	5.16	71.6	51	12.6	100	100
4110	24	5.17	71.7	51	12.6	100	100
4140	24	5.18	71.8	51	12.6	100	100
4170	24	5.2	72	51	12.6	100	100
4200	24	5.21	72.1	51	12.6	100	100
4230	24	5.22	72.2	51	12.6	100	100
4260	24	5.23	72.3	51	12.6	100	100
4290	24	5.24	72.4	51	12.6	100	100
4320	24	5.25	72.5	51	12.6	100	100
4350	24	5.26	72.6	51	12.6	100	100
4380	24	5.28	72.8	51	12.6	100	100
4410	24	5.29	72.9	51	12.6	100	100
4440	24	5.3	73	51	12.6	100	100
4470	24	5.31	73.1	51	12.6	100	100
4500	24	5.32	73.2	51	12.6	100	100
4530	24	5.33	73.3	51	12.6	100	100

Table 3: Data Run#1 Conducted on 08Jun05 Recorded Data for Voltage Source Inverter with no water supplied to heat sink							
Experimental Time (Seconds)	Ambient Temperature (°C)	Analog Voltage (Volts)	ΔT_j (°C)	DC Bus Voltage (Volts)	DC Current from Rectifier (Amps)	Load Voltage (Volts)	Load Current (Amps)
4560	24	5.34	73.4	51	12.6	100	100
4590	24	5.35	73.5	51	12.6	100	100
4620	24	5.36	73.6	51	12.6	100	100
4650	24	5.37	73.7	51	12.6	100	100
4680	24	5.38	73.8	51	12.6	100	100
4710	24	5.39	73.9	51	12.6	100	100
4740	24	5.4	74	51	12.6	100	100
4770	24	5.41	74.1	51	12.6	100	100
4800	24	5.42	74.2	51	12.6	100	100
4830	24	5.43	74.3	51	12.6	100	100
4860	24	5.44	74.4	51	12.6	100	100
4890	24	5.45	74.5	51	12.6	100	100
4920	24	5.45	74.5	51	12.6	100	100
4950	24	5.46	74.6	51	12.6	100	100
4980	24	5.47	74.7	51	12.6	100	100
5010	24	5.48	74.8	51	12.6	100	100
5040	24	5.49	74.9	51	12.6	100	100
5070	24	5.5	75	51	12.6	100	100
5100	24	5.51	75.1	51	12.6	100	100

Table 3: Data Run#1 Conducted on 08Jun05 Recorded Data for Voltage Source Inverter with no water supplied to heat sink							
Experimental Time (Seconds)	Ambient Temperature (°C)	Analog Voltage (Volts)	ΔT_j (°C)	DC Bus Voltage (Volts)	DC Current from Rectifier (Amps)	Load Voltage (Volts)	Load Current (Amps)
5130	24	5.52	75.2	51	12.6	100	100
5160	24	5.53	75.3	51	12.6	100	100
5190	24	5.53	75.3	51	12.6	100	100
5220	24	5.54	75.4	51	12.6	100	100
5250	24	5.55	75.5	51	12.6	100	100
5280	24	5.56	75.6	51	12.6	100	100
5310	24	5.56	75.6	51	12.6	100	100
5340	24	5.57	75.7	51	12.6	100	100
5370	24	5.58	75.8	51	12.6	100	100
5400	24	5.59	75.9	51	12.6	100	100
5430	24	5.59	75.9	51	12.6	100	100
5460	24	5.6	76	51	12.6	100	100
5490	24	5.61	76.1	51	12.6	100	100
5520	24	5.61	76.1	51	12.6	100	100
5550	24	5.62	76.2	51	12.6	100	100
5580	24	5.63	76.3	51	12.6	100	100
5610	24\	5.63	76.3	51	12.6	100	100
5640	24	5.64	76.4	51	12.6	100	100
5670	24	5.65	76.5	51	12.6	100	100

Table 3: Data Run#1 Conducted on 08Jun05 Recorded Data for Voltage Source Inverter with no water supplied to heat sink							
Experimental Time (Seconds)	Ambient Temperature (°C)	Analog Voltage (Volts)	ΔT_j (°C)	DC Bus Voltage (Volts)	DC Current from Rectifier (Amps)	Load Voltage (Volts)	Load Current (Amps)
5700	24	5.66	76.6	51	12.6	100	100
5730	24	5.66	76.6	51	12.6	100	100
5760	24	5.66	76.6	51	12.6	100	100
5790	24	5.67	76.7	51	12.6	100	100
5820	24	5.68	76.8	51	12.6	100	100
5850	24	5.68	76.8	51	12.6	100	100
5880	24	5.69	76.9	51	12.6	100	100
5910	24	5.69	76.9	51	12.6	100	100
5940	24	5.7	77	51	12.6	100	100
5970	24	5.7	77	51	12.6	100	100
6000	24	5.71	77.1	51	12.6	100	100
6030	24	5.71	77.1	51	12.6	100	100
6060	24	5.72	77.2	51	12.6	100	100
6090	24	5.72	77.2	51	12.6	100	100
6120	24	5.73	77.3	51	12.6	100	100
6150	24	5.74	77.4	51	12.6	100	100
6180	24	5.74	77.4	51	12.6	100	100
6210	24	5.75	77.5	51	12.6	100	100
6240	24	5.76	77.6	51	12.6	100	100

Table 3: Data Run#1 Conducted on 08Jun05 Recorded Data for Voltage Source Inverter with no water supplied to heat sink							
Experimental Time (Seconds)	Ambient Temperature (°C)	Analog Voltage (Volts)	ΔT_j (°C)	DC Bus Voltage (Volts)	DC Current from Rectifier (Amps)	Load Voltage (Volts)	Load Current (Amps)
6270	24	5.76	77.6	51	12.6	100	100
6300	24	5.77	77.7	51	12.6	100	100
6330	24	5.77	77.7	51	12.6	100	100
6360	24	5.78	77.8	51	12.6	100	100
6390	24	5.78	77.8	51	12.6	100	100
6420	24	5.79	77.9	51	12.6	100	100
6450	24	5.79	77.9	51	12.6	100	100
6480	24	5.8	78	51	12.6	100	100
6510	24	5.8	78	51	12.6	100	100
6540	24	5.81	78.1	51	12.6	100	100
6570	24	5.81	78.1	51	12.6	100	100
6600	24	5.82	78.2	51	12.6	100	100
6630	24	5.82	78.2	51	12.6	100	100
6660	24	5.83	78.3	51	12.6	100	100
6690	24	5.83	78.3	51	12.6	100	100
6720	24	5.84	78.4	51	12.6	100	100
6750	24	5.84	78.4	51	12.6	100	100
6780	24	5.84	78.4	51	12.6	100	100
6810	24	5.85	78.5	51	12.6	100	100

Table 3: Data Run#1 Conducted on 08Jun05 Recorded Data for Voltage Source Inverter with no water supplied to heat sink							
Experimental Time (Seconds)	Ambient Temperature (°C)	Analog Voltage (Volts)	ΔT_j (°C)	DC Bus Voltage (Volts)	DC Current from Rectifier (Amps)	Load Voltage (Volts)	Load Current (Amps)
6840	24	5.85	78.5	51	12.6	100	100
6870	24	5.86	78.6	51	12.6	100	100
6900	24	5.86	78.6	51	12.6	100	100
6930	24	5.86	78.6	51	12.6	100	100
6960	24	5.87	78.7	51	12.6	100	100
6990	24	5.87	78.7	51	12.6	100	100
7020	24	5.88	78.8	51	12.6	100	100
7050	24	5.88	78.8	51	12.6	100	100
7080	24	5.88	78.8	51	12.6	100	100
7110	24	5.89	78.9	51	12.6	100	100
7140	24	5.89	78.9	51	12.6	100	100
7170	24	5.89	78.9	51	12.6	100	100
7200	24	5.89	78.9	51	12.6	100	100
7230	24	5.9	79	51	12.6	100	100
7260	24	5.9	79	51	12.6	100	100
7290	24	5.91	79.1	51	12.6	100	100
7320	24	5.91	79.1	51	12.6	100	100
7350	24	5.91	79.1	51	12.6	100	100
7380	24	5.91	79.1	51	12.6	100	100

Table 3: Data Run#1 Conducted on 08Jun05 Recorded Data for Voltage Source Inverter with no water supplied to heat sink							
Experimental Time (Seconds)	Ambient Temperature (°C)	Analog Voltage (Volts)	ΔT_j (°C)	DC Bus Voltage (Volts)	DC Current from Rectifier (Amps)	Load Voltage (Volts)	Load Current (Amps)
7410	24	5.91	79.1	51	12.6	100	100
7440	24	5.92	79.2	51	12.6	100	100
7470	24	5.92	79.2	51	12.6	100	100
7500	24	5.92	79.2	51	12.6	100	100

Table 3. Data Run#1 Conducted on 08Jun05 Recorded Data for Voltage Source Inverter with no water supplied to heat sink

The plotted thermal resistor temperature for data run #1 is shown **Figure 40**.

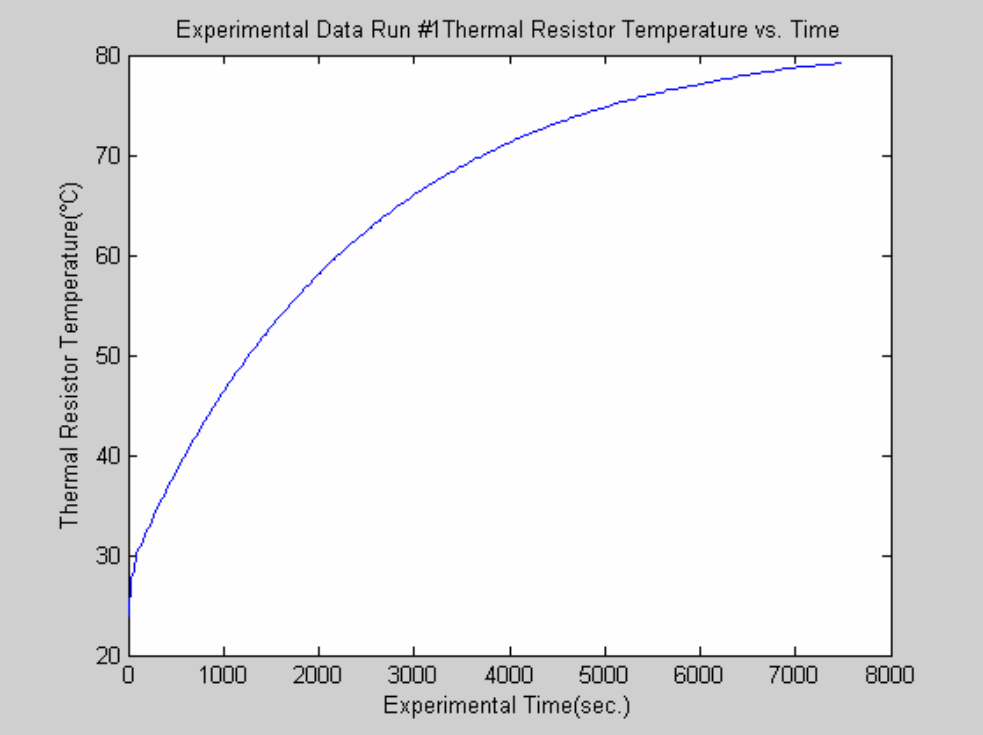

Figure 40. Matlab Plot of Rise in Thermal Resistor Temperature with no coolant flow and input power of 642 Watts for Semikron Source Inverter SKiiP942GB120-317CTV with an ambient temperature of 24°C.

The experimental data plotted above correlates to the expected response of a exponential buildup function. The above data was then used to determine the time constant of the entire thermal system based on the first order thermal model of the system (**Figure 41**) [6].

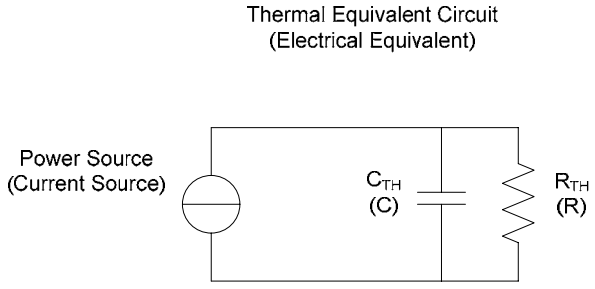

Figure 41. Thermal Model Approximation of 1st Order System [6].

Next the following basic equations in **Table 4** were used to extract the time constant of the above first order thermal model.

$$\tau = R_{TH} \cdot C_{TH}$$

$$Temp(t) = A(1 - e^{-\frac{t}{\tau}}) + C$$

$$I = \frac{V}{R} \rightarrow V = I \cdot R \text{ (Electrical Equivalent)}$$

$$\text{Power} = \frac{\text{Temperature}}{R_{TH}} \text{ where } R_{TH} = \text{thermal resistance} \rightarrow V = I \cdot R \text{ (Theramal Equivalent)}$$

From Plotted Data A=Max Temp-Ambient Temp $\Rightarrow A = 79.2 - 24 = 55.2(\Delta°C)$

C=Ambient Temperature=24°C

Table 4. Equations Relating First Order Solution of the Thermal System to the Electrical Equivalent Circuit[7]

The time constant (tau) was computed using Matlab Cftool box and plot on the data collected in data run #1 (**Figure 42)**.

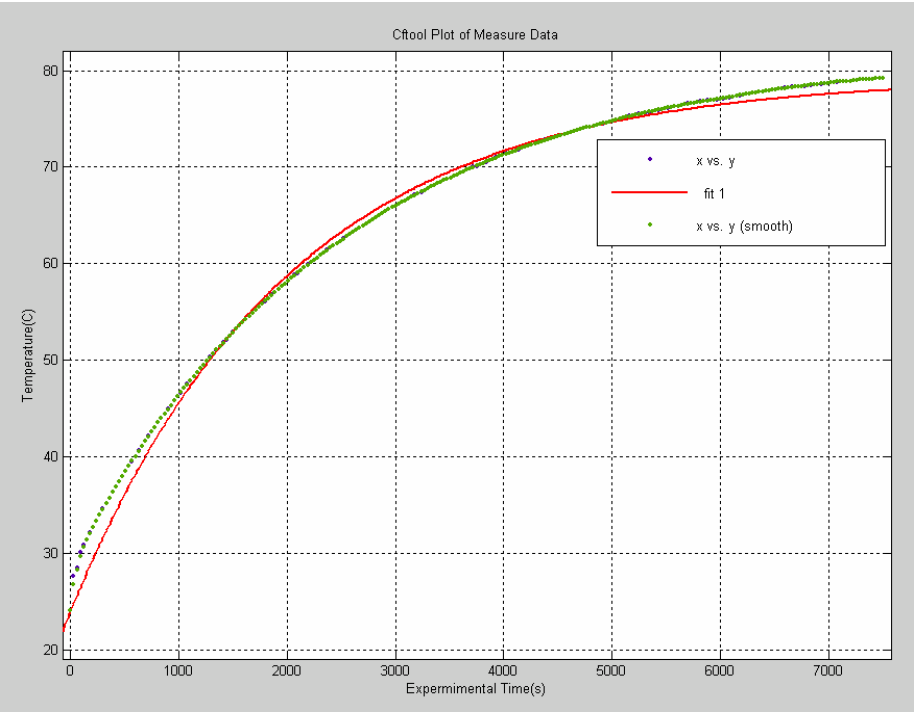

Figure 42. CFTOOL fitting of Thermal Data to extract tau= R x C.

CFTOOL OUTPUT:
General model:
f(y) = a*(1-exp(-y/z))+c
Coefficients (with 95% confidence bounds):
a = 55.3 (fixed at bound)
C = 24 (fixed at bound)
z = 2018 (1999, 2037)
Goodness of fit:
SSE: 283.8
R-square: 0.9941
Adjusted R-square: 0.9941
RMSE: 1.065

Table 5. Matlab CFTOOL Output for solving 1st Order Equivalent of Thermal System

The tau was determined to be 2018 from using the above Matlab CFTool best fit function. Then using the thermal equation for electrical equivalent circuit from **Table 4** the thermal resistance was solved for.

$$V(temp) = Power \cdot R_{th} \Rightarrow\ 55.2 = 642.6W \cdot \mathrm{R_{TH}} \Rightarrow\ \mathrm{R_{TH}} = \frac{55.2°\mathrm{C}}{642.6W} = 0.0859\ \frac{°\mathrm{C}}{W} \qquad (17)$$

Equation 15. Solving Thermal Resistance of VSI System from Data Run #1 as a Single Order System

Next, the constant **A** for the Temperature buildup equation in **Table 5** must be calculated based on the maximum design input power for the inverter in order to compute the time to shutdown for a loss of coolant casualty. The Calculations and Assumptions are shown in **Table 6**.

$625kW$ Max Design Power for ONR Fuel Cell Reformer Project (6) 3 Phase Inverters in system 18 Inverter Half Bridges P_{Max} One Half Bridge= 625kW/18=34722W $A=P_{max} \cdot R_{th} = 34722W \cdot 0.0859 \frac{°C}{W} = 2982.7°C$

Table 6. Calculations and Assumptions for Determining the constant A in Buildup Equation in Table 5.

Finally in order to predict the time to shutdown with a loss of coolant casualty the buildup equation was constructed using the solved parameters from the data from data run #1. A Matlab script file was created in order to compute the time to shutdown using 110°C as a shut down temperature and 25°C as ambient temperature (Equations and Script file shown in **Table 7**).

$Temp(t) = A(1-\exp^{-\frac{t}{tau}}) + C$
$Temp(t) = 2982.7(1-\exp^{-\frac{t}{2018}}) + 25$
Matlab CODE
z=linspace(0,10000,100000);
a = 2982.7*(1-exp(-z./2018))+25;
figure
plot(z,a)
time_shutdown=2018*(-log(-(((125-25)/2982.7)-1)))
time_shutdown = 68.8170 seconds

Table 7. Equations and Matlab Code to Determine Time to Shutdown with a Loss of Coolant Casualty

Therefore, the predicted time to shutdown for a LOCC was **68.8 seconds** based on the thermal data collected on the voltage source inverter in data run #1. The plot of predicted junction temperature based on a loss of coolant casualty with the maximum design input power is shown in **Figure 43.**

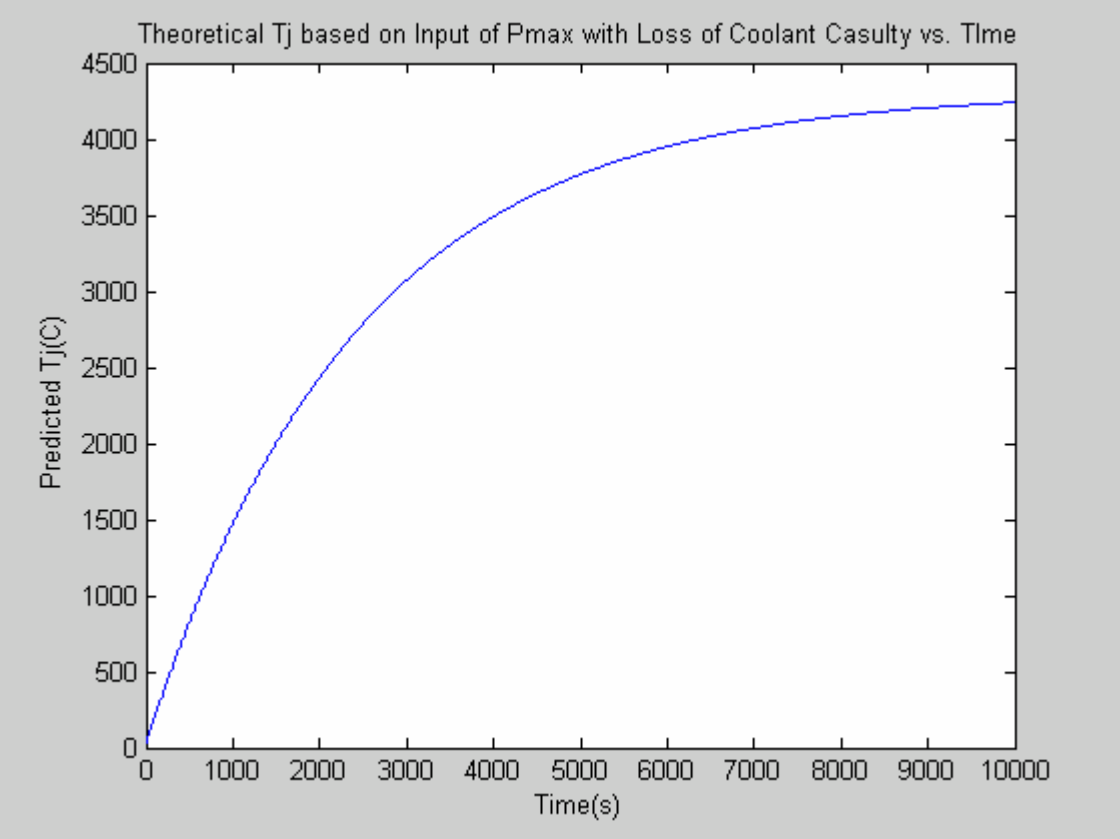

Figure 43. Predicted Theoretical T_j based on Input of P_{max} with a Loss of Coolant Casualty

2. Second Data Run with Coolant Flow Conducted on 07Jul05.

The second data run was completed in order to capture data to validate the simulated power losses and thermal model data. The data run was completed with coolant flow to the water heat exchanger in order to match vendor design criteria. The FPGA based controller card was configured to provide a load current of 100 A_{rms}. The measured DC bus current was 5.78 Amps, which was measured on a AEMC SL206 AC/DC current probe that was connected to a EXTECH INSTRUMENTS MultiMaster 560 True RMS meter set to the V_{DC} mode. The actual voltage that was measured was 0.0578mV with a scaling factor of 10mV/A. This equated to the 5.78 Amps**.** The DC Bus voltage was measured with a EXTECH INSTRUMENTS MultiMaster 560 True RMS meter set to the V_{DC} mode measured 100VDC. The output voltage was measured as 100Vrms with a TEXTRONIC TDS 3012B Oscilloscope using a high voltage differential probe set to 1/500 scale and is calculated in **Equation 18** (**Figure 44**). The

Output Current was measured with two TEXTRONIC AS6303 current probes that were inputted to the two channels of a TEXTRONIC TDS 3012B Oscilloscope and summed together using the summing function. Two current probes were used because the value of current was above the rating of each current probe individually. The current was measure to be 100 Amps seen in **Figure 45** and calculated in Equation 19**.** The ambient room temperature was recorded to be 25.4°C with a BRAUN SS CO. CAT. No. 610 Laboratory Grade Thermometer. The coolant temperature was recorded to be 21.5°C with a BRAUN SS CO. CAT. No. 610 Laboratory Grade Thermometer. The flow rate was calibrated by filling a five gallon bucket four times and averaging the flow rate. The average was controlled until it was calculated to be 1.40gal/min. This corresponded to a flow rate of 5.3 l/min, which corresponded to a thermal resistance of 0.018K/W which was the thermal resistance of the heatsink used for the simulation (**Figure 30**). This was done in order to match experimental conditions to previously computer simulated conditions.

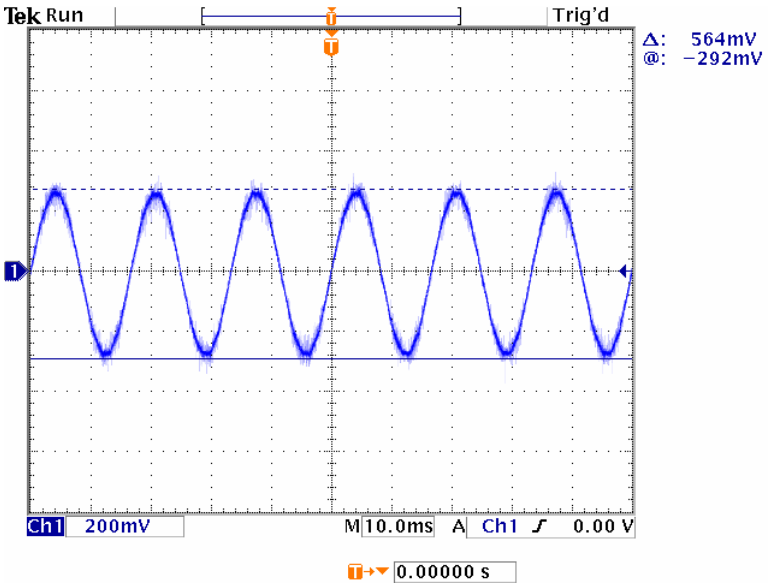

Figure 44. Load Voltage 564mVpp using a High Voltage Differential Probe on Scale 1/500: Therefore showing $100V_{rms}$ (Equation 18).

$$V_{LOAD\ (RMS)} = \left[\frac{\left(564*10^{-3}\right)}{2}*\frac{500}{\sqrt{2}}\right] = 99.7\ V_{rms} \approx 100\ V_{rms} \qquad (18)$$

Equation 18. Calculation of Load Voltage for Data Run #2

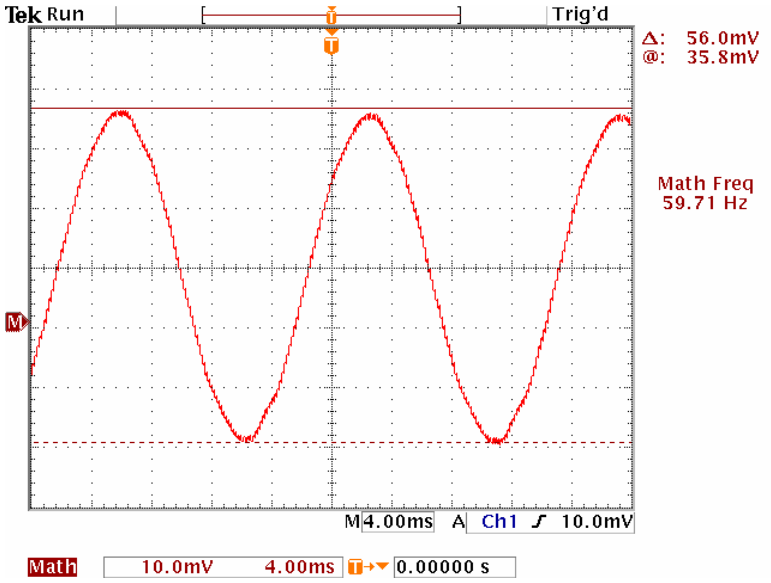

Figure 45. Load Current for Data Run #2of 56.0mVpp using two current probes and the summing function with 50A/div at the 10mV scale (Equation 19).

$$I_{LOAD\,(RMS)} = \left[\frac{\left(56.0*10^{-3}\,mV_{pp}\right)}{div} * \frac{50Amps}{div} * \frac{div}{10mV} * \frac{1A_p}{2A_{pp}} * \frac{1A_{rms}}{\sqrt{2}A_p}\right] = 99.26\ A_{rms} \approx 100\ A_{rms} \quad (19)$$

Equation 19. Calculation of Load Current Voltage for Data Run #2.

The experimental time was measured with a SEIKO ARCTURA stopwatch. The thermal data that was collected every thirty seconds for until equilibrium was reached which was 40 minutes. The recorded data is shown in **Table 9.**

Table 8: 2 Data Run 07Jul05 Recorded Data for Voltage Source Inverter with water supplied to heat sink at a rate of 5.3ll/min with water at a temperature of 21.5°C.

Experimental Time (Seconds)	Ambient Temperature (°C)	Analog Voltage (Volts)	ΔT_j (°C)	DC Bus Voltage (Volts)	DC Current from Rectifier (Amps)	Load Voltage (Volts)	Load Current (Amps)
0	25.4	0.63	25.494	100	5.78	100	100
30	25.4	0.64	25.632	100	5.78	100	100
60	25.4	0.64	25.632	100	5.78	100	100
90	25.4	0.64	25.632	100	5.78	100	100
120	25.4	0.64	25.632	100	5.78	100	100
150	25.4	0.65	25.77	100	5.78	100	100
180	25.4	0.65	25.77	100	5.78	100	100
210	25.4	0.65	25.77	100	5.78	100	100
240	25.4	0.65	25.77	100	5.78	100	100
270	25.4	0.66	25.908	100	5.78	100	100
300	25.4	0.66	25.908	100	5.78	100	100
330	25.4	0.66	25.908	100	5.78	100	100
360	25.4	0.66	25.908	100	5.78	100	100
390	25.4	0.67	26.046	100	5.78	100	100
420	25.4	0.67	26.046	100	5.78	100	100
450	25.4	0.67	26.046	100	5.78	100	100
480	25.4	0.67	26.046	100	5.78	100	100
510	25.4	0.67	26.046	100	5.78	100	100

Table 8: 2 Data Run 07Jul05 Recorded Data for Voltage Source Inverter with water supplied to heat sink at a rate of 5.3ll/min with water at a temperature of 21.5°C.

Experimental Time (Seconds)	Ambient Temperature (°C)	Analog Voltage (Volts)	ΔT_j (°C)	DC Bus Voltage (Volts)	DC Current from Rectifier (Amps)	Load Voltage (Volts)	Load Current (Amps)
540	25.4	0.68	26.184	100	5.78	100	100
570	25.4	0.68	26.184	100	5.78	100	100
600	25.4	0.68	26.184	100	5.78	100	100
630	25.4	0.68	26.184	100	5.78	100	100
660	25.4	0.68	26.184	100	5.78	100	100
690	25.4	0.69	26.322	100	5.78	100	100
720	25.4	0.69	26.322	100	5.78	100	100
750	25.4	0.69	26.322	100	5.78	100	100
780	25.4	0.69	26.322	100	5.78	100	100
810	25.4	0.69	26.322	100	5.78	100	100
840	25.4	0.7	26.46	100	5.78	100	100
870	25.4	0.7	26.46	100	5.78	100	100
900	25.4	0.7	26.46	100	5.78	100	100
930	25.4	0.7	26.46	100	5.78	100	100
960	25.4	0.7	26.46	100	5.78	100	100
990	25.4	0.71	26.598	100	5.78	100	100
1020	25.4	0.71	26.598	100	5.78	100	100
1050	25.4	0.71	26.598	100	5.78	100	100

Table 8: 2 Data Run 07Jul05 Recorded Data for Voltage Source Inverter with water supplied to heat sink at a rate of 5.3ll/min with water at a temperature of 21.5°C.

Experimental Time (Seconds)	Ambient Temperature (°C)	Analog Voltage (Volts)	ΔT_j (°C)	DC Bus Voltage (Volts)	DC Current from Rectifier (Amps)	Load Voltage (Volts)	Load Current (Amps)
1080	25.4	0.71	26.598	100	5.78	100	100
1110	25.4	0.71	26.598	100	5.78	100	100
1140	25.4	0.72	26.736	100	5.78	100	100
1170	25.4	0.72	26.736	100	5.78	100	100
1200	25.4	0.72	26.736	100	5.78	100	100
1230	25.4	0.72	26.736	100	5.78	100	100
1260	25.4	0.72	26.736	100	5.78	100	100
1290	25.4	0.73	26.874	100	5.78	100	100
1320	25.4	0.73	26.874	100	5.78	100	100
1350	25.4	0.73	26.874	100	5.78	100	100
1380	25.4	0.73	26.874	100	5.78	100	100
1410	25.4	0.73	26.874	100	5.78	100	100
1440	25.4	0.73	26.874	100	5.78	100	100
1470	25.4	0.73	26.874	100	5.78	100	100
1500	25.4	0.73	26.874	100	5.78	100	100
1530	25.4	0.74	27.012	100	5.78	100	100
1560	25.4	0.74	27.012	100	5.78	100	100
1590	25.4	0.74	27.012	100	5.78	100	100

Table 8: 2 Data Run 07Jul05 Recorded Data for Voltage Source Inverter with water supplied to heat sink at a rate of 5.3ll/min with water at a temperature of 21.5°C.

Experimental Time (Seconds)	Ambient Temperature (°C)	Analog Voltage (Volts)	ΔT_j (°C)	DC Bus Voltage (Volts)	DC Current from Rectifier (Amps)	Load Voltage (Volts)	Load Current (Amps)
1620	25.4	0.74	27.012	100	5.78	100	100
1650	25.4	0.74	27.012	100	5.78	100	100
1680	25.4	0.74	27.012	100	5.78	100	100
1710	25.4	0.74	27.012	100	5.78	100	100
1740	25.4	0.74	27.012	100	5.78	100	100
1770	25.4	0.74	27.012	100	5.78	100	100
1800	25.4	0.75	27.15	100	5.78	100	100
1830	25.4	0.75	27.15	100	5.78	100	100
1860	25.4	0.75	27.15	100	5.78	100	100
1890	25.4	0.75	27.15	100	5.78	100	100
1920	25.4	0.75	27.15	100	5.78	100	100
1950	25.4	0.75	27.15	100	5.78	100	100
1980	25.4	0.75	27.15	100	5.78	100	100
2010	25.4	0.75	27.15	100	5.78	100	100
2040	25.4	0.75	27.15	100	5.78	100	100
2070	25.4	0.75	27.15	100	5.78	100	100
2100	25.4	0.75	27.15	100	5.78	100	100
2130	25.4	0.75	27.15	100	5.78	100	100

Table 8: 2 Data Run 07Jul05 Recorded Data for Voltage Source Inverter with water supplied to heat sink at a rate of 5.3ll/min with water at a temperature of 21.5°C.							
Experimental Time (Seconds)	Ambient Temperature (°C)	Analog Voltage (Volts)	ΔT_j (°C)	DC Bus Voltage (Volts)	DC Current from Rectifier (Amps)	Load Voltage (Volts)	Load Current (Amps)
2160	25.4	0.75	27.15	100	5.78	100	100
2190	25.4	0.75	27.15	100	5.78	100	100
2220	25.4	0.75	27.15	100	5.78	100	100
2250	25.4	0.75	27.15	100	5.78	100	100
2280	25.4	0.75	27.15	100	5.78	100	100
2310	25.4	0.75	27.15	100	5.78	100	100
2340	25.4	0.75	27.15	100	5.78	100	100
2370	25.4	0.75	27.15	100	5.78	100	100
2400	25.4	0.75	27.15	100	5.78	100	100

Table 8. Data Run #2 Completed on 07Jul05.Recorded Data for Voltage Source Inverter with water supplied to heat sink at a rate of 5.31 l/min with water at a temperature of 21.5°C.

The plotted thermal resistor temperature from data run #2 is shown in **Figure 46**.

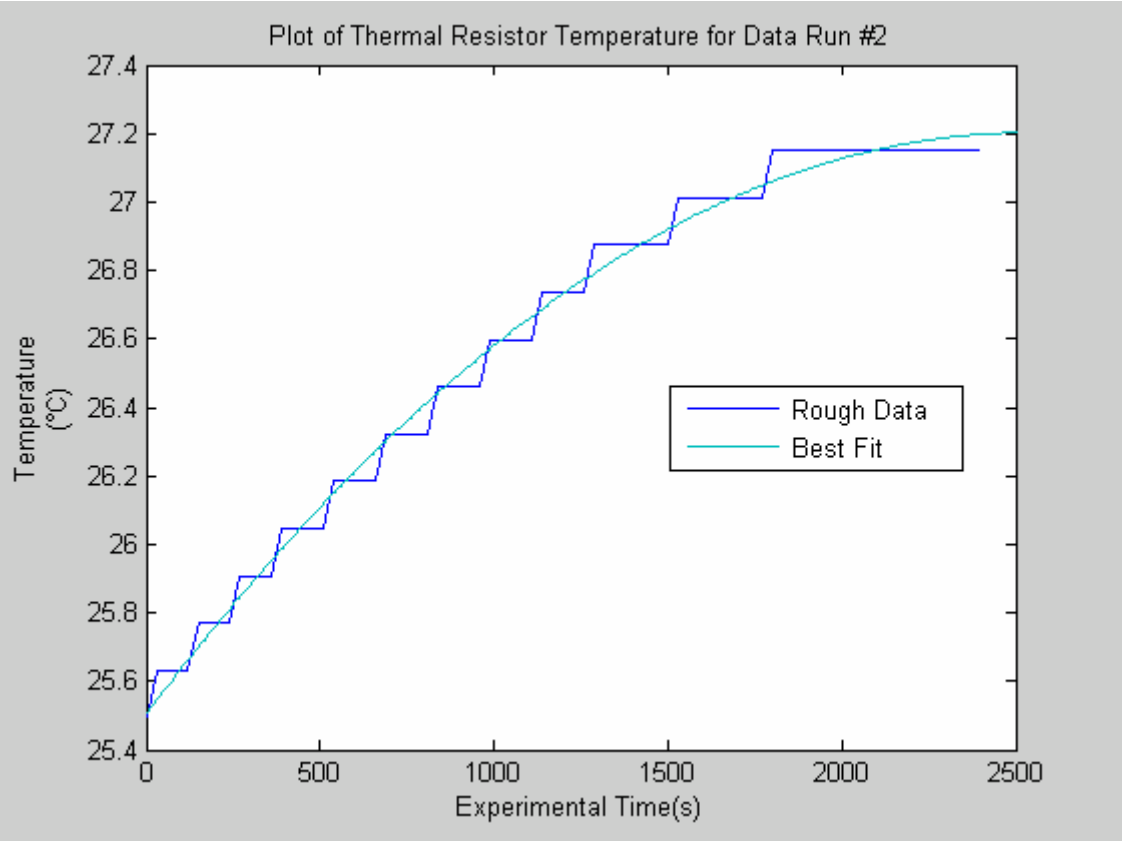

Figure 46. Matlab Plot of Rise in Thermal Resistor Temperature with coolant flow and input power of 578 Watts for Semikron Source Inverter SKiiP942GB120-317CTV with an ambient temperature of 25.4°C.

The experimental data plotted above correlates to the expected response of a exponential buildup function. The thermal resistor indicated a rise of 1.75°C for a input power of 578 W. The experimental temperature rise will be compared to the simulated data in Chapter V, in order to validate the thermal and power losses models. Once the models are validated they will be used to answer the research questions. The next chapter will address the validation of the power losses and thermal models.

D. SUMMARY

The experimental thermal response of the VSI system was a buildup function as expected. In the plotted thermal data in **Figure 46** from data run #2 one can see the Analog to Digital (A/D) resolution of the A/D converter on the Semikron module as the temperature steps in incremental amounts. The extrapolated time to shutdown with a LOCC indicated shutdown in **68.8 seconds**. This time is assuming that the system can be modeled as a first order system. The data was also recorded at a relatively low power compared to the max design operating power. If the system was operating at the maximum design power the extrapolated time to shutdown for a LOCC probably would have been sooner. The lab equipment prevented running the equipment at maximum design power. The summary of data collected and extracted from data runs 1&2 are shown in **Tables 9&10**. In the next Chapter, the experimental data and simulated data will be compared and the research questions will be addressed.

Data Run #1	Input Power	Output Voltage (AC rms)	Ouput Current (AC rms)	Temperature Rise/ for Simulation Time of 7500 seconds	Extracted Max Time to S/D With a LOCC
No Coolant	642.6W	100V	100 A	55.2°C	68.8 seconds

Table 9. Summary of Collected and Extracted Data from Data Run #1.

Data Run #2	Input Power	Output Voltage (AC rms)	Output Current (AC rms)	Temperature Rise/ for Simulation Time of 2400 seconds
Coolant	578	100V	100 A	1.3°C

Table 10. Summary of Collected and Extracted Data from Data Run #2.

THIS PAGE INTENTIONALLY LEFT BLANK

VI. VALIDATION OF MODELS AND RESEARCH QUESTIONS ANSWERED

A. INTRODUCTION

In this chapter, a comparison of the simulated data and the experimental data will be made in order to validate the thermal and power losses models. Each model will be examined separately and a discussion about its assumptions and ways to improve the model will be discussed. In the next Chapter, conclusions will be stated and opportunities for future research explored.

B. VALIDATATION OF MODELS

1. Power Losses Simulation vs. Total Experimental Input Power

The simulation power losses are shown below in **Tables 11, 12, & 13**. The experimental input power is shown in **Table 14**. As seen in **Table 15**, the percent error between the input power and the simulated power was 11%. With all the assumptions made for the simulation the percent error is low enough that this a correlation between the simulated power losses and the experimental power losses. Therefore the power losses model is validated and could be used to predict the system response based on the assumptions made in the simulation chapter.

Switching Losses Upper IGBT	Switching Losses Lower IGBT	Conduction Losses Lower IGBT	Conduction Losses Upper IGBT	Total IGBT Power Losses One Inverter Pole	Total IGBT Power Losses One Three Phase Inverter
16.62W	16.62	48.98W	42.84W	125.06	375.18

Table 11. Summary of Simulated IGBT Power Losses.

Conduction Losses Upper Power Diode	Conduction Losses Lower Power Diode	Reverse Recovery Losses Upper Power Diode	Reverse Recovery Losses Lower Power Diode	Total Diode Power Losses One Inverter Pole	Total Diode Power Losses One Three Phase Inverter
33.14W	31.31W	2.22W	2.22W	68.89W	206.67W

Table 12. Summary of Simulated Power Diode Power Losses.

. Total IGBT Power Losses One Three Phase Inverter	Total Diode Power Losses One Three Phase Inverter	Total Three Phase Inductor Conduction Losses	Total Power Losses on one Three Phase Inverter
375.18W	206.67W	60W	641.85W

Table 13. Summary of Simulated Power Losses for One Three Phase Inverter.

DC Input Current	DC Input Voltage	Total Power Losses on one Three Phase Inverter
5.78 A	100V	578W

Table 14. Summary of Experimental Input Power

Simulated Total Power Losses One Three Phase Inverter	Experimental Total Input Power for One Three Phase Inverter	Percent Error $\left[\frac{P_S - P_E}{P_E} \times 100\right]$
641.85	578W	11%

Table 15. Comparison of Experimental and Simulated Power Losses Data with Percent Error

2. Thermal Model Simulation Junction Temperatures vs. Experimental IGBT Junction Temperature

The simulated thermal response and experimental thermal response is summarized in **Table 16** from data collected in the simulation and experimental chapters. As seen in **Table 17**, the percent error between the simulated thermal response and experimental thermal response was 28%. The percent error seems higher than expected but since the change is temperature was small the percent error looks high. If the lab equipment would support higher currents then the percent error should be lower. With all the assumptions made for the simulation the percent error is low enough that a correlation between the simulated thermal response and the experimental thermal response exists. Therefore the thermal model is validated and could be used to predict the systems thermal response based on the assumptions made in the simulations chapter.

	Matlab Simulated Data (C°)	Lab Experimental Data	Percent Error
Rise in T(j) (C°)	2.4	1.75	27.4%

Table 16. Comparison of Simulated vs. Experimental Thermal Response with Percent Error

C. SIMULATION TO ANSWER RESEARCH QUESTION

1. Simulation to Determine IGBT Junction Temperature at Different Frequencies at Maximum Design Conditions for the 625KW Fuel Cell Reformer Project for ONR

The many simulations were run at different PWM frequencies at the maximum design operating conditions for the 625KW Fuel Cell Reformer Project for ONR. Some assumptions were made about worst case conditions for ambient temperature and a twenty percent tolerance was added to ensure overheating doesn't occur. The maximum ambient temperature was chosen to be 40°C which corresponds to 104°F. This

temperature was based on the worst anticipated ship conditions in the Persian Gulf. The results of the simulations are shown in **Figures 47, 48, and 49**. The summary of the results are shown in **Table 17**.

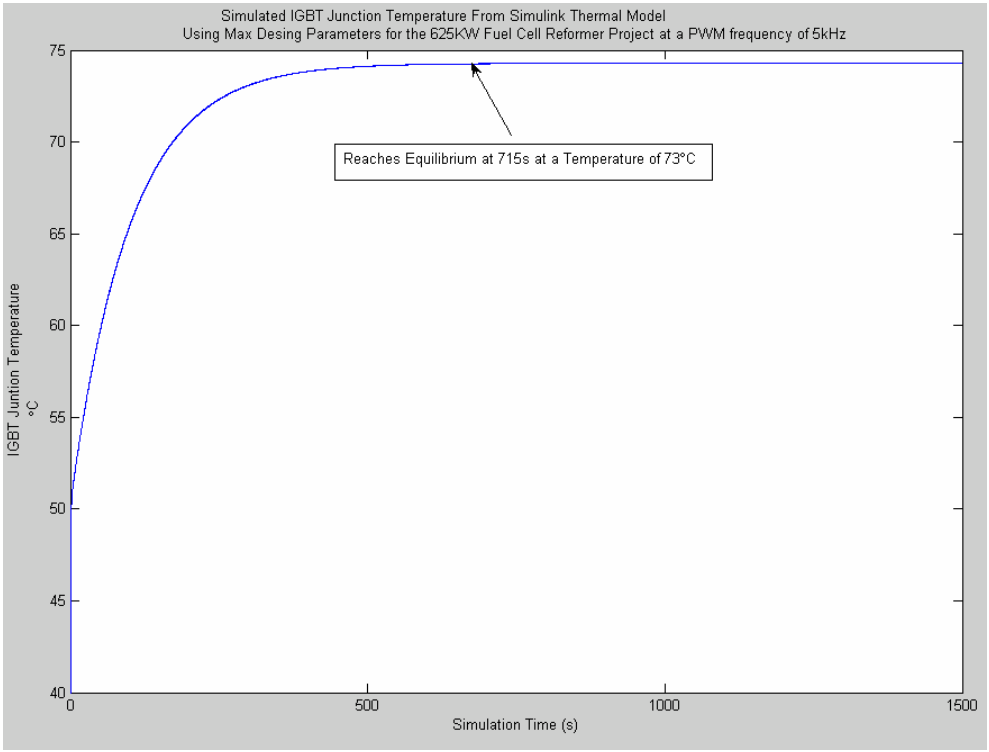

Figure 47. Simulated IGBT Junction Temperature from Simulink Thermal Model Using Maximum Design Parameters for the 625Kw Fuel Cell Reformer Project at a PWM switching frequency of 5kHz.

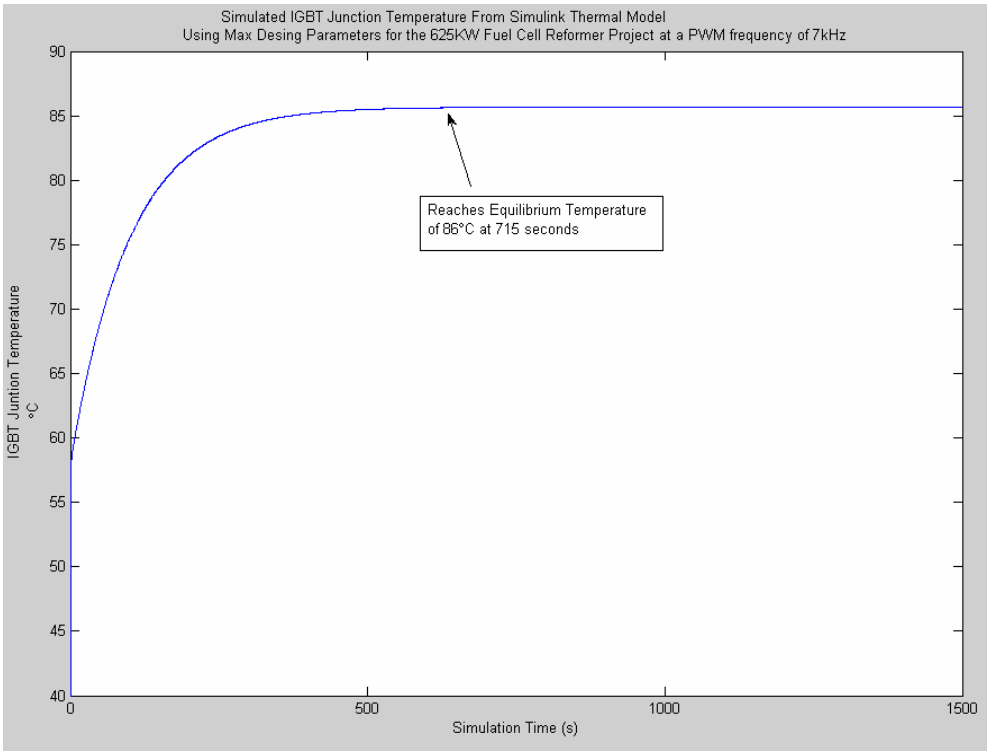

Figure 48. Simulated IGBT Junction Temperature from Simulink Thermal Model Using Maximum Design Parameters for the 625Kw Fuel Cell Reformer Project at a PWM Switching frequency of 7 kHz.

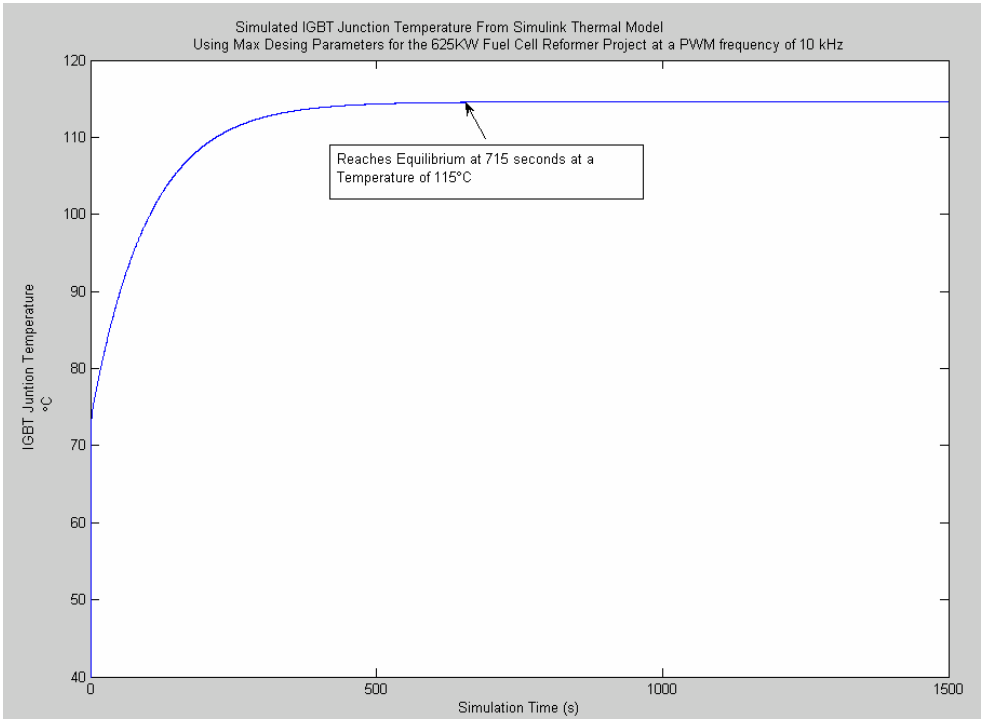

Figure 49. Simulated IGBT Junction Temperature from Simulink Thermal Model Using Maximum Design Parameters for the 625Kw Fuel Cell Reformer Project at a PWM switching frequency of 7 kHz.

PWM Switching Frequency (kHz)	Simulated Hottest Junction Temperature (C°)	% Margin to Over Temperature Protection (110°C)
5	73	34 %
7	**86**	**22%**
10	115	Over-Temp Fault

Table 17. Summary of Simulated IGBT Junction Temperature for 625 Fuel Cell Reformer Demonstration for different Frequencies based on Maximum Design Parameters and Maximum Ambient Temperature

The IGBT Junction temperature was the hottest junction temperature at the maximum design parameters for the 625kW Fuel Cell Reformer Demonstration for ONR. The maximum design parameters were an input of 350 VDC input with an output of 440VAC at 400 Amps at 60 Hz. The over-temperature protection of the Semikron module had a temperature range from 110-120 °C. The low range value of 110 was used and a engineering margin of 20% was added to ensure an over-temperature condition didn't exist because of the PWM frequency. The simulated ambient temperature was increased from the 25.5 °C to 40°C to account for the worst case possible ambient temperature in a ship environment. As you can see in **Table 17**, the maximum PWM switching frequency recommended is 7 kHz which allowed an 20% margin to over temperature protection set point of 110°C.

D. RESEARCH QUESTIONS READDRESSED

In this section all the research questions will be discussed and decided whether the research goals were met and/or obtained. The goals of this thesis were to model the power losses for three phase voltage source inverter system using Simulink, model the thermal response of VSI system using Simulink, build lab system that matches computer model and collect data in order to validate the computer models, quantify the accuracy of

the estimated thermal impedance of an IGBT module, predict the maximum switching frequency without violating thermal limits for the 625 Fuel Cell Reformer Project of ONR, predict the time to shutdown on a Loss of Coolant Casualty (LOCC), and quantify the characteristics of the heat-sink needed to dissipate the heat under worst case conditions.

The simulated power losses of the three phase VSI inverter had an accuracy of 11 % (**Table 15**) compared to the experimental data. This shows that by taking the vendor data one can accurately create a power losses model of a half bridge VSI by counting switching events of the four semiconductor devices and determining when each one is conducting. Although the experimental data was taken at low power due to insufficient lab equipment one could expect the same or a better response at higher power.

The simulated delta thermal response of the IGBT Junction temperature of a half-bridge VSI inverter had an percent error of 27 % (**Table 16**). Although, the percent error seems high at the low power the experiment was conducted at the percent error should decrease when run at a higher power because the change in temperature will be larger and the difference smaller. A thermal model of a half bridge VSI can be created by taking the vendor data and creating a model of the system. The cost of design and production of half-bridge IGBT VSI's can be reduced if one takes the time to create and validate a power losses and thermal models. These tools can allow designers and manufactures to create a product that will work and won't have to create many different prototypes to achieve the desired results.

The predicted time to shutdown on a LOCC was **68.8 seconds** for the 625kW Fuel Cell Reformer project. The maximum PWM switching frequency for the 625kW Fuel Cell Reformer project is 7 kHz which allowed an 20% margin to over temperature protection set point of 110°C.

THIS PAGE INTENTIONALLY LEFT BLANK

VII. CONCLUSIONS

A. CHAPTER OVERVIEW

This chapter summarizes the research performed in this thesis and discusses the results of Thermal and Power Loss Models of a Voltage Source Inverter. Also, possible areas for future research are also discussed.

B. SUMMARY

The goal of this thesis was to show that one can take the vendor data for a voltage source inverter given a valid electrical model and accurately simulate a power loss and thermal model and that these models would allow one to reduce the cost of design and production, increase reliability, quantify the accuracy of the estimated thermal impedance of an IGBT module, predict the maximum switching frequency without violating thermal limits and to quantify the characteristics of the heat-sink needed to dissipate the heat under worst case conditions. This thesis particularly was focused on a voltage source inverter used in the development of a 625KW Fuel Cell and Reformer demonstration for ONR (Office of Naval Research).

The power losses model of the Semikron VSI module was initially created in Simulink with input variables set to an obtainable lab conditions so that experimental data could be collected. The thermal model was defined and then created in Simulink and calibrated to the Semikron VSI Module and heatsink with an input that was the average power output of the semiconductor devices of the power losses model. The power losses model was then simulated and data collected. The thermal model was then simulated with the average power outputs of the semiconductor devices from the power losses model simulation. The experimental lab conditions were set up to match the models simulated conditions. Two data runs were performed, one without coolant in order to calculated the time to shutdown on over-temperature protection on a LOCC. The second experimental data run with coolant flow was to collect experimental data to compare to the simulated models in order to validate them. The data was compared and it was determined that a strong correlation was present between the experimental data and

the simulated data. The power losses and thermal simulation were then run many times to determine the maximum PWM switching frequency for the 625 Kw Fuel Cell Reformer Project of ONR.

C. CONCLUSIONS

This thesis indicates one can take the vendor data for a VSI given a valid electrical model and accurately simulate power loss and thermal models. Once created the validated models will allow engineers to reduce the cost of design and production, increase reliability, quantify the accuracy of the estimated thermal impedance of an IGBT module, predict the maximum switching frequency without violating thermal limits, and to quantify the characteristics of the heat-sink needed to dissipate the heat under worst case conditions. The summary of the results of this thesis are shown in **Table 18**.

	Matlab Simulated Data	Lab Experimental Data	Percent Error
Rise in ΔT(j) (C°)	2.4	1.75	27.4%
Power Losses (W)	636.7	578	9%
Extrapolated Time to Shutdown on LOCC (seconds)	68	NA	NA
Maximum PWM Switching Frequency (kHz)	7	NA	NA

Table 18. Summary of Thesis Results and Goals

D. FUTURE WORK

There are several opportunities for future work in this area. Additional investigation would be best suited to try collecting experimental and simulated data at the maximum design ratings of the 625KW fuel cell reformer project. The correlation

between simulated data and the data collected at the maximum design ratings should be higher. Currently, the lack of adequate lab equipment and power precludes this from happening. Another area for future research would be the method of switching could be varied to see which method of switching (PWM, space vector, hysteresis, etc) gives the best quality power with the least amount of heat generated.

THIS PAGE INTENTIONALLY LEFT BLANK

APPENDIX A

SKiiP 942GB120-317CTV

SEMIKRON

I. Power section

Absolute maximum ratings		T_s = 25°C unless otherwise specified	
Symbol	**Conditions**	**Values**	**Units**
IGBT			
V_{CES}		1200	V
V_{CC} 1)	Operating DC link voltage	900	V
V_{GES}		± 20	V
I_C	T_s = 25 (70) °C	900 (675)	A
Inverse diode			
$I_F = -I_C$	T_s = 25 (70) °C	900 (675)	A
I_{FSM}	T_j = 150 °C, t_p = 10ms; sin	6480	A
I^2t (Diode)	Diode, T_j = 150 °C, 10ms	210	kA^2s
T_j , (T_{stg})		-40 (-25) ...+150 (125)	°C
V_{isol}	AC, 1min.	3000	V

Characteristics	T_s = 25°C unless otherwise specified				
Symbol	**Conditions**	**min.**	**typ.**	**max.**	**Units**
IGBT					
V_{CEsat}	I_C = 750A, T_j = 25 (125)°C	–	2,6 (3,1)	3,1	V
V_{CEO}	T_j = 25 (125) °C	–	1,2 (1,3)	1,5 (1,6)	V
r_{CE}	T_j = 25 (125) °C	–	1,8 (2,3)	2,1 (2,7)	mΩ
I_{CES}	V_{GE}=0,V_{CE}=V_{CES},T_j=25(125) °C	–	(45)	1,2	mA
$E_{on} + E_{off}$	I_C=750A, Vcc=600V	–	–	225	mJ
	T_j=125°C Vcc=900V	–	–	397	mJ
$R_{CC'-EE'}$	terminal chip, T_j = 125 °C	–	0,17	–	mΩ
L_{CE}	top, bottom	–	5,0	–	nH
C_{CHC}	per phase, AC-side	–	4,2	–	nF
Inverse diode					
$V_F = V_{EC}$	I_F= 750A; T_j = 25(125) °C	–	2,1 (2,0)	2,6	V
V_{TO}	T_j = 25 (125) °C	–	1,3 (1,0)	1,4 (1,1)	V
r_T	T_j = 25 (125) °C	–	1,1 (1,3)	1,5 (1,7)	mΩ
E_{RR}	I_C=750A Vcc=600V	–	–	29	mJ
	T_j=125°C Vcc=900V	–	–	37	mJ
Mechanical data					
M_{dc}	DC terminals, SI Units	6	–	8	Nm
M_{ac}	AC terminals, SI Units	13	–	15	Nm
w	SKiiP® 2 System w/o heat sink	–	2,7	–	kg
w	heat sink	–	6,6	–	kg
Thermal characteristics (P16 heat sink; 295 m^3/ h); "r" reference to temperature sensor					
$R_{thjrIGBT}$	per IGBT	–	–	0,030	K/W
$R_{thjrdiode}$	per diode	–	–	0,083	K/W
R_{thra}	per module	–	–	0,036	K/W

Z_{th}	R_i (mK/W) (max.)				tau_i(s)			
	1	2	3	4	1	2	3	4
$IGBT_{jr}$	3	23	4	–	1	0,13	0,001	–
$diode_{jr}$	9	64	10	–	1	0,13	0,001	–
$heatsink_{ra}$	11,1	18,3	3,5	3,1	204	60	6	0,02

SKiiP® 2

SK integrated intelligent Power 2-pack

SKiiP 942GB120-317CTV

Case S3

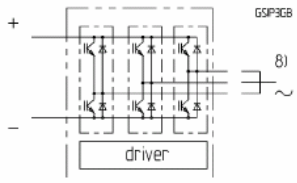

Features

- SKiiP technology inside
- low loss IGBTs
- CAL diode technology
- integrated current sensor
- integrated temperature sensor
- integrated heat sink
- IEC 60721-3-3 (humidity) class 3K3/IE32 (SKiiP® 2 System)
- IEC 68T.1 (climate) 40/125/56 (SKiiP® 2 power section)

1) with assembly of suitable MKP capacitor per terminal (SEMIKRON type is recommended)

8) AC connection busbars must be connected by the user; copper busbars available on request

NWK 40

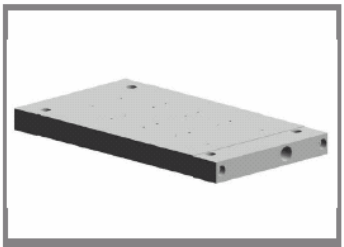

SEMIKRON Heatsinks

Standard lengths	n	b / d Ø mm	$R_{th(s-w)}$ (SKiiP 2) $R_{th(sensor-water)}$ K/W	$R_{th(r-w)}$ (SKiiP 3) $R_{th(sensor-water)}$ K/W	w kg
		SKiiP 2	50% glycol ; 8 l/min		
NWK 40/180		2-fold	0,0148		4,26
NWK 40/240		3-fold	0,0125		5,18
NWK 40/300		4-fold	0,010		6,14
		SKiiP 3		50% glycol ; 8 l/min	
NWK 40/180		2-fold		0,012	4,26
NWK 40/240		3-fold		0,011	5,18
NWK 40/300		4-fold		0,009	6,14

For SKiiP 2 + 3

NWK 40

Features

- Intended for water/liquid cooling of 2-fold, 3-fold + 4-fold versions of SKiiP 2 + 3
- Different side parts available for different directions/positions of In/Out coolant nozzles (contact SEMIKRON for more info)

Dimensions in mm

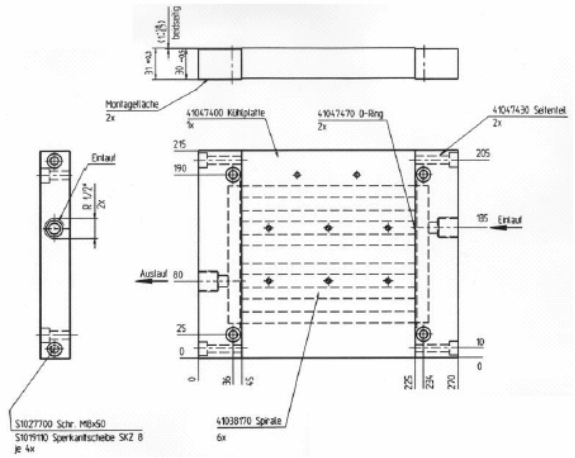

NWK 40/180 for SKiiP 2 (Identical for SKiiP 3 except for position of drilling holes)

Dimensions in mm

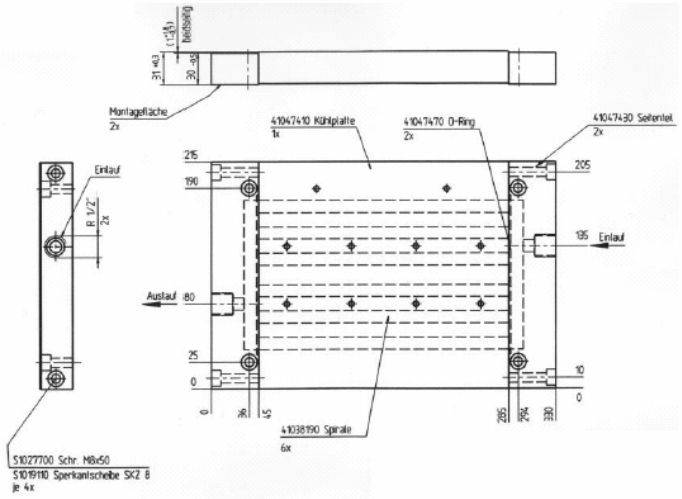

NWK 40/240 for SKiiP 2 (Identical for SKiiP 3 except for position of drilling holes)

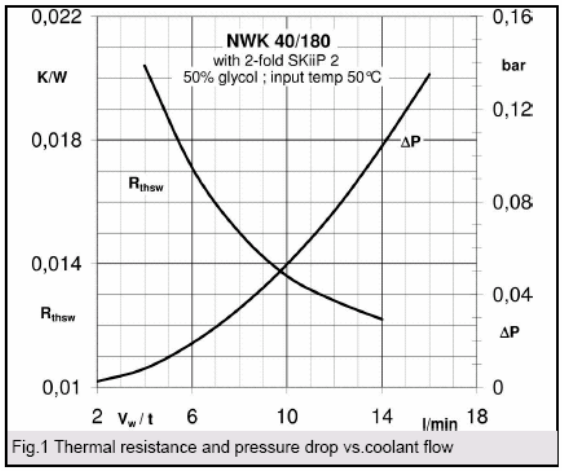

Fig.1 Thermal resistance and pressure drop vs.coolant flow

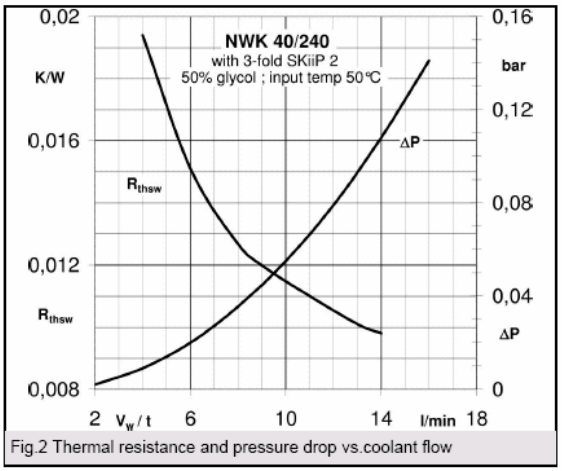

Fig.2 Thermal resistance and pressure drop vs.coolant flow

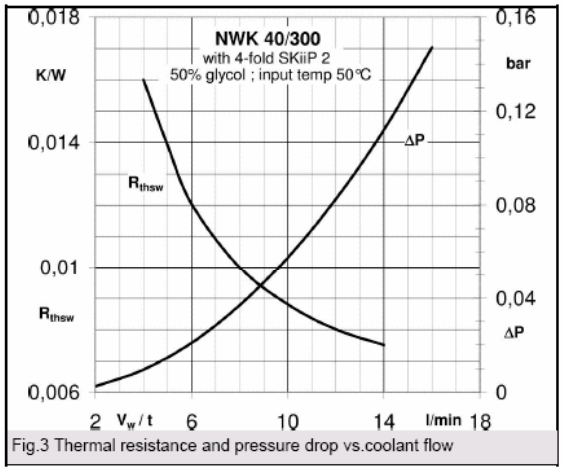

Fig.3 Thermal resistance and pressure drop vs.coolant flow

THIS PAGE INTENTIONALLY LEFT BLANK

APPENDIX B

A. MATLAB M-FILE FOR POWER LOSSES MODEL

Filename: fuel_cell_intlab5.m

```
i_load=100;              %Sets load current%
ffilter=4000;
Tsw = (2*100*10^-6);     %PWM switching frequency
f_fund = 60;             %Fundamental output frequency%
Vdc=100;                 %Input Voltage to inverters
omega=2*pi*60;
oversample=1;
tstep = Tsw/100;         %sets step size%
tstop=20/f_fund          %sets simulation stop time%
Lfa=90*10^-6;
Lfb=Lfa;
Lfc=Lfa;
Cf= (170+6*45)*1e-6*3;
Cfa=Cf;
Cfb=Cfa;
Cfc=Cfb;
alpha=0*2*0.2*sqrt(Lfa*Cfa)/Vdc;%active damping gain
Loa=900*10^-6;
Lob=Loa;
Loc=Loa;
Roa=0.023; %current is in phase winding, system is characterized for a
delta connected winding
Rob=Roa;
Roc=Roa;
%Kp_i=sqrt(3)/Vdc/8;
%Ki_i=1000*sqrt(3)/Vdc/8;    %Current control loop gain
Kp_i=.01;%current PI gain is amplified to account for the SV modulation
scaling
Ki_i=.5;    %Current control loop gain
%Kp_v=.2;
Kp_v=.5;
Kp_rms=0;
Ki_rms=0;    %Voltage control loop gain

%Kp_i=.0005/2;
%Ki_i=10/4;
%Kp_v=.00005*200;
%Ki_v=20*4;

Amat_indI = zeros(2);
Bmat_indI = inv([Lfa -Lfb;Lfc Lfb+Lfc]);
Cmat_indI = [1 0 ;0 1 ;-1 -1 ];    %Ic = -Ia-Ib
Dmat_indI = zeros(3,2);
```

Filename: fuel_cell_intlab5.m(continued)

```
Amat_caps = zeros(3);
Bmat_caps = [1/Cfa 0 0; 0 1/Cfb 0; 0 0 1/Cfc];
Cmat_caps = eye(3);
Dmat_caps = zeros(3);

Amat_load = [-Roa/Loa 0 0; 0 -Rob/Lob 0; 0 0 -Roc/Loc];
Bmat_load = [1/Loa 0 0; 0 1/Lob 0 ; 0 0 1/Loc];
Cmat_load = eye(3);
Dmat_load = zeros(3);

one_zero_state=0;       %Set to one so that only one zero state is used
in modulation
if one_zero_state == 1
    gain1 = 1;
    gain2 = 0;
else
    gain1 = 1/2;
    gain2 = 1;
end

turns_ratio=208/480/sqrt(3);
trans1=turns_ratio*sqrt(3)/2*[sqrt(3) 1 0;-1 sqrt(3) 0;0 0 0];
trans1_qd=trans1(1:2,1:2);
trans2=turns_ratio*sqrt(3)/2*[sqrt(3) -1 0;1 sqrt(3) 0;0 0 0];
trans2_qd=trans2(1:2,1:2);
trans3=1/(turns_ratio*sqrt(3)/2)*[sqrt(3)/4 1/4 0;-1/4 sqrt(3)/4 0; 0 0
0];
```

LIST OF REFERENCES

[1] William F. Weldon, et al. "*Roadmap to an Electric Naval Force*," NRAC Report 02-01, NRAC, Arlington, VA, March 2003

[2] Brad P. Bittle, "Hysteresis Control of Parallel Connected Hybrid Inverters", Masters Thesis, Naval Post Graduate School, Monterey California, September 2005.

[3] Mike Collins, "*DD(X) IPS Revolution in Shipboard Power*," NAVSEA PEO-510 Internal Presentation, Washington D.C., February 2003

[4] R. Steck, et al. "Surface Ship Thermal Management Survery-Part 1," CARDIVNSWC-TR-92-03-21, CARDDIVNSWC, Philadelphia, PA, July 2003

[5] IEEE Power Electronics Subcommittee Task Force 2, "*Power Electronics Building Block Concepts*," IEEE Power Engineering Society Report 04TP170, IEEE Press, New York, 2004

[6] "Semikron Application Notes for Skiip Modules" Semikron website, www.semikron.com, last accessed 19 January 2006

[7] A. Bruce Carlson, "CIricuits" pp (254-258), Brooks/Cole Thomson Learning, Inc., 511 Forest Lodge Rd. Pacific Grove, California, 2000

[8] Ned Mohan, Tore M Undeland, and William P Robbins, "*Power Electronics, 3rd Edition*," pp (225-248), John Wiley and Sons, Inc., Hoboken, New Jersey, 2003

[9]Vladimir Blasko, Rich Lukaszewski, and Ray Sladky, "Online Thermal Management Strategy of a Three Phase Voltage Source Inverter", *Proc. IEEE Industry Applications Society 34th Annual Meeting,* pp. 1423-1431, 1999.

[10] Zhaohui Luo, Hyungkeun Ahn and Mahnoud A El Nokali, "A Thermal Model for Insulated Gate Bipolar Transistor Module", *Proc. IEEE Transactions on Power Electronics VOL. 19. No. 4.,* pp. 902-907, July 2004.

[11]H. Alan Mantooth and Allen R. Hefner. Jr. " Electo-thermal Simulation of an IGBT PWM Inverter", National Institute of Standards and Technology, pp. 77-84, 1993.

[12] Zhaohui Luo, Hyungkeun Ahn and Mahnoud A El Nokali, "A Thermal Model for Insulated Gate Bipolar Transistor Module", *Proc. IEEE Transactions on Power Electronics VOL. 19. No. 4.,* pp. 902-907, July 2004.

[13] L. W. Nagel, "SPICE2: A computer Program to simulate semiconductor circuits", ERL Memo. ERL-M-520, University of California, Berkley, 1975.

[14] G. N. Ellision, "Thermal Computations for Electronic Equipment", Van Nostrand Reinhold: New York, 1984.

[15] A. R. Hefner, "Semiconductor Measurement Technology: INTANT-IGBT Network Simulation and Transient Analysis Tool", NIST Special Publication 400-88, 1992.

[16] A. R. Hefner and D. M. Diebolt, "An Experimentally Verified IGBT Model Implemented in the Saber Circuit Simulator," IEEE PESC Conf. Rec., 1991.

[17] A. R. Hefner and D. L. Blackburn, "Simulating the Dynamic Electro-Thermal Behavior of Power Electronics Circuits and Systems," Conf, Rec. IEEE Workshop on Computers in Power Electronics, 1992.

[18] A. R. Hefner, "A Dynamic Electro-Thermal Model for the IGBT," IEEE IAS Conf. Rec., 1992.

[19] A. R. Hefner and D. L. Blackburn, "Thermal Component Models for Electro-Thermal Network Simulation," Proc. IEEE Semiconductor Thermal Measurement and Management SEMI-THERM Symposium, 1993.

[20] Brian E. Souhan, "Closed Loop Control of Cascaded Multi-level Converter to minimize Harmonic Distortion", Masters Thesis, Naval Post Graduate School, Monterey California, June 2005.

INITIAL DISTRIBUTION LIST

1. Defense Technical Information Center
   Ft. Belvoir, VA

2. Dudley Knox Library
   Naval Postgraduate School
   Monterey, CA

3. Naval Surface Warfare Center Carderock Division
   Code 984
   Attn: Tom Fikse
   Philadelphia, PA

4. Office of Naval Research
   Code 334, Room 669
   Attn: Terry Ericksen
   Arlington, VA

5. Dr. Jeffrey Knorr, Chairman, Department of Electrical and Computer Engineering
   Code EC/Ko
   Naval Postgraduate School
   Monterey, CA

6. Dr. Robert W. Ashton, Department of Electrical and Computer Engineering
   Code EC/Ah
   Naval Postgraduate School
   Monterey, CA

7. Dr. Alexander Julian, Department of Electrical and Computer Engineering
   Code EC/Jl
   Naval Postgraduate School
   Monterey, CA